

https://dspace.org/

Optical properties of synthetic diamond of different synthesis origin.

Fish, Michael Lester.

1995
https://hdl.handle.net/10539/24379

Downloaded from a DSpace repository. https://dspace.org/

OPTICAL PROPERTIES OF SYNTHETIC DIAMOND OF DIFFERENT SYNTHESIS ORIGIN

Michael Lester Fisk

A research report submitted to the Faculty of Science, University of the Witwatersrand, Johannesburg in partial fulfilment of the requirements for the degree of Master of Science

Johannesburg 1995

DECLARATION

I declare that this research report is my own work and that it has not been submitted for any degree or examination in any other University.

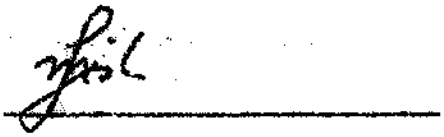

M L Fish

9 February 1995

ACKNOWLEDGEMENTS

The support, funding of De Beers Industrial Diamond Division (Pty) Ltd is gratefully acknowledged.

I thank my supervisor, Prof. J D Comins, for his patience and support and my colleagues, particularly Drs S H Robertson, C N Dodge, and G J Davies, for their encouragement and advice.

I acknowledge, with gratitude, the extraordinary patience and support of my employers, the Diamond Research Laboratory.

Mrs C Van Rooyen is thanked for her considerable assistance in preparing this manuscript.

Finally, I thank my family for their forbearance and understanding.

TABLE OF CONTENTS

		PAGE
ABSTRACT		1
1.	INTRODUCTION	2
1.1	The synthetic diamond industry	3
1.2	Diamond synthesis	5
1.2.1	Thermodynamics and kinetics of diamond synthesis	5
1.3	Morphology	12
1.4	Internal structure of synthetic diamond	14
1.4.1	Lattice defects	14
1.4.2	Inclusions	14
1.4.3	Dislocations and stacking faults	15
1.5	Differences between growth sectors	16
1.6	Control over the properties of synthetic diamond	19
1.6.1	HPHT graphite conversion	20
1.6.2	HPHT reconstitution	22
1.7	Nomenclature	23
1.8	Physical properties of diamond	24
1.9	Optical properties of diamond	29
1.9.1	Electronic	30
1.9.2	Vibrational: one-phonon and defect induced IR	30
1.9.3	Vibrational: Raman	31
1.9.4	Vibronic	33
1.10	Point defects in diamond	37
1.10.1	Overview	37
1.10.2	Aggregation of point defects	39
1.10.3	Single substitutional nitrogen	40

1.10.4 Neutral vacancy 40

1.10.5 The 1.945 eV Centre 41

1.10.6 The H3 centre 41

1.10.7 The 575 nm centre 44

1.11 Heat treatment of synthetic diamond 44

1.12 Plastic deformation of diamond and the creation of point defects 45

1.13 Line broadening 46

2. EXPERIMENTAL 52

2.1 Apparatus 52

2.1.1 Overview 52

2.1.2 Laser 52

2.1.3 Optics 52

2.1.4 Cryostat 57

2.1.5 Monochromator 59

2.1.6 Photon counting system 60

2.2 Samples 61

2.2.1 Sample type 61

2.2.2 Sectioned SDA samples 64

2.2.3 Powder samples 67

2.2.3.1 Large area luminescence 68

2.2.3.2 Small area luminescence 68

2.2.4 Large crystals 72

2.3 Measurement conditions 73

2.3.1 Choice of laser line 74

2.3.2 Temperature 74

2.4 Normalisation of the spectra 75

3. RESULTS 76

3.1 Comparison with previous work 76

3.2 Intensities due to different defects 80

3.3 Reproducibility of measurements on powder 80

3.4 Comparison of representative spectra 90

3.4.1 The H3 centre 103

3.4.2 The 1.945 eV centre 103

3.4.3 The 575 nm centre 104

3.5 Statistical analysis 105

3.5.1 Correlations between different defects within samples 105

3.5.1.1 Large area luminescence 105

3.5.1.2 Small area luminescence 107

3.5.2 Frequency distributions 114

3.5.2.1 Introduction 114

3.5.2.2 The 1.945 eV centre 114

3.5.2.3 The H3 centre 115

3.5.2.4 The 575 nm centre 115

3.6 Lineshape analysis 120

3.6.1 Analysis of the shape of the 1.945 eV ZPL 120

3.6.2 Linewidths of the 1.945 eV ZPL 132

4. DISCUSSION 133

4.1 Intensities due to different defects and comparison with previous work 133
4.1.1 The luminescence intensities from the H3 defect 138
4.1.2 The luminescence intensities from the 1.945eV defect 140
4.1.3 The luminescence intensities from the 575nm defect 143
4.2 Statistical analysis 144
4.2.1 Correlations between different defects within samples 144
4.2.2 Frequency distributions 146
4.3 Lineshape analysis 147
4.3.1 Linewidths 147
4.3.2 Lineshapes 148
4.4 Summary 151
4.5 Conclusions and suggestions for further work 152
4.5.1 Conclusions 152
4.5.2 Suggestions for future work 153

REFERENCES 155

LIST OF TABLES

		PAGE
1.1	The nomenclature used for the three important vibronic defects and the Raman line encountered in this work.	24
1.2	Classification of diamonds.	25
1.3	The Knoop hardness of diamond.	28
1.4	The elastic properties of diamond.	28
1.5	Fracture strength values for diamond.	29
1.6	Pertinent data concerning the three centres which dominate photoluminescence spectra of synthetic diamond.	37
1.7	Some of the simpler point defects found in diamond.	38
1.8	Some more complex defects found in diamond.	38
1.9	Defects in diamond resulting from aggregation processes.	39
2.1	Measurement conditions used for general scans.	73
2.2	Measurement conditions used for zero-phonon line scans.	73
3.1	Comparison of measured spectra with previous work.	79
3.2	One way ANOVA for the 1.945 eV one-phonon sideband normalised luminescence.	85
3.3	One way ANOVA for the H3 one-phonon sideband normalised luminescence.	86
3.4	One way ANOVA for the 1.945 eV ZPL FWHH.	8
3.5	Refence table for sample labelling and identity.	90
3.6	Table summarising the normalised luminescence intensities for the representative spectra of the different sample types.	91

3.7	Correlation of intensity of one-phonon [illegible] for all small area luminescence samples.	110
3.8	Correlation of intensity of one-phonon lines for >50 # samples.	112
3.9	Correlation of intensity of one-phonon lines for 50/60 # samples.	113
3.10	Summary of the frequency distributions of the intensities of the luminescence of the different centres.	116
3.11	Lineshape parameters found by fitting the Voigt profile to the 1.945 eV ZPLs.	121

LIST OF FIGURES

		PAGE
1.1	The effect of the solvent/catalyst on the kinetic barrier.	8
1.2a)	Phase diagram for carbon.	9
1.2b)	Detail from figure 1.2a).	10
1.3	Schematic of variation of morphology with synthesis pressure and temperature.	13
1.4	Example photoluminescence spectra of synthetic diamond.	26
1.5	IR spectra of different diamond types.	32
1.6	Configurational co-ordinate diagram.	34
2.1	Block diagram of the experimental photoluminescence set-up (90° arrangement).	53
2.2	Schematic of the experimental photoluminescence set-up (90° arrangement).	54
2.3	Block diagram of the experimental photoluminescence set-up (180° arrangement).	55
2.4	Schematic of the experimental photoluminescence set-up (180° arrangement).	56
2.5	Octahedral single crystal, identified as Oh.	62
2.6	Cubo-octahedral single crystal, identified as CO.	62
2.7	Cubic single crystal, identified as Cu.	63
2.8	CDA 140/170 # powder sample	63
2.9	SDA 40/45 # powder sample, identified as S11	65
2.10	SDA 40/45 # powder, heat treated under argon for 40 minutes at 1120° C.	65

2.11	Sectioned SDA mounted in a low temperature braze matrix with {111} polished faces exposed.	66
2.12	Modified sample holder for the Oxford Instruments CF1204 Cryostat used for large sample luminescence.	70
2.13	Sample holder for the Oxford Instruments CF1204 Cryostat used for small sample luminescence.	71
3.1	Room temperature photoluminescence spectrum of polycrystalline diamond, SYNDITE.	77
3.2	Example SDA photoluminescence spectra.	78
3.3a)	Replicate spectra of powder sample of CDA. λ_{exc} = 488 nm.	81
3.3b)	Replicate spectra of powder sample of CDA. λ_{exc} = 514 nm.	81
3.4a)	Replicate spectra of powder sample of SDA, S11. λ_{exc} = 488 nm.	82
3.4b)	Replicate spectra of powder sample of SDA, S11. λ_{exc} = 514 nm.	82
3.5a)	Replicate spectra of powder sample of heat treated SDA, HT11. λ_{exc} = 488 nm.	83
3.5b)	Replicate spectra of powder sample of heat treated SDA, HT11. λ_{exc} = 514 nm.	83
3.6	Plot of means of the 1.945 eV 1-phonon luminescence intensity for the powder samples.	87
3.7	Plot of means of the H3 1-phonon luminescence intensity for the powder samples.	88
3.8	Plot of means of the 1.945 eV ZPL FWHH for the powder samples.	89
3.9a)	Averaged photoluminescence spectrum of powder sample of CDA. λ_{exc} = 488 nm.	92

3.9b)	Averaged photoluminescence spectrum of powder sample of CDA. λ_{exc} = 514 nm.	92
3.10a)	Averaged photoluminescence spectrum of powder sample of SDA, S11. λ_{exc} = 488 nm.	93
3.10b)	Averaged photoluminescence spectrum of powder sample of SDA, S11. λ_{exc} = 514 nm.	93
3.11a)	Averaged photoluminescence spectrum of powder sample of heat treated SDA, HT11. λ_{exc} = 488 nm.	94
3.11b)	Averaged photoluminescence spectrum of powder sample of heat treated SDA, HT11. λ_{exc} = 514 nm.	94
3.12a)	Photoluminescence spectrum of {111} sectioned SDA: sample 011. λ_{exc} = 488 nm.	95
3.12b)	Photoluminescence spectrum of {111} sectioned SDA: sample 011. λ_{exc} = 514 nm.	95
3.13a)	Photoluminescence spectrum of {100} sectioned SDA: sample C11. λ_{exc} = 488 nm.	96
3.13b)	Photoluminescence spectrum of {100} sectioned SDA: sample C11. λ_{exc} = 514 nm.	96
3.14a)	Photoluminescence spectrum of octahedral face of octahedral crystal Oh. λ_{exc} = 488 nm	97
3.14b)	Photoluminescence spectrum of octahedral face of octahedral crystal Oh. λ_{exc} = 514 nm.	97
3.15a)	Photoluminescence spectrum of octahedral face of cubo-octahedral crystal COO. λ_{exc} = 488 nm	98
3.15b)	Photoluminescence spectrum of octahedral face of cubo-octahedral crystal COO. λ_{exc} = 514 nm.	98
3.16a)	Photoluminescence spectrum of cubic face of cubo-octahedral crystal COC. λ_{exc} = 488 nm	99

3.16b)	Photoluminescence spectrum of cubic face of cubo-octahedral crystal COC. λ_{exc} = 514 nm.	99
3.17a)	Photoluminescence spectrum of cubic face of cubic crystal Cu. λ_{exc} = 488 nm.	100
3.17b)	Photoluminescence spectrum of cubic face of cubic crystal Cu. λ_{exc} = 514 nm.	100
3.18	Variation in intensity of the H3 photoluminescence as a function of sample type.	101
3.19	Variation in intensity of the 1.945 eV photoluminescence as a function of sample type.	101
3.20	Photoluminescence spectrum of cubic face of cubo-octahedral crystal COC, showing the 575 nm luminescence. λ_{exc} = 514 nm.	102
3.21	Scattergraph showing the evident lack of correlation between the luminescence due to the 1.945 eV and the H3 centres.	106
3.22	A rough check on the comparability of measurements performed on the same samples, using different excitation wavelengths.	108
3.23	Correlation between the one-phonon sidebands intensities of the 575 nm and the H3 centre.	108
3.24	Correlation between the one-phonon sidebands intensities of the 575 nm and the 1.945 eV centres.	111
3.25	Correlation between the one-phonon sidebands intensities of the 1.945 eV and the H3 centres.	111
3.26	Distribution of the 1.945 eV ZPL intensities for SDA grit.	117
3.27	An expanded view of the distribution of the 1.945 eV ZPL intensities of the 40/45 # SDA grit from figure 3.26.	117

3.28	The distribution of the H3 ZPL intensities of SDA grit.	118
3.29	The distribution of the 575 nm ZPL intensities for SDA grit.	119
3.30	An expanded view of the distribution of the 575 nm ZPL intensities for 40/45 # SDA grit from figure 3.29.	119
3.31	Replicate spectra of 1.945 eV ZPL of powder sample of CDA. λ_{exc} = 514 nm.	123
3.32	Replicate spectra of 1.945 eV ZPL of powder sample of SDA: S11. λ_{exc} = 514 nm.	123
3.33	Replicate spectra of 1.945 eV ZPL of powder sample of SDA: HT11. λ_{exc} = 514 nm.	124
3.34	Spectrum of 1.945 eV ZPL of {111} sectioned SDA: sample 011. λ_{exc} = 514 nm.	124
3.35	Replicate spectra of 1.945 eV ZPL of {100} sectioned SDA: sample C11. λ_{exc} = 514 nm.	125
3.36	Spectrum of 1.945 eV ZPL of octahedral crystal: sample Oh. λ_{exc} = 514 nm.	125
3.37	Replicate spectra of 1.945 eV ZPL of octahedral face of cubo-octahedral crystal: COO. λ_{exc} = 514 nm.	126
3.38	Replicate spectra of 1.945 eV ZPL of cubic face of cubo-octahedral crystal: COC. λ_{exc} = 514 nm.	126
3.39	Spectrum of 1.945 eV ZPL of cubic crystal: Cu. λ_{exc} = 514 nm.	127
3.40	Spectrum of 1.945 eV ZPL of {111} sectioned SDA: sample 011, showing deconvolution into two Voigt profile components. λ_{exc} = 514 nm.	127
3.41	The lineshapes of the 1.945 eV ZPLs of the powder samples.	128

3.42	The lineshapes of the 1.945 eV ZPLs of the two sectioned SDA samples.	128
3.43	The lineshapes of the 1.945 eV ZPLs of the three single crystal samples.	129
3.44	Example of Gaussian (formfactor $\alpha = 0.5$) and Lorentzian (formfactor $\alpha = 1$) lineshape.	129
3.45	Lorentzian fraction Γ_L/Γ of the 1.945 eV ZPL lineshapes.	130
3.46	Gaussian fraction Γ_G/Γ of the 1.945 eV ZPL lineshapes.	130
3.47	Fitted FWHH of the 1.945eV ZPLs.	131
4.1	Estimation of stress in diamond from the FWHH.	150

ABSTRACT

The aim of this work was to evaluate the measurement of the optical properties as a means of obtaining information on the growth history of synthetic diamond. A suite of samples of known synthesis origin representing the different types of commercially produced synthetic diamond was analysed by photoluminescence.

The photoluminescence intensity was normalising by using the area of the Raman peak. This allowed a semi-quantitative comparison of the defect concentration.

Three photoluminescent centres were identified, H3, 575 nm and 1.945 eV (with zero-phonon lines at 2.463 eV, 2.156 eV, and 1.945 eV respectively). Differences between the intensities of the luminescence due to these centres were observed as a function of the type of diamond. The H3 and the 1.945 eV intensity was found to increase with the proportion of cubic growth sector. In addition the 1.945 eV intensity was found to increase with heat treatment and was higher in {100} than in {111} growth sectors.

As all three defects detected involve vacancies and nitrogen impurity, an analysis was done to quantify any correlation between the luminescent intensities from the different defects in the same SDA powder sample. The 1.945 eV and 575 nm intensities were observed to be correlated.. An additional correlation was found between the 575 nm and the H3 intensities in the case of finer particle size samples. The luminescence intensity for all three defect types was observed to be a function of the particle size of the sample.

The shapes and widths of zero-phonon lines were related to the types and concentration of lattice defects present in a crystal according to line broadening theory.

An attempt was made to explain the results in the context of the known synthesis origin and growth conditions.

1. INTRODUCTION

The main commercial value of diamond derives in part from its visual attractiveness as a gemstone. This is perhaps a fitting pointer to a fascinating field of scientific endeavour in the study of diamond - the study of its optical properties. For a considerable number of years the main thrust of the work has been to use optical measurements of various optical centres as a means of following the various aggregation reactions that occur between these, mainly nitrogen related, defects. At this juncture, much is understood of the processes which are responsible for the conversion of the typically deep yellow freshly grown diamond (as represented today by synthetic type Ib diamonds) to the perfectly colourless, but no purer, well annealed gem-type diamond (as represented by a natural type Ia diamond). The bulk of this study has been performed on diamonds of natural origin, mainly because of the scarcity of suitably large synthetics (a problem which is fast disappearing because of the growing commercial production of large crystals and because of advances in instrumentation).

It has been said that diamond is "a letter to us from the depths" (Sir Charles Frank, quoted in Field, 1979). In the same metaphor, the advances in this field have been such that the optical properties of the diamond make a large contribution to our ability to read this letter. One important reason for studying the optical properties of a diamond is the potential to learn something of its growth history. This has long been appreciated and applied to natural diamond, but is only now coming of age for synthetic diamond. One practical application of studies of the optical properties of sintered polycrystalline synthetic diamond products in this respect may be found in a paper by Evans et al (1984) where photoluminescence was used to infer temperature gradients which existed during sintering across the diameter of a sintered compact.

The aim of this work was to evaluate the usefulness of the study of the optical properties of synthetic diamond as a means of generating information on the growth history of various types of commercial synthetic diamond. The starting point was to study a set of samples covering the extremes of the various types of commercially produced synthetic diamond. The means used to achieve this was specifically photoluminescence.

1.1 The Synthetic Diamond Industry

The synthetic diamond industry arose out of a need for ever increasing amounts of diamond for abrasive uses which natural sources could not supply (current requirement of the "Western" world market is about 80 tonnes a year (Tomlinson 1992)). Laboratory synthesis of diamond was first reported in 1955 by a team from General Electric although synthesis had been achieved in the laboratory prior to this in Sweden by ASEA (Busch et al 1991). Commercial production has grown rapidly since then, reaching a situation today where 90% of the requirement for industrial diamond is supplied by synthetic diamond produced in many different countries around the globe (Tomlinson 1992).

Initially, the major application for diamond abrasive was for grinding of hard, brittle materials such as tungsten carbides, ceramics and glasses (Busch 1979). Today, in addition to traditional abrasives applications such as polishing, grinding, sawing and drilling of stone, rock and concrete, which exploit the hardness and abrasion resistance of diamond, various non-abrasive applications exist which utilise other unique properties of diamond. These include : application as heat sinks, radiation detectors, lasers, high pressure anvils and surgical blades (Seal 1992).

While the ultimate goal of diamond-based electronic chips remains elusive, the infant chemical vapour deposition (CVD) diamond industry already offers products such as CVD-diamond coated ceramic cutting tool inserts , and free-standing polycrystalline diamond film for thermal management and optical windows (Sussman 1993). An example of a thermal management application is the use of CVD diamond films as heat spreaders in laser diode assemblies used in optical communication systems.

The early successful attempts at diamond synthesis were all achieved by "high pressure, high temperature" (HPHT) synthesis where a carbon source (graphite), in the presence of a metallic solvent/catalyst is subjected to pressures and temperatures in the diamond stable region of the carbon phase diagram. (Severe kinetic barriers prevent

the direct conversion of carbon to diamond except at exceptionally high pressures and temperatures.) This approach still forms the basis of the synthetic diamond abrasives industry today, with graphite (usually in the form of discs and powders) as the carbon source , and alloys of cobalt, iron and nickel and manganese as the most frequently used solvent/catalyst. Other materials used as solvent/catalysts include chromium and tantalum as well as various carbides, carbonates, sulphates and hydroxides (Burns and Davies 1992). Diamonds of up to 1mm are typically grown by this HPHT graphite conversion technique process.

A variation on this approach is to replace the graphite in the above scheme with diamond powder. In this arrangement, the source carbon is separated from the growing crystals (which are nucleated on seeds arranged within the capsule) by a solvent/catalyst metal bath. This approach is known as the HPHT reconstitution technique of diamond growth. Despite the fact that slow growth rates of <5 mg/h (Vagarali et al 1990) are characteristic of this process this technique is favoured for the growth of large synthetic crystals, the largest recorded such crystal, grown by De Beers, weighing 34.8 carat (Koivula et al 1993). Diamonds grown by this method are used for applications such as single point turning tools, microtome knives, surgical blades, wire drawing dies and heat sinks.

A method which is becoming increasingly important is the synthesis of diamond at low pressures under conditions where graphite and not diamond is the stable form of carbon, usually by deposition from a vapour (CVD diamond growth). CVD diamond synthesis can be described as involving the dissociation of carbon-based gases and hydrogen at below atmospheric pressure by electric discharges (plasmas) or heating elements (often tungsten) to deposit diamond onto a substrate. Diamond films have also been produced using oxy-acetylene flame techniques.

1.3 Diamond Synthesis

While there are many types of diamond synthesis have been mentioned, this section will concentrate on the HP/HT methods using a solvent/catalyst. The two main types are: [illegible] and graphite conversion. Recent reviews include those by Wedlake [illegible] (1990), DeVries (1991), and Vagarali et al (1990), Burns and Davies [illegible] documentation of the history of diamond synthesis research at [illegible] is given by Strong (1989).

Thermodynamics and Kinetics of Diamond Synthesis

Diamond and graphite are simply different allotropes of carbon with graphite being more thermodynamically stable at atmospheric pressure and diamond the stable form at elevated pressure. The stability of the metastable diamond phase at ambient conditions is an obvious fact of everyday life. As discussed by Berman (1979) thermodynamic stability is measured by the Gibbs free energy, G, and the fact that the difference in free energies of graphite and diamond changes as a result of pressure can be expressed as

$$(\delta\Delta G/\delta P)_T = \Delta V \qquad \text{....1}$$

where $\Delta G = G_d - G_g$ *and* $\Delta V = V_d - V_g$

Here subscripts d and g refer to the diamond or graphite phase respectively (Berman 1979).

1.2 Diamond Synthesis

While three main types of diamond synthesis have been mentioned, this section will concentrate on the HPHT methods using a solvent/catalyst. The two main types are: reconstitution and graphite conversion. Recent reviews include those by Wedlake (1979), Muncke (1979), DeVries (1991), and Vagarali et al (1990), Burns and Davies (1992). An interesting documentation of the history of diamond synthesis research at General Electric is given by Strong (1989).

1.2.1 Thermodynamics and Kinetics of Diamond Synthesis

Diamond and graphite are simply different allotropes of carbon with graphite slightly more thermodynamically stable at atmospheric pressure and diamond the stable form at elevated pressure. The stability of the metastable diamond phase at ambient conditions is an obvious fact of everyday life. As discussed by Berman (1979) thermodynamic stability is measured by the Gibbs free energy, G, and the fact that the difference in free energies of graphite and diamond changes as a result of pressure can be expressed as

$$(\delta\Delta G/\delta P)_T = \Delta V \qquad \ldots.1$$

where $\Delta G = G_d - G_g$ *and* $\Delta V = V_d - V_g$

Here subscripts d and g refer to the diamond or graphite phase respectively (Berman 1979).

Since diamond is much denser than graphite, ΔV is negative. From equation 1 above this implies that, at constant temperature ΔG decreases as pressure increases. This has the consequence that there exists some pressure at which $\Delta G = 0$; here graphite and diamond are in equilibrium (Berman 1979).

The problem of diamond synthesis might thus appear to be one of achieving the pressures and temperatures at which diamond is the stable form of carbon. However, the presence of an appreciable kinetic barrier, which is the result of a large positive activation volume, results in failure of all attempts at synthesising diamond by simply applying the appropriate pressure and temperature for thermodynamic diamond stability. (In fact, applying the high pressures required to achieve the thermodynamically stable diamond situation itself opposes the achievement of the increased volume of the transition state, requiring higher temperatures to overcome the activation barrier, which in turn would require higher pressures.) In HPHT diamond synthesis, the activation energy is lowered by the use of "solvent/catalysts", usually from the group VIII transition metals. The effect of the solvent/catalyst on the kinetic barrier is represented in figure 1.1 where "a" and "b" are the high and low energy intermediate states between graphite and diamond respectively (DeVries 1991).

A further thermodynamic constraint is that the solvent/catalyst is required to be in the liquid state at the pressure being used. The melt line for the solvent/catalyst in question thus provides a lower limit to the useful temperature range for diamond synthesis. As can be seen in figure 1.2 b) the diamond graphite equilibrium line and the melt line of the solvent/catalyst form boundaries in pressure temperature space to form a "v" - the so-called v-notch region for HPHT diamond growth. The shaded areas in figures1.2 a) and 1.2 b) represent the temperatures and pressures used for HPHT synthesis (Wentorf 1965).

Achieving a situation where diamond can precipitate from the melt as the stable form of carbon is not the whole story however. The presence or formation of initial diamond nuclei are also required. It has been observed that the nucleation density increases with the overpressure (ΔP_e) which is the amount by which the applied pressure exceeds the minimum pressure required (at the temperature in question) to achieve a graphite/diamond equilibrium (Strong and Hanneman 1967, Bezrukov et al 1972). The latter authors noted that nucleation of new crystals was essentially confined to the initial stages (2 minutes) of the synthesis time, an observation confirmed by Wakatsuki (1984) and explained in terms of the increase in wetting energy as the solvent/catalyst solution becomes saturated with carbon (Fedoseev and Semenova-Tyan-Shanskaya 1986). In the reconstitution method it is customary to provide diamond seeds in the synthesis cell, obviating the necessity for spontaneous nucleation. However, unless ΔP_e is kept low, spontaneous nucleation occurs in addition to growth on the seeds. It was also noted that it was possible to nucleate and grow graphite even at conditions where diamond and not graphite is the stable phase. Furthermore, Wakatsuki (1984) observed that diamond nucleation on this re-crystallised graphite was not as efficient as nucleation on "fresh" graphite. Using the fact that it is possible, at negative ΔP_e, to nucleate graphite exclusively, he developed an approach for controlling the diamond nucleation density by "passivating" the surface of graphite source with re-crystallised graphite.

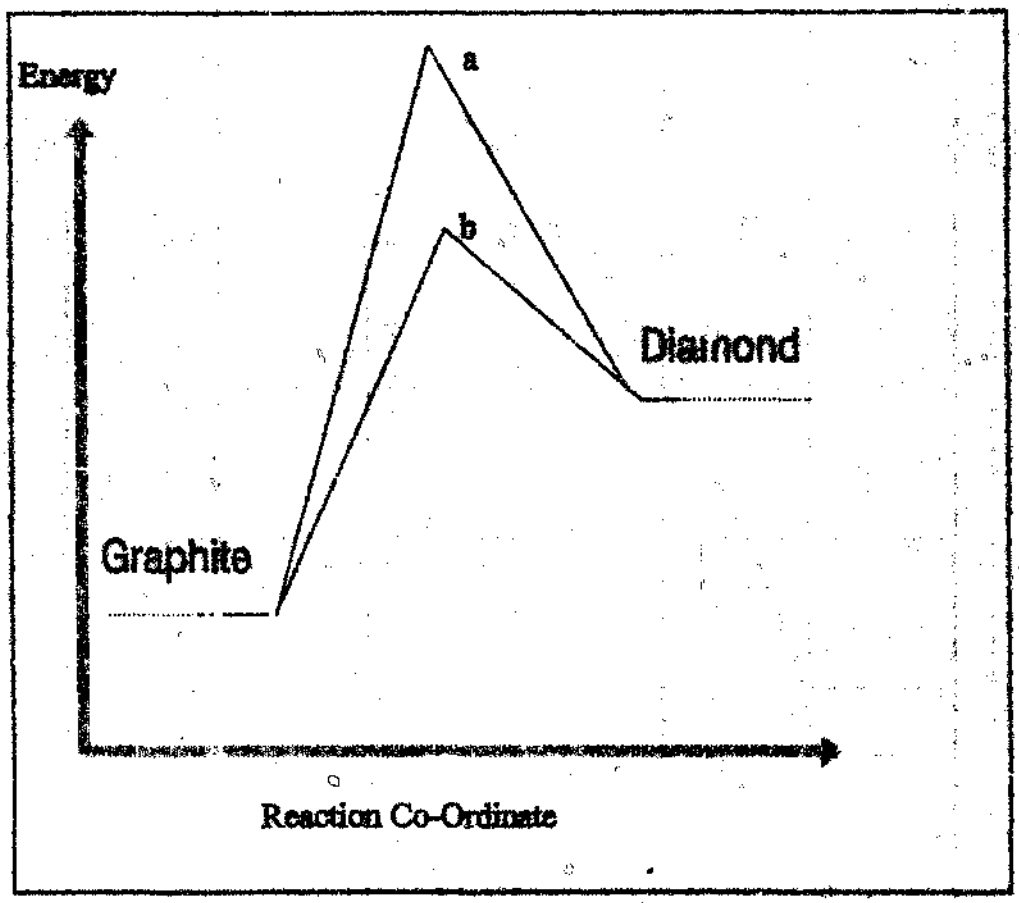

Figure 1.1 The effect of the solvent/catalyst on the kinetic barrier. The solvent/catalyst provides an alternative, lower energy reaction path for the compound to transform from graphite to diamond (DeVries 1991).

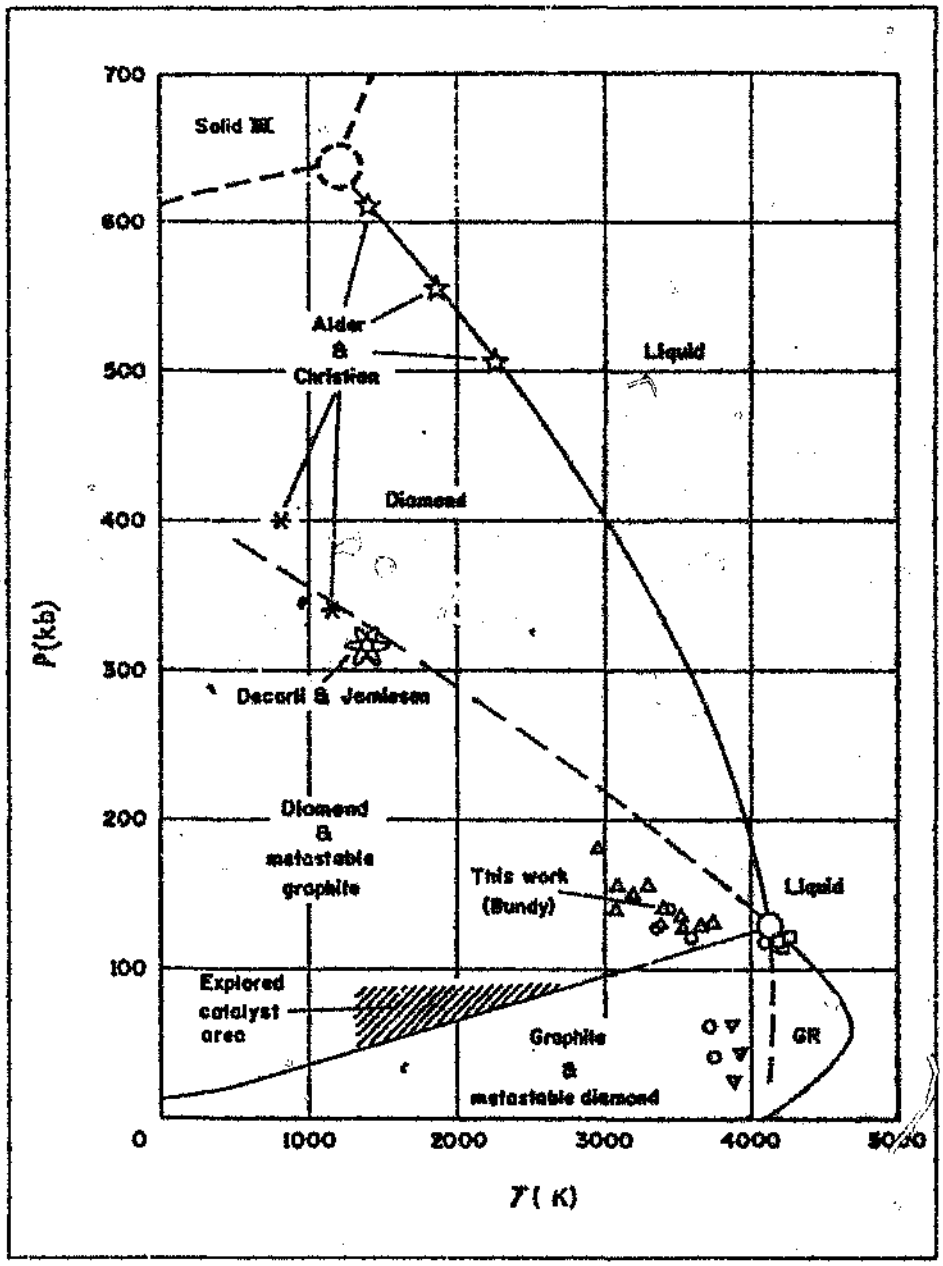

Figure 1.2 a) Phase diagram for carbon (Wentorf 1965). The area from 0 to 100kb and 0 to 3000K is expanded in figure 1.2 b).

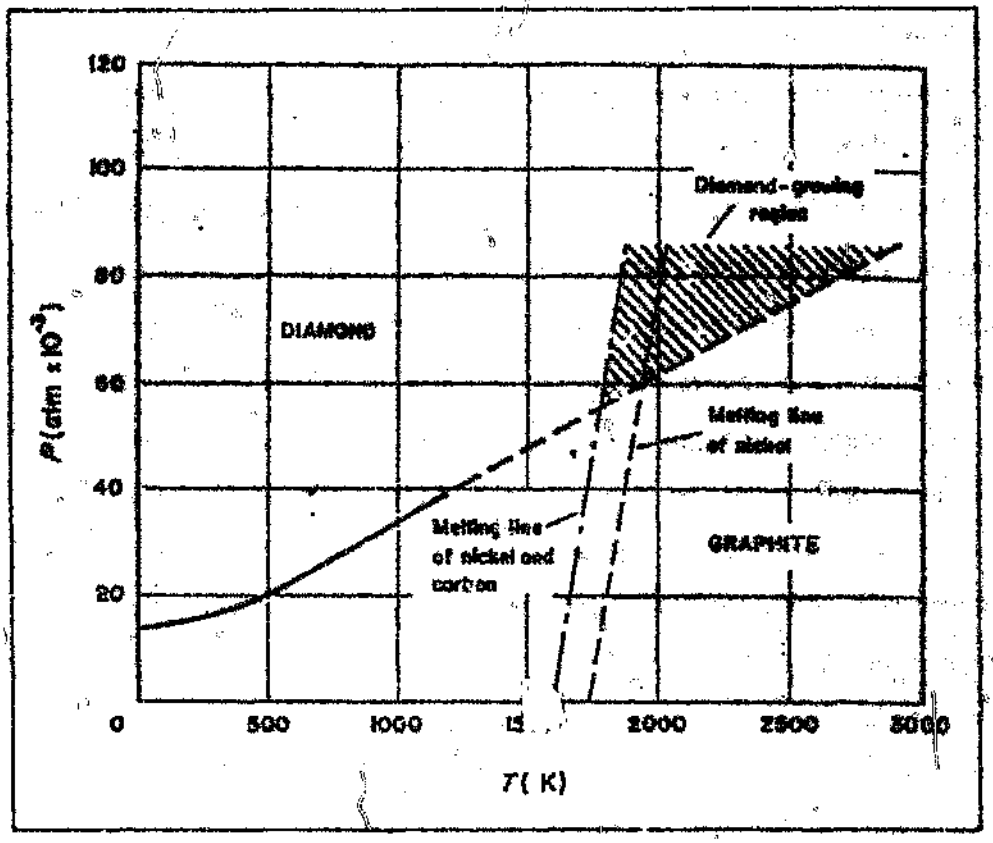

Figure 1.2 b) Detail from figure 1.2 a). The angle formed by the melting line of carbon-saturated nickel and the diamond/graphite equilibrium line (bold, broken line) forms the "v-notch" - the area used for HPHT diamond synthesis (shaded area). (Wentorf 1965)

The existence of viable diamond nuclei and the correct conditions to ensure diamond stability do not guarantee useful reaction rates. Studies of the kinetics of HPHT diamond growth using nickel solvent/catalysts show that, at moderate temperatures, the rate of diamond growth is controlled by the rate of diffusion of carbon through the metal film surrounding the growing diamond (Strong and Hanneman 1967). This has the consequence that the growth rate per unit area is inversely proportional to the thickness of the metal film separating the diamond and graphite. The diffusion constant is proportional to the concentration gradient across the film, which in turn depends on the difference between the solubility of graphite and diamond in the metal. This solubility difference is the thermodynamic driving force for the reaction and is proportional to ΔP_s for constant temperature (implied by equation 1), or to ΔT_d for constant pressure. (Here ΔT_d equals the amount by which the temperature exceeds the liquid/graphite/diamond eutectic temperature (Strong and Hanneman 1967).) While it is noted that the growth rate is dependent on ΔT_d, the free energy difference between diamond and graphite due to their respective structures dominates to such an extent that graphite will be converted to diamond even in situations where the graphite is at a lower temperature than the growing diamond (Wentorf 1965). The dependence of growth rate on ΔP_s may become problematic during attempts to grow high quality single crystal diamond as the growth rate is sensitive to changes in pressure which are smaller in magnitude than the pressure stability of conventional synthesis systems (Wakatsuki and Takano 1987). The HPHT reconstitution or "temperature gradient" approach largely overcomes this difficulty as the driving force in this case is the difference in the solubility of diamond in the solvent/catalyst metal as a function of temperature and this is essentially independent of pressure (provided that the thermodynamic stability of diamond is maintained) (Wakatsuki and Takano 1987).

1.3 Morphology

The morphology of synthetic diamonds is a strong function of the thermodynamic conditions prevailing during growth (Giardini and Tydings 1962). At growth conditions close to the graphite diamond equilibrium line, octahedral morphology dominates, gradually progressing through cubo-octahedral morphology to cubic as the growth conditions approach the melt line for the solvent/catalyst in use as illustrated in figure 1.3 (Muncke 1979). In addition to the change in the crystal morphology as a function of the thermodynamic conditions for growth, differences in surface features such as growth spirals and steps associated with different microscopic growth mechanisms are also observed (e.g. Giardini and Tydings 1962).

Fast growing growth sectors terminate in facets which diminish as growth proceeds, leaving a crystal bounded by the facets of the slower growing sectors. Usually, the higher the number of atoms per surface area of a face, the slower the growth rate of the corresponding growth sector will be. In the case of diamond, this suggests that the {111} octahedral growth sector will be the slowest growing, and hence octahedral faces will dominate the morphology of diamond crystals. This is indeed observed for natural diamond. Dodecahedral diamond, bounded by {110} faces is believed to form as a result of dissolution of octahedral forms. So-called natural cubic diamond rarely has flat {100} faces and generally occurs as result of fibrous growth. Synthetic diamond, on the other hand, is generally found with both cubic and octahedral faces in the form of cubo-octahedral crystals, although dodecahedral and other low-index faces are also found, generally as minor facets. This difference between natural and synthetic diamond suggests differences in the growth mechanism for the two types of diamond (Sunagawa 1984).

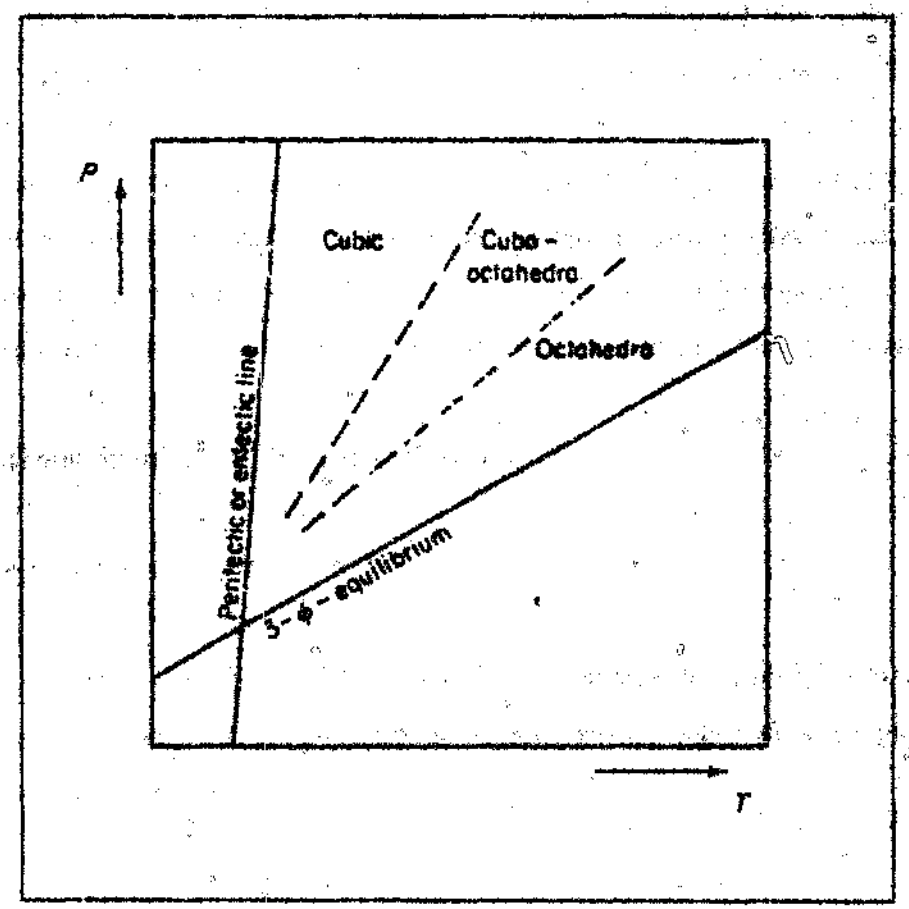

Figure 1.3 Schematic of variation of morphology with synthesis pressure and temperature (Muncke 1979). The peritectic or eutectic line is the melting line of the carbon-saturated metal. The 3-ϕ-equilibrium is the liquid/diamond/graphite equilibrium line.

In diamond synthesis the rate of growth of the {100} and {111} sectors depends to different extents on the growth temperature with the result that different morphologies dominate at different growth temperatures. This can be explained in terms of the different wetting energies of the different surfaces (Yazu 1985, Perevertailo 1992) or in terms of the periodic bond chain (PBC) model which invokes different microscopic growth mechanisms at work on each of the faces (Giling and Van Enckevoort 1985, Sunagawa 1990, Burns and Davies 1992). The simple PBC model successfully explains the observed morphologies and surface structures of the different faces of natural diamond, but fails for synthetic diamond. Giling and Van Enckevoort (1985) propose that surface reconstruction, together with surface chemistry effects, account for the difference in the case of synthetics, while Sunagawa (1990) proposes that growth in synthetics occurs by addition of larger growth units than single atomic entities.

1.4 Internal Structure of Synthetic Diamond

1.4.1 Lattice Defects

The phrase "lattice defects" usually encompasses inclusions, stacking faults and dislocations and point defects; the latter will be dealt with in a separate section (Section 1.10).

1.4.2 Inclusions

Inclusions in diamond are well known. In natural diamonds, they serve to identify the geological and physical environments that existed during growth (Harris 1992). Similarly, the inclusions in synthetic diamond consist largely of amounts of the solvent/catalyst entrapped or otherwise included during growth.

In general, the visible inclusions are of two types: large inclusions of up to several tenths of a millimetre which may occur at any point within the crystal; and sheets of microscopic inclusions lying on planes formed by joining the nucleation point and the corners of any edges at which two facets with the

same kind of crystallographic indices meet (Wakatsuki 1984). The sheets of microscopic inclusions entrapped between like growth zones noted by Kamiya and Lang (1965) and the "whisker inclusions" reported by Kurdadze et al (1992) are believed to be of this sort. It has been observed in diamonds grown between metal and graphite discs, that these bands of inclusions extend only towards the side of the diamond growing into the graphite where the metal film through which the carbon flux must diffuse is thinner (Kanda et al 1981). These asymmetries are not observed in crystals grown by the temperature gradient method in which the thickness of the metal layer through which the carbon must diffuse is large. Scanning electron micrographs of sections through these inclusions showed them to be contained within holes having the same morphology as the external crystal, and to be smaller than 10 micrometers (Wakatsuki 1984).

X-ray diffraction studies of the included metal in both nickel and cobalt grown diamond show that metal phases oriented parallel to the diamond matrix can be detected (Woods 1973). The occurrence of sub-microscopic metal inclusions has been detected by low angle X-ray scattering. The presence of lamellar inclusions 80 Angstroms thick and parallel to {111}, {100} and {113} growth planes was inferred (Woods 1970).

Nickel is capable of being included in the diamond lattice as a point defect and gives rise to optical absorption, cathodoluminescence and photoluminescence features (Collins 1991). Some evidence for "Me-X", where Me is a metal atom and X is either nitrogen or carbon, has also been presented (Malogolovets et al 1978; Malogolovets et al 1993).

1.4.3 Dislocations and Stacking Faults

Both natural and synthetic diamonds are prone to contain dislocations, but stacking faults, and strain-producing growth sector boundaries are only common in synthetic diamonds. Dislocation bundles are often associated with

the macroscopic seeds used in HPHT reconstituted diamond growth (natural diamonds generally grow from sub-microscopic seeds and hence have far fewer dislocations associated with the nucleus). Natural diamonds usually comprise only {111} growth sectors, while synthetics also contain {100} and, less frequently, {110} and {113} growth sectors, each of which has a different tendency to contain impurity atoms. This gives rise to slight differences in lattice constant in the different growth sectors, and hence to strain (Lang et al 1992).

Grown-in dislocations are identified by having direction normal to growth planes (Woods and Lang 1975; Wierzchowski et al 1991) . Other dislocations in the <110> direction were also observed from cathodoluminescent decorations (luminescing pink/orange or blue) by Woods and Lang (1975), and dislocations parallel to (001) surfaces of reconstituted diamond crystals, originating from metallic inclusions have been reported by Wierzchowski et al (1991).

In HPHT graphite conversion diamond, the above convention would suggest that most dislocations would appear to be grown in (Kanda and Lang 1965; Kurdadze et al 1992). The dissimilar lattice constants in the different growth sectors give rise to strain, visible in birefringence microscopy as in the case of diamond grown by HPHT reconstitution.

1.5 Differences between Growth Sectors

The different growth sectors of synthetic diamond may differ significantly in various properties :

1) Single substitutional nitrogen

The concentration of single substitutional nitrogen varies in the sequence {111} > {100} >> {113} > {110} (Woods and Lang 1975, Burns et al 1990) but the situation for diamonds grown at low temperatures may alter to {100} having the

highest nitrogen concentration (Satoh et al 1990). It has also been noted that "cold shaped" diamond (more cubic diamond, grown under lower temperature conditions than usual) displayed a murky green coloration in the cubic growth zones. This was found to be associated with a broad absorption band peaking at 1.9 eV that exhibits thermochromic behaviour, disappearing on cooling to 77 K. This effect, observed for diamond grown by both HPHT reconstitution and graphite conversion, and in both cobalt-iron and iron-nickel solvent/catalysts, was also associated with very high nitrogen concentrations (about 800 ppm) (Collins and Lawson 1989).

It should be noted that the growth sector dependence above for nitrogen will affect any other point defects formed by aggregation with nitrogen. For example, the 1.945 eV defect (NV) was shown in photoluminescence tomography measurements to occur at a much higher concentration in the {111} growth zones than in the {100} and {113} sectors, in accordance with the nitrogen concentration (Van Enckevoort and Lochs 1988).

2) Ni-related defects

It has been shown that the nickel related, optically active point defects are confined exclusively to {111} growth sectors (Collins et al 1990: Satoh et al 1990). Wakatsuki (1991) reports quantitative measurements of this substitutional Ni defect which showed that concentrations in the {111} growth sectors were as high as 100 ppm, but less than 0.1 ppm in the {100} growth sectors. Iron was also detected in the {100} growth sectors at levels of up to 1 ppm (Wakatsuki 1991).

3) The H3 Defect

The bright green cathodoluminescence of the H3 centre, restricted mainly to the {100} growth sectors, is a major feature of the cathodoluminescence of synthetic diamonds (Woods and Lang 1975; Burns et al 1990). This cathodoluminescence displays marked banding parallel to the {100} crystal faces, and is optically polarised in each {100} growth sector in the <110> directions parallel to the {100} face of the sector. A similarity between the luminescence distribution noted by

Woods and Lang and that occurring in CVD diamond is noted by Kawarada et al (1989), but not identified as H3. These phenomena, which are not observed when H3 centres are generated by creating vacancies and allowing them to be trapped by A centres during annealing, are explained as the result of these defects being grown in for synthetic diamonds (Dodge 1986).

4) Lattice parameter

In their seminal paper, Kaiser and Bond (1959) showed a clear correlation between the lattice spacing and the nitrogen content of synthetic diamond and used the magnitude of this dilation to argue that the nitrogen was present predominantly as substitutional nitrogen. In general, any point or lattice defects at high enough concentration can perturb the lattice spacing. Precise measurements of the lattice spacing in specific growth sectors, coupled with the quantification of the concentration of the point defects responsible, provide valuable data to assist in verifying models of defect structure. As an example, measurements associated with single substitutional nitrogen show that the effective volume for the nitrogen atom in diamond is 1.41±0.06 times that of the carbon atom displaced (Lang et al 1992).

Precise measurements of the lattice spacing by x-ray diffraction techniques have detected differences between the lattice spacing of different growth sectors in HPHT reconstituted diamond of the order of 10's of parts per million with an accuracy of 1.5 ppm (Wierzchowski et al 1991). The lattice spacing decreased in the sequence {111}>{100}>{110},{113}, in good agreement with the sequence observed for the substitutional nitrogen concentration noted above (Burns et al 1990).

5) Other features

Stability of growth sector: the {111} faces are least affected by fluctuation in growth parameter, followed by {100}. The presence of the faces {110} and {113} are intermittent (they appear and disappear intermittently during the growth of a crystal) and are very sensitive to growth conditions (Kanda et al 1981).

Boron is incorporated in the lattice of synthetic diamond substitutionally in a highly inhomogeneous manner (Burns et al 1990).

The cleavage energy for the different crystallographic planes increase in the order {111}<{110}<{311}<{100}, and this has a major influence over the manner in which diamond fractures, the favoured cleavage plane being {111} (Field 1979).

Abrasion resistance varies with growth sector (Woods and Lang 1975). In addition, the abrasion resistance within a growth sector is distinctly anisotropic (Wilks and Wilks 1965).

Hardness, measured by indentation, varies as a function of direction in a crystal face, with Knoop hardness in the <110> direction being smaller on the {111} face than on the {110} and {100} faces (Brookes 1992).

1.6 Control Over the Properties of Synthetic Diamond

The growth in the use of synthetic diamond is partly attributable to the ability of the synthesis processes to produce diamond with specifically tailored mechanical properties (Wedlake 1979, Tomlinson 1992). While the exact "recipes" for tailoring the various synthetic diamond properties are "closely guarded industrial secrets" (Wedlake 1979) a fair amount may be gleaned from the literature. The problem of growing synthetic diamond in the presence of an appropriate solvent/catalyst was broken down to five components above: achieving the thermodynamic conditions required for diamond growth; simultaneously achieving conditions for the solvent/catalyst to be in a molten state; achieving an appropriate degree of nucleation; obtaining a suitable growth rate; and maintaining constant growth conditions during synthesis. We shall see that the art of tailoring diamond properties essentially consists in manipulating these

Using these variables, the synthetic diamond industry produces a wide variety of abrasive products, varying mainly in particle size and strength. In this way, it is

possible, for example, to mass produce fine, friable diamond abrasives for application in resin bonded grinding wheels, or relatively coarse, tough and thermally stable diamond abrasives for sintering into metal segments for use in sawing granite.

1.6.1 In HPHT Graphite Conversion

Wedlake (1979) notes that variables used to achieve control over the properties of diamond produced include: pressure and temperature cycles; the nature of the solvent/catalyst and the carbonaceous material, and even doping with poisons to achieve poor crystallinity and imperfection.

The growth of perfectly crystalline, non-included diamond requires that the nucleation density is controlled at a sufficiently low level to prevent adjacent crystals interpenetrating as they grow, as well as low growth rates to facilitate perfectly formed, flat surfaces and minimal inclusions. Both the low nucleation density and the layer growth mechanism are achieved by maintaining a low over-pressure (pressure in excess of the pressure for graphite/diamond equilibrium) as discussed in section 1.2.1. An alternative approach to reducing nucleating density, by passivating the graphite surface by achieving a degree of coverage with re-precipitated graphite, has been developed (Wakatsuki 1984).

An important aspect to grasp is that in typical HPHT graphite conversion diamond synthesis processes, appreciable gradients may exist within the high pressure cell. This has the consequence that crystals growing in different parts of the cell may well be growing under different thermodynamic conditions. The effect of this on the size distribution of crystals grown from a non-ideal high pressure cell are considered by Fedoseev and Semenova-Tyan-Shanskaya (1986). The consequences of these distributions of growth environment is that the properties of the resultant diamond even from a single synthesis run are distributed over a wide range. The distributions found for some technologically important crystal properties are discussed by Nevstruev et al (1992).

The presence of trace impurities in the synthesis cell may have considerable effects on diamond nucleation and subsequent growth. Some early observations suggested that elements electronegative with respect to carbon, such as sulphur selenium and oxygen, act as poisons, while those electropositive, such as aluminium and boron act as nucleation enhancers (Cannon and Conlin 1964). The presence of water in the crystal growth environment has been demonstrated to have a major effect on the crystal growth mechanism, the crystal growth type changing from flat through hopper to dendritic as the amount of water available increases (Sunagawa 1990). In a recent review Burns and Davies (1992) briefly mention the role of nitrogen and aromatic ring structures in preventing the formation of diamond, and the relative lack of any apparent harmful role of hydrogen in the conversion of hydrocarbons. An example of the manner in which trace impurities can have a profound effect on the type of diamond grown is illustrated by the report that the successful use of glassy carbon as a carbon source with cobalt, iron, and nickel solvent/catalysts depends strongly on the hydrogen concentration. A maximum permissible level for hydrogen is reported to be 2200 parts per million (Miyamoto et al 1991). This same report illustrates well how variations in the carbon source and the solvent/catalyst can affect the properties of the diamond produced. When iron rich solvent/catalysts were used in conjunction with a carbon source with a flat, smooth surface, irregular, needle-like crystals, highly elongated in the <100> direction, could be grown. The same type of crystal was grown from both non-graphitic glassy carbon and highly graphitised pyrolytic graphite. The authors attribute the phenomenon to the enhanced nucleation density which arises from the smooth, pore-free surface of the carbons in conjunction with the use of iron as the solvent/catalyst, followed by a process of geometric selection as the crystals simultaneously grow out radially from the site of nucleation.

As mentioned in the earlier section on morphology, diamonds grown at different relative pressures and temperatures end up with different morphologies. There are many references to other consequences of growth at different relative pressures and temperatures. Two such examples are: increasing growth pressures and temperatures such that the favoured morphology is octahedral results in a reduction of the concentration of both epitaxially and randomly included matter (Giardini and Tydings 1962); and increasing the growth rate results in a decrease of the strength of the diamonds (because of increases inclusion capture and growth defects) (Fedoseev and Semanova-Tyan- Shanskaya 1987, and Novikov and Borlinsky 1992).

1.6.2 In HPHT recrystallization

The major control variable in this process is the thermodynamic driving force for diamond growth, namely the temperature induced solubility difference between the source diamond and the growing diamond. This is manipulated by varying the temperature difference between the parts of the high pressure cell where these are respectively situated.

As for the case of HPHT graphite conversion growth, the growth temperature and pressure have a profound effect on the morphology and general crystal perfection. Strong and Chrenko (1971) remark on the need to keep growth rates low in order to limit the entrapment of metal.

Variations in the source diamond such as the isotope ratio (C^{12}:C^{13}), and addition of nitrogen getters, can result in production of a variety of different diamond types, from isotopically pure or isotope enriched type IIa to type IIb diamond (Anthony et al 1990).

1.7 Nomenclature

The naming of optically active point defects found in diamond often causes confusion. Attempts at introducing a systematic approach have been made but no single set of rules appears to be followed. For vibronic centres, the zero-phonon line (ZPL) is usually called by the energy or wavelength at which it occurs, but sometimes by a letter followed by a number following a scheme such as the one discussed by Walker (1979). This number is further confused by the adoption of a different naming scheme for defect centres observed by ESR. The same centre may also be observed by optical techniques, and be given a different name.

Further confusion may arise from the practices generally adopted regarding the description of the spectral energy associated with a defect. For defects which absorb or emit in the infra red such as single substitutional nitrogen, wavenumber (cm^{-1}) is usually used. For defects absorbing or emitting in the visible or ultra-violet (e.g. the centre known as H3, with ZPL at 2.463 eV), energy (eV) or wavelength is used.

The practice adopted here is the one used by Collins (1992) where the most frequently used name is chosen. No attempt is made to adherere to a single naming scheme or energy unit. This results in some apparent oddities as one defect encountered (H3) adheres to the nomenclature of Walker (1979), one defect is known by its ZPL wavelength (575 nm), and one defect is known by its ZPL energy (1.945 eV). For describing peak positions and spectral features, wavenumber will be used to allow for reference to the figures. For reference, a list of some of the nomenclature is given below in table 1.1. The "Label" column gives the label used for this defect in the spectra.

Table 1.1

Name	Structure	Label	Wavelength (nm)	Energy (eV)	Wavenumber (cm^{-1})
H3	N-V-N	H3	503.2	2.463	19871
575 nm	N_i-V	575 nm	575	2.156	17391
1.945 eV	N-V	1.945 eV	637.5	1.945	15692
Raman λ_{exc}=514.5 nm		Raman	552.4	2.25	18104
Raman λ_{exc}=488 nm		Raman	521.9	2.38	19160
Laser line λ_{exc}=514.5 nm		? =514 nm	514.5	2.410	19436
Laser line λ_{exc}=488 nm		λ_{exc}=488 nm	488.0	2.540	20491

The nomenclature used for the three important vibronic defects, the Raman and laser excitation lines encountered in this work. The the energies are given in various units for reference.

An example spectrum showing these vibronic defe s and the Raman line is given in figure 1.4.

1.8 Physical Properties of Diamond

Diamond is a unique material with many outstanding properties. The extreme hardness of diamond is its best known characteristic and arises directly out of the extreme rigidity of the diamond lattice, as do most of its unique properties. This rigid lattice comprises an extended network of carbon-carbon bonds extending tetrahedrally from each carbon atom, each being in the sp^3 hybridisation state. There are two crystallographic forms of diamond: cubic (most natural and synthetic diamond), and hexagonal (shock diamond).

Diamond generally contains impurities, the most important being nitrogen which occurs in a variety of forms. A classification system based on the nitrogen content exists and is widely used (table 1.2).

Table 1.2

Type	Form of Nitrogen	Abundance
Ia	A and B aggregates and platelets	98% of natural
Ib	Single substitutional (C centres)	0.1% of natural, most synthetics
IIa	Virtually no nitrogen	2% of natural
IIb	Virtually no nitrogen but semiconducting due to boron	Rare for natural diamond
(IaA)	Predominantly A aggregates	Subgroup of Ia
(IaB)	Predominantly B aggregates	Subgroup of Ia

Classification of diamonds (after Field 1991)

Other important impurities are hydrogen and oxygen, and mineral or metallic inclusions of the growth medium (depending on whether the diamonds are natural or synthetic). Many elements have been detected in diamond, particularly using nuclear probes (Sellschop 1992).

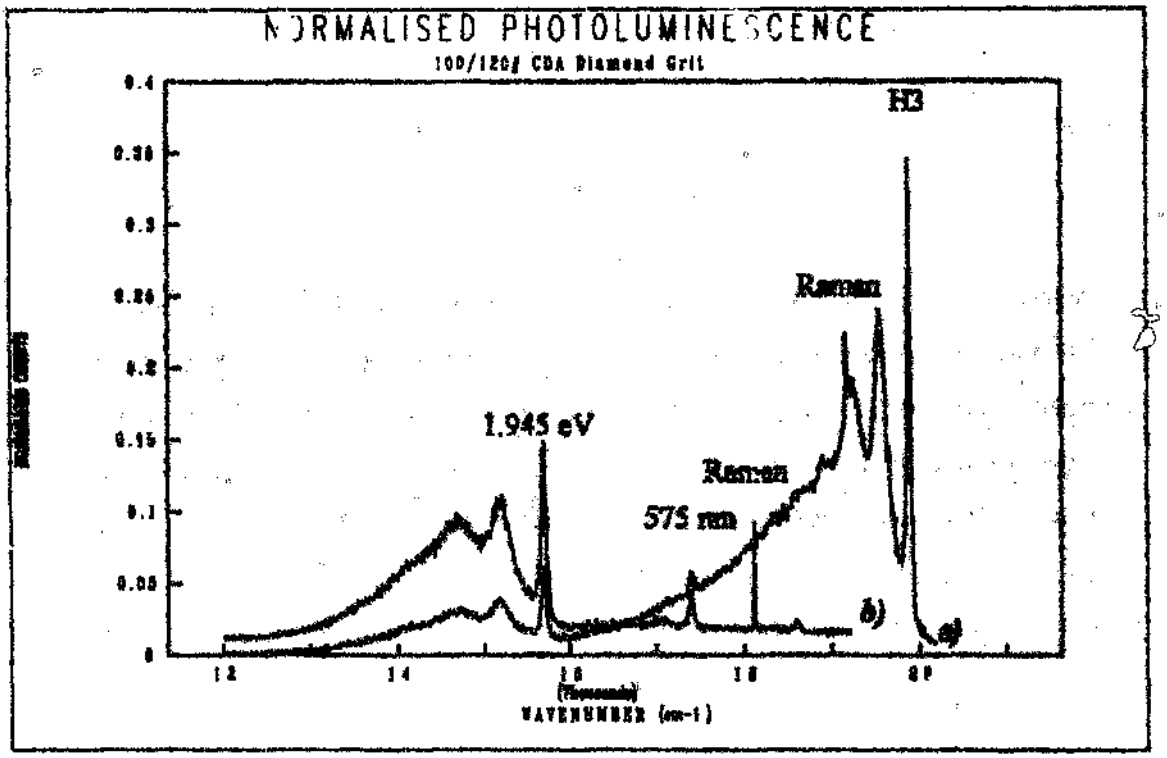

Figure 1.4 Example photoluminescence spectra (λ_{exc} = 488 nm a), λ_{exc} = 514 nm b)) of synthetic diamond showing the vibronic luminescence spectra of the three main defects that are encountered in this work (refer to table 1.1). The Raman line occurs at different wavenumber depending on λ_{exc} as it occurs Stokes-shifted by a constant shift from λ_{exc}

The thermal conductivity of diamond is very high (about 5 times that of copper at room temperature), which is another consequence of the rigid lattice and low nuclear mass of carbon. Thermal conductivity is reduced by the presence of impurities and dislocations, and even by isotopic scattering. The production of synthetic diamond with very low C^{13} concentration yielded a greater than expected improvement in thermal conductivity - attributed primarily to the effect on Umklapp processes (Field 1991).

Diamond has a relatively large band gap of 5.48 eV (Field 1991), making it a very good insulator, transparent to light right across the visible into the UV. Impurities may give rise to absorption bands which give rise to coloured diamonds - single substitutional nitrogen in particular, introduces an absorption band in the UV, the tail of which absorbs in the visible, giving synthetics their characteristic yellow coloration.

Diamond is chemically inert under most circumstances - another feature of the strong sp^3 carbon-carbon bonds. It is resistant to most chemical attack but is susceptible to oxidation at high temperatures. Some metals such as tungsten, tantalum, and zirconium react with diamond to form their carbides, while other metals such as iron manganese, cobalt, chromium and the platinum group metals in the molten state dissolve carbon.

Some mechanical properties of diamond are listed in the following tables (table 1.3, table 1.4, and table 1.5).

Table 1.3

Diamond Type	Face	Orientation	Knoop Hardness
Type I	(001)	<100>	98 GPa
Type I	(001)	<110>	83 GPa
Type I	(111)	<110>	56 GPa
Type I	(111)	<112>	63 GPa
Type II	(001)	<100>	103 GPa
Type II	(001)	<110>	91 GPa
Type II	(111)	<110>	76 GPa
Type II	(111)	<112>	110 GPa

The Knoop hardness of diamond. The face for which the hardness is quoted is given in the column "Face" while the orientation given is the direction of the long axis of the indenter. From Brookes (1992).

Table 1.4

Young's Modulus	11.41×10^{11} Nm^{-2}
Poisson's Ratio	0.07
Bulk Modulus	4.42×10^{11} Nm^{-2}

The elastic properties of diamond. Values given are the isotropic aggregate values. (Data from the appendix of Field (1992).)

Table 1.5

Cleavage Energy	γ=5.5±0.15 Jm^{-2} {111}
Fracture Toughness	K_{Ic}=3.4 to 5.0 $MNm^{-3/2}$ (depending on surface)
Tensile Strength	ca. 300 $kgmm^{-2}$
Compressive strength	ca. 1000 $kgmm^{-2}$ (Synthetic SDA100 grit)

Fracture strength values for diamond. (Data from appendix of Field (1992).)

More comprehensive listings of the properties of diamond are listed in an appendix in the books edited by Field (1979; 1992) and in Field (1991).

1.9 Optical Properties of Diamond

Light can interact with the diamond lattice in a number of ways. In each case, absorption of light corresponds with the excitation of the lattice in some manner, increasing its energy by the energy of the photon absorbed . (In an analagous manner, emission of light corresponds to the relaxation of the lattice, decreasing its energy by the energy of the emitted photon.) Infrared photons have energies appropriate to the excitation of lattice vibrations, while the wavelength of visible light is too short to excite vibrations and too long to excite valence electrons from the valence band to the conduction band (i.e. diamond is transparent to visible light). In fact, the bandgap of diamond 5.48 eV at 77 K means that diamond is transparent well into the UV. However, impurities may well have energy levels in the band gap, giving rise to absorption of light of energies in this otherwise transparent region. It is precisely this phenomenon of a very large bandgap which makes the optical properties of diamond such a rich field as impurities and defects with a wide range of energies can give rise to features in this otherwise featureless energy range.

1.9.1 Electronic

Electrons can only be excited from the valence band to the conduction band in combination with phonon absorption and emission. This results in increasing absorption just below the band edge as temperature (and hence the phonon distribution density) increases (Collins 1993).

Luminescence ("edge emission") may occur by recombination of free excitons resulting from the generation of electron-hole pairs by absorption of UV light or as cathodoluminescence generated by energetic electrons (Collins 1993).

The major impurity in synthetic diamond is single substitutional nitrogen. This defect can act as a donor with a donor level in the band gap. As a result, it is possible for donor electrons from the nitrogen impurity to be excited to the conduction band by photons with energy greater than 2.0 eV (Collins 1993), giving rise to an absorption continuum above this level. It is this which gives rise to the characteristic yellow colour of synthetic diamond.

1.9.2 Vibrational: One-phonon and Defect Induced IR absorption

Absorption of infrared (IR) wavelength light occurs as result of the excitation of vibrational modes in the lattice. There will be an upper limit to the frequency of vibration related to the mass of the carbon atoms and the strength of the carbon-carbon bonds. This limit has a value of 1332 cm^{-1} which is the Raman frequency in diamond. The mass dependence means that diamonds grown with different isotopes of carbon will have their vibrational modes shifted in energy. The ability to grow C^{12} and C^{13} diamond has allowed a much greater understanding of localised modes to be established (see for example Collins 1991). The diamond structure has no intrinsic electric moment associated with it, and hence the absorption of light by a phonon ("one phonon absorption") is forbidden. There are, however, two important ways in which absorption of

light by pure vibrational means can occur: multi-phonon processes; and defect-induced one phonon absorption.

In the case of multi-phonon absorption, one vibrational mode induces a temporary electric moment. Absorption of light can cause further vibration of these electric moments. This process is known as two-phonon absorption. Two and three-phonon absorption provide the only intrinsic vibrational absorption processes that are seen in diamond. They are characteristic of the diamond lattice and are hence common to all diamond types.

In defect-induced one-phonon absorption, an impurity atom gives rise to an electric moment, allowing coupling of one-phonon vibrational modes to radiation. The most important such vibrational modes are those associated with nitrogen and aggregated nitrogen impurities. In fact the analysis of the infrared absorption spectrum provides the most useful means of identifying the type to which a diamond belongs (see figure 1.5). In cases where the defect is a single atom, a "localised mode" may occur where the associated vibrational mode forms a sharp, localised band of vibrational frequencies, rather than the broad envelope observed for lattice vibrations.

1.9.3 Vibrational: Raman

We have seen that defect free diamond should be transparent between the upper limit for the three-phonon absorption at about 3996 cm^{-1} (0.5 eV) and the absorption edge at about 44630 cm^{-1} (5.5 eV) (Davies 1977(a)). The only optical processes that can occur in this region are Raman processes. In these, incident light may exchange energy with the diamond lattice to be inelastically scattered as Raman scattered light. This light will have an energy differing from the incident light by an amount equal to that transferred - the energy "shift" which may be the result of gaining energy from (anti-Stokes process) or losing energy (Stokes process) to the lattice. The selection rules and the nature of the

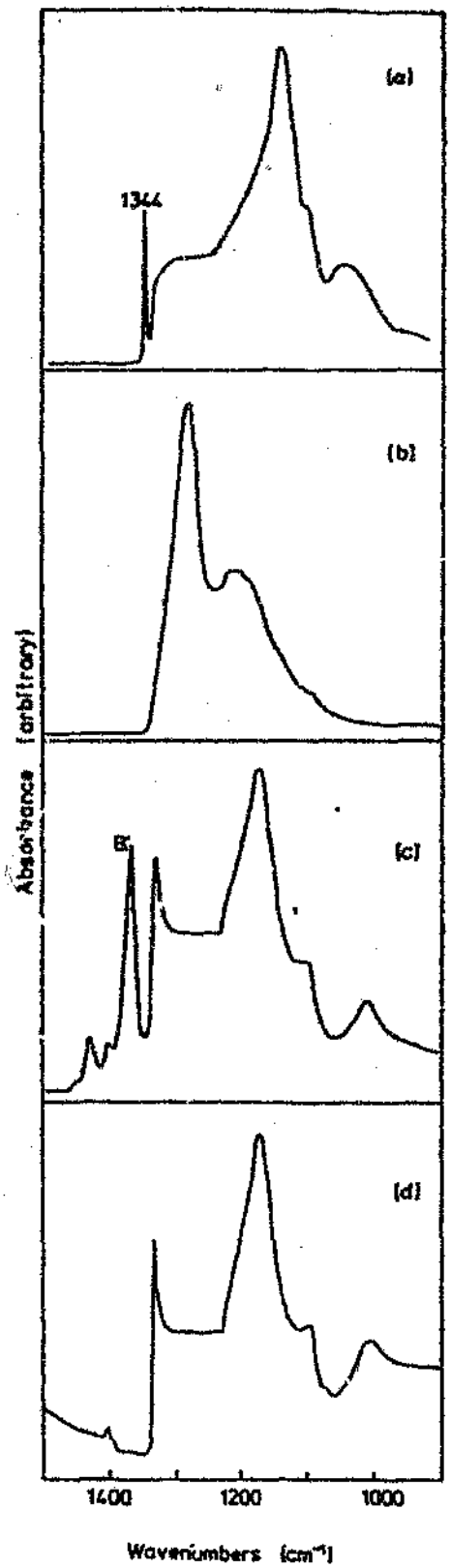

Figure 1.5 IR spectra of type Ib a), IaA b), IaB (with platelet peak) c), IaB (without platelets) d). (After Collins (1993).) These nitrogen related absorption systems are examples of defect induced, one-phonon absorptions and are the basis of the most important classification of diamond into types (see table 1.2).

optical modes of diamond are such that the first-order Raman spectrum of diamond consists of a single line shifted by 1332 cm^{-1} ((Davies 1977(a)). The Stokes Raman line appears in all photoluminescence spectra in this work superimposed on the second phonon replicate of the H3 band for 488 nm excitation (see, for example, figure 1.4), and as the single sharp line to the high energy side of the 1.945 eV and 575 nm bands in 514 nm excited spectra. (The wavenumber at which the Raman line occurs in this work is 18104 cm^{-1} when 514 nm excitation is used and 19160 cm^{-1} when 488 nm excitation is used.) As explained later, the Raman line is used to normalise the photoluminescence spectra to allow semi-quantitative comparisons of luminescence intensities between spectra.

1.3.4 Vibronic

A photon of radiation may be absorbed by a defect in the diamond lattice by the excitation of an electron from the ground electronic state to an excited electronic state. The effect of the electronic excitation is to create a new spatial distribution of the electrons of the defect. Because of this rearrangement, the nuclei surrounding the defect will have to move to new equilibrium positions to accommodate the new electron distribution. We see that an electronic excitation results in atomic vibrations - the process cannot be considered a purely electronic phenomenon, but rather a vibronic phenomenon. Vibronic transitions can be simply explained by configurational co-ordinate diagrams (see figure 1.6).

The configurational model summarises the Born-Oppenheimer approximation. Physically, the Born-Oppenheimer approximation considers the light electrons to respond instantaneously to vibrations of the nuclei, however the massive nuclei respond only to the average position of the electrons.

In figure 1.6, the vibrations of the lattice in the ground and excited electronic states are approximated by harmonic potentials, each with its own harmonic

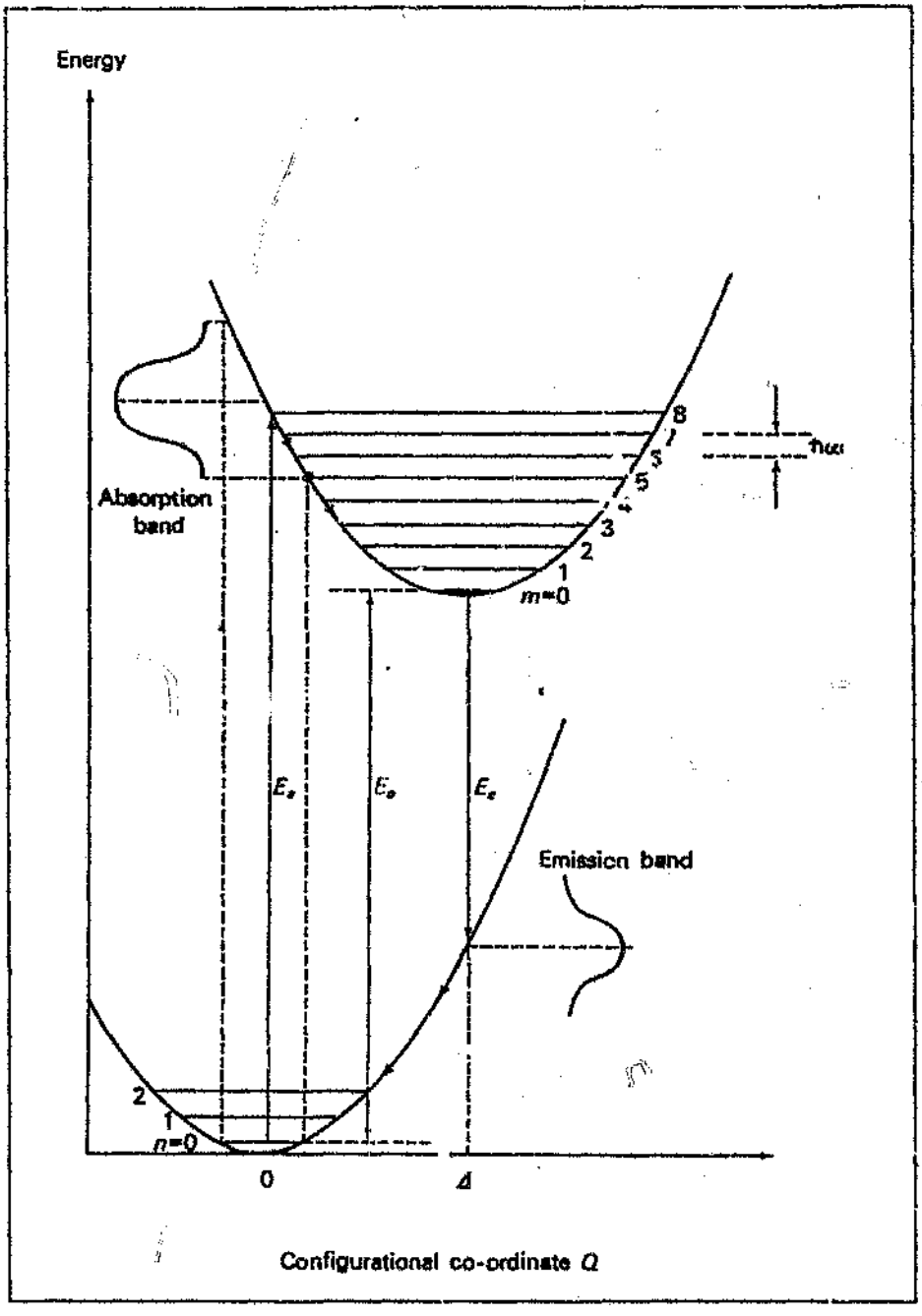

Figure 1.6 Configurational co-ordinate diagram. The parabola represent the ground and excited electronic states. The equilibrium point in the excited state is shifted to a new configurational co-ordinate. As a result, vertical electronic transitions result in an excited vibrational state. (From Henderson (1972).)

oscillator energy levels, n and m respectively. Considering the case for a temperature of 0 K, only the lowest vibrational energy level of the ground state will be populated and all electronic transitions will start at this level. As the time taken for an electronic transition is very small compared to the rate at which the vibrating nuclei are moving, the nuclei involved in the defect can be considered to be static during the transition, giving rise to a vertical transition in the configurational co-ordinate diagram (the Franck-Condon principle) to the vibrational state $m>0$ of the excited electronic state . This means that the configurational co-ordinate, Q, from which the excitation is initiated becomes the extreme lower limit for Q of the excited state vibrational level. In time, the nuclei of the defect in the excited electronic state will rearrange themselves with an equilibrium position of $Q=\Delta$. (The above example describes the situation where the nuclei of the excited state are more widely separated than those of the ground state - usually the case as excited states tend to be more anti-bonding in nature). The transition to the excited state occurs with the absorption of a photon of energy $E_a=E_0+m\hbar\omega$. Once an electronic transition has occurred, the defect will be in the excited vibrational state of the excited electronic state. The vibrational energy will be emitted non-radiatively as m phonons until the $m=0$ vibrational state is reached. The defect will then decay to the ground electronic state radiatively, emitting a photon of energy $E_e = E_0 - n\hbar\omega$. The difference between E_a and E_e is the Stokes shift. Clearly, the higher the number of phonons involved in the absorption transition, the larger the Stokes shift i.e. the stronger the coupling between the electronic and vibrational energies (the electron-phonon coupling). Also, since the probability distribution of the configurational co-ordinate for any vibrational energy level, n, is a Gaussian centred around $Q=0$ (Henderson 1972), the lower the coupling, the greater the probability of a transition involving no phonons (a zero-phonon transition). The above is summed up in the relationship giving the probability of a transition at 0 K involving the excitation of S phonons :

$$P_{0m} = e^{-S}S^m/m!$$

where S is also called the Huang-Rhys constant and is an indicator of both the degree of coupling (large S, large coupling) as well as the probability of a zero-phonon transition (the smaller S, the larger the probability). For large S, the absorption or emission band becomes Gaussian, centred about $S=m$.

The above discussion has involved some severe simplifications :
The temperature was confined to 0 K, and coupling to only one vibrational mode was considered. The effect of increased temperature is that the $n>0$ energy levels become increasingly populated according to the Boltzmann distribution. The reduced population in the $n=0$ (and $m=0$ in the excited state) vibrational level reduces the zero-phonon line (ZPL) intensity for absorption (and emission) (which is one of the reasons for doing measurements at low temperatures). Similarly, the width of the absorption or emission band, while remaining around $S=m$, broadens with temperature.

The effect of considering coupling to additional vibrational modes is to broaden all the phonon assisted transitions, while leaving the ZPL unchanged. It is this feature that results in the characteristic shape of vibronic lines in diamond measured at low temperatures where a sharp ZPL can be seen with a series of broader phonon sidebands. It is this, too, which makes the ZPLs so suitable for using as a probe of the environment of the absorbing or luminescing defect - its sharpness allows the discernment of splitting in uniaxial stress fields (e.g. Davies and Hamer 1976), and analysis of the line shape (e.g. Davies 1970(a)).

In this work, the 1.945 eV centre was chosen for analysis of the lineshape. Uniaxial stress measurements have been made on the 1.945 eV vibronic centre by Davies and Hamer (1976). They were able to conclude that the absorption band due to the centre is the result of an A_1 to E transition at a trigonal centre. Small differences between the absorption and emission spectra were shown to be consistent with a substitutional nitrogen, vacancy pair (which is supported by the results of annealing studies).

involved in this conversion, results in a volume of high stress. As the thermal expansion of diamond is particularly low compared to that of the included solvent/catalyst materials, the faster rate of thermal expansion of the inclusions also exacerbates the build up of internal stress during heating of the diamond.

In synthetic abrasive diamond products, the effects of this process are seen as a reduction in the grit strength, while in similar heat treatment of natural diamond (which contain no metallic solvent/catalyst), an increase in strength occurs, probably as result of annealing out of internal strains (Field 1992). As the end use for such diamond products usually requires a high temperature step in the manufacture of abrasive tools, this "thermal degradation" is of considerable commercial importance.

1.12 Plastic Deformation of Diamond and the Creation of Point Defects

Diamond, despite its extreme hardness, undergoes plastic deformation at temperatures in excess of about 1000 °C when indented by a conical indenter made of softer material than diamond (cubic boron nitride) . The temperature at which plastic flow is observed depends on the diamond type under scrutiny: 750 °C for synthetic, 950 °C for type Ia and 1100 °C for type IIa (Brookes et al 1990). Plastic deformation occurs via dislocation movement, which, in cases of non-conservative dislocation movement gives rise to the creation of vacancies. It was shown (Brookes et al 1993) that slip traces created during plastic deformation on synthetic type Ib and natural type IaA were decorated by 575 nm and band A (not to be confused with the A nitrogen defect), and H3 cathodoluminescence respectively. At the temperatures under which plastic deformation is generated using the soft indenter technique, vacancies generated during plastic deformation are mobile and will diffuse until they are trapped at impurities in the lattice giving rise to the luminescent defects observed. The defect responsible for the 575 nm cathodoluminescence is nitrogen in a split interstitial form plus a vacancy (Zaitsev 1991), band A luminescence is attributed to dislocations, H3 is the result of a vacancy plus an A centre (predominant in type IaA). Photoluminescence measurements confirmed the presence of the 1.945 eV luminescence due to the N-V defect that one might expect to be formed as a

consequence of the creation of vacancies in synthetic diamond. The H3 luminescence displayed considerably broadened ZPLs. (Unfortunately, no comment on the breadth of the 1.945 eV ZPL was made.)

Earlier, Evans et al (1984) showed that natural diamond compacts sintered at temperatures increasing from 1300 °C showed increasing H3 photoluminescence, while synthetic diamond compacts showed 1.945 eV and 575 nm photoluminescence increasing to about 1500 °C and then decreasing, while the H3 photoluminescence increased until 1800 °C, when the other two luminescence types had virtually disappeared. The authors explained the results in terms of the creation of vacancies by the plastic deformation which occurs during sintering, and their subsequent trapping by the predominant point defects (A centres in the natural diamond, and substitutional nitrogen in the synthetic diamond). At temperatures above 1300 °C, the single substitutional nitrogen was believed to diffuse by the vacancy enhanced mechanism (as N-V pairs) and to combine with other nitrogen atoms to form H3.

1.13 Line Broadening

The luminescence ZPLs of defect centres are always observed to be broadened from the ideal single energy transition. The major reasons for this may include lifetime broadening, quadratic electron-phonon coupling effects and inhomogeneous broadening due to strain and electric fields and field gradients due to defects. In the diamond lattice inhomogeneous strain broadening dominates (Davies 1977(a)). As the phonon energy distribution is a function of temperature, any electron-phonon coupling is expected to be temperature dependent. For a variety of colour centres in diamond, it has been shown that broadening due to electron-phonon coupling is negligible below 80 K (Davies 1974)

Inhomogeneous strain broadening of optical ZPLs arises because in each measurement, very many emitting optical centres contribute to the overall signal that gives rise to the optical line. As the lattice site of each of these many centres is in a different environment determined by the cumulative effect of the surrounding defects

The following table (table 1.6), extracted from Davies (1981), gives pertinent data concerning the three vibronic systems encountered in this study.

Table 1.6

ZPL Energy	Point Group	Structure	S	$\hbar\omega$
1.945 eV	C_{3v}	N-V	3.73	65 meV
2.463 eV	C_{2v}	N-V-N	2.9	40 meV
2.156 eV	C_{2v}*	N_i-V	~2	75 meV

Pertinent data concerning the three centres which dominate photoluminescence spectra of synthetic diamond (Davies 1981, *Zaitsev et al 1991).

1.10 Point Defects in Diamond

1.10.1 Overview

A vast amount of research effort in the area of the optical properties of diamond has been spent in unravelling the mechanisms of formation of the more common point defects found. Central to the origin of many complex defects is aggregation of various simpler point defects. Nitrogen was identified as early as 1959 as being the major source of impurity in type I diamond (Kaiser and Bond 1959). Consequently the major components in many defects in diamond are nitrogen and the vacancy.

Some of the simpler examples are listed in table 1.7 below :

Table 1.7

[illegible]	[illegible]	[illegible]
[illegible]	Neutral vacancy	Dominant in IIa *
[illegible]	Negative vacancy	Dominant in Ib*
[illegible] centre	Substitutional N	Type Ib

[illegible] of the simpler point defects found in diamond. [illegible] introduced into specimens for study by irradiation.

Some complex examples are given in table 1.8 below :

Table 1.8

[illegible]	[illegible]	[illegible]
A centre	N-N	Occurs in Ia
B centre	N N-V-N N	Occurs in Ia
N3 centre	N V-N N	Formed under the same conditons as B centres

Some more complex defects found in diamond.

1.10.3 Aggregation of Point Defects

Examples of some of the simple aggregation processes are listed in table 1.9 below.

Table 1.9

[illegible]	Aggregation Product
[illegible] + C centre	A centre (N-N)
[illegible] + Vacancy	H3 (N-V-N)
[illegible] + Vacancy	1.945 eV centre (N-V)
[illegible] + Vacancy	H4
Three Nitrogens and a vacancy	N3
Aggregation of carbon interstitials	Platelets*

Defects in diamond resulting from aggregation processes.
**** The platelets produced are extended defects rather than point defects.***

A summary of the model for aggregation taken from Woods (1986) is as follows

Nitrogen is incorporated in single substitutional form (as in synthetics) - at sufficiently high temperatures these aggregate to form A centres - at higher temperatures, B centres and some N3 centres are formed, the vacancies required for the process being formed simultaneously with interstitial carbon which is believed to aggregate to form platelets (large defects of the order of tens of nanometres to micrometers). Platelets, in turn can degrade by combining with vacancies, leaving only dislocation loops.

A more detailed discussion of the defects important to this work follows in the sections below.

1.10.3 Single Substitutional Nitrogen

Synthetic diamond, unless specific steps are taken to exclude nitrogen (Dyer et al 1956), are yellow in colour, due to the presence of single substitutional nitrogen (Chrenko et al 1971). This nitrogen is the origin of the C centre, which gives rise to a characteristic EPR signal, an absorption in the one-phonon region of the infrared spectrum, and the blue absorption due to electron transitions between the nitrogen donor and the conduction band which gives rise to the typical yellow colouration mentioned above.

1.10.4 Neutral Vacancy

The optical centre with ZPL = 1.673 eV (the GR1 band resulting from radiation damage) is attributed to the neutral vacancy (Walker 1979). Irradiation is frequently used to generate a high concentration of vacancies. The carbon interstitials produced at the same time are highly mobile at relatively low temperatures (>50 K (Davies et al 1992)) and remove some of the vacancies formed by recombination. The vacancy becomes mobile at approximately 500 °C, and at temperatures above this is trapped at various forms of nitrogen or precipitates at internal surfaces (such as dislocations etc.) or external surfaces. In synthetic diamond with its abundance of substitutional nitrogen which can act as an electron donor, the preferred form of the vacancy is in the negatively charged form (optical centre ND1 with ZPL = 3.510 eV). It has been shown that only the neutral form is mobile and that the activation energy for migration of the vacancy is 2.3±0.3 eV (Davies and Collins 1993).

Vacancies can also be thermally created. In the case of diamond, however, the vacancy formation energy of 7.2 eV (Bernholc et al 1992) makes the temperatures required for vacancy formation very high. In an experiment designed to evaluate the efficiency of thermal vacancy creation, heat treatment at 1800 °C for 30 minutes failed to create any detectable luminescence from the

centres expected to have formed if vacancies had been created (Evans et al 1984).

Vacancies are also produced as result of plastic deformation by interaction between moving dislocations and by non-conservative dislocation movement. The numbers involved become appreciable in the case of diamond sintered at high pressures and temperatures, as, for example in the manufacture of sintered polycrystalline diamond products (Davey et al 1984). The photoluminescence due to vacancy related optical centres was observed to increase as a function of increasing temperature and pressure, and decreasing size of the diamond grains involved. This observation was explained by the authors as resulting from an increased volume fraction of plastically deformed diamond being formed in the sintering process. The number of vacancies created by sintering was calculated at approximately 10^{15} cm^{3} (Dodge 1986).

1.10.5 The 1.945 eV Centre

This vibronic optical centre is usually referred to by the energy of its ZPL. It can be observed in absorption and photoluminescence, but not in cathodoluminescence. The centre displays trigonal symmetry (Walker 1979). Davies and Hamer (1976) concluded that the 1.945 eV centre, which is the dominant end product of annealing radiation damage in diamonds containing substitutional nitrogen, is either substitutional nitrogen plus a vacancy, or nitrogen plus interstitial nitrogen. The nitrogen-vacancy pair model was confirmed by ESR work of Loubser and van Wyk (1977). The 1.945 eV centre may be summarised as N + V giving rise to N-V.

1.10.6 The H3 Centre

This is one of the so-called H lines (Walker 1979), vibronic ZPLs that were first noted as resulting from heat treatment following irradiation of diamonds. (This illustrates some of the problems associated with this system of systematic

nomenclature, as this centre also arises in untreated synthetic diamonds.) It has a ZPL at 2.463 eV.

This defect is the end product of annealing radiation damage in diamonds containing A centres (Davies 1972). Its properties are reviewed by Davies (1977(b)). It can be observed in absorption, photoluminescence and cathodoluminescence, emitting bright green light in luminescence. Uniaxial stress and polarisation studies show the centre to display C_{2v} symmetry and a forbidden transition appears under uniaxial stress. This latter factor results in a difference between the shape of the absorption and luminescence bands. The C_{2v} symmetry means that one of the nitrogen atoms in the A centre exchanges places with the vacancy when it is trapped at an A centre ; i.e. the H3 centre, formed from N-N + V, rearranges to become N-V-N.

Although associated with annealed radiation damage in diamonds containing A centres, H3 is also found in unirradiated diamond, being associated with slip traces, dislocations and platelets (Hanley et al 1977), and in plastically deformed type Ia diamond (Brookes et al 1993), and in as-grown synthetics (e.g. Collins 1991).

Different mechanisms are proposed for the origin of this defect in natural and HPHT synthetic diamond. In natural diamonds, the defect was shown to arise from the trapping of radiation products (vacancies) by A centres (substitutional nitrogen pairs) together with the simultaneous formation of H4 from B centres by the same mechanism (Davies 1972). Nitrogen pairs, however, are rare in synthetic diamonds unless they have been exposed to high temperatures (1600 to 2000 °C - requiring the use of pressures in the diamond stable region in order to prevent graphitisation) for relatively long periods (Chrenko et al 1977), or annealed at 1500 °C after radiation damage (Collins 1980). The rate of aggregation of substitutional nitrogen was calculated to be increased by about 50 times by the creation of approximately 5 ppm of vacancies. This enhancement was explained in terms of the creation of the N-V centre (1.945

eV), which moves rapidly through the lattice at elevated temperatures, combining with a substitutional nitrogen to form N-V-N (H3), which is unstable at high temperatures and decomposes to form a substitutional nitrogen pair (A centre) and a vacancy. The vacancy is thus made available to form another N-V centre allowing the process to be repeated ad infinitum. Apart from aggregation of nitrogen to form A centres after synthesis, A centres may be formed during growth, providing sufficiently high temperatures (1350 to 1500 °C) are experienced. A report by Vins et al (1991) noted A centres appearing at growth temperatures above 1430 °C, and increasing with growth temperature, until all nitrogen is in the form of A centres at a growth temperature of 1740 °C. In tests in which synthetic type Ib diamond was subjected to similar temperatures and pressures, no aggregation was observed until temperatures of 1600 °C. They conclude that A centres formed during growth at temperatures below 1600 °C are the result of these centres being grown-in, while at temperatures above 1600 °C, aggregation begins to occur as well. An Arrhenius activation energy for the incorporation of A centres during growth was calculated at 2.8±0.3 eV (Vins et al 1991). The activation energy given by Chrenko (Chrenko et al 1977) appears too low to be consistent with the above findings, and the author suggest that the value of 3.6 eV given by Klyuev et al (1982) is more appropriate.

Despite the unlikely conditions required for forming H3 by aggregation in synthetic diamond, H3 is ubiquitous in synthetic diamond, where it is usually confined to the {100} growth sectors and its luminescence displays polarisation parallel to the <110> vectors lying within the growth plane (Burns et al 1990). This phenomenon has been explained by Dodge (1986) as resulting from the defect being "grown in" during synthesis.

The presence of H3 thus either indicates the simultaneous presence of the A defect and vacancies, or to HPHT synthesis as the origin of the diamond. As vacancies may arise from irradiation or plastic deformation, the presence of H3

in unirradiated natural diamond is quoted as evidence of plastic deformation (Evans et al 1984).

1.10.7 The 575 nm Centre

Zaitsev et al (1991) have proposed a structure consisting of a vacancy together with nitrogen in a split interstitial site for this defect. This defect can be created in all diamonds by irradiation followed by annealing (Walker 1979), or as result of plastic deformation. An elegant demonstration of the association of the formation of the 575 nm defect and slip is seen in the cathodoluminescence images of type Ib diamond surfaces indented by a soft indenter at high temperatures (Brookes et al 1990). Very striking photographs of the same phenomenon in polished sections of large De Beers synthetic diamonds appear in Ponahlo (1992). These orange red needles oriented in <110> are associated by the author with a broad cathodoluminescence band at 820 nm; however, the 575 nm ZPL can be clearly seen in the spectra. Diamond which has undergone severe plastic deformation during sintering displays high intensities of 575 nm photoluminescence (Davey et al 1984).

A feature of this defect is that it is readily detected in cathodoluminescence, but far less readily in photoluminescence.

1.11 Heat Treatment of Synthetic Diamond

In the presence of included solvent/metal catalyst and in the absence of high pressures to stabilise the diamond phase, heat treatment results in the "reverse synthesis" reaction - the conversion of diamond to graphite. This phenomenon has been studied by Evans (1992) for metal films on diamond surfaces under UHV and displayed a very rapid onset at temperatures above 750 °C (whereas un-catalysed graphitisation of diamond in UHV occurs at much higher temperatures of 1500 to 1900 °C). The catalytic graphitisation of diamond in the presence of internal metallic solvent/catalysts was also observed by Woods (1971). The large volume expansion

consequence of the creation of vacancies in synthetic diamond. The H3 luminescence displayed considerably broadened ZPLs. (Unfortunately, no comment on the breadth of the 1.945 eV ZPL was made.)

Earlier, Evans et al (1984) showed that natural diamond compacts sintered at temperatures increasing from 1300 °C showed increasing H3 photoluminescence, while synthetic diamond compacts showed 1.945 eV and 575 nm photoluminescence increasing to about 1500 °C and then decreasing, while the H3 photoluminescence increased until 1800 °C, when the other two luminescence types had virtually disappeared. The authors explained the results in terms of the creation of vacancies by the plastic deformation which occurs during sintering, and their subsequent trapping by the predominant point defects (A centres in the natural diamond, and substitutional nitrogen in the synthetic diamond). At temperatures above 1300 °C, the single substitutional nitrogen was believed to diffuse by the vacancy enhanced mechanism (as N-V pairs) and to combine with other nitrogen atoms to form H3.

1.13 Line Broadening

The luminescence ZPLs of defect centres are always observed to be broadened from the ideal single energy transition. The major reasons for this may include lifetime broadening, quadratic electron-phonon coupling effects and inhomogeneous broadening due to strain and electric fields and field gradients due to defects. In the diamond lattice inhomogeneous strain broadening dominates (Davies 1977(a)). As the phonon energy distribution is a function of temperature, any electron-phonon coupling is expected to be temperature dependent. For a variety of colour centres in diamond, it has been shown that broadening due to electron-phonon coupling is negligible below 80 K (Davies 1974)

Inhomogeneous strain broadening of optical ZPLs arises because in each measurement, very many emitting optical centres contribute to the overall signal that gives rise to the optical line. As the lattice site of each of these many centres is in a different environment determined by the cumulative effect of the surrounding defects

in the lattice, the energy of the transition being observed at each of these optical centres is perturbed to a different degree, resulting in a spread of energies for that transition. In the case of strain broadening, the lattice at the site of each of the many optical centres experiences a strain. This is the sum of the strain introduced into the lattice by all other sources of strain such as point defects (primarily substitutional nitrogen in the case of synthetic diamond), which have relatively short range strain fields, and dislocations (the strain fields of which decay much more slowly with distance). The net result of this statistical distribution of strain inducing defects and optical centres is a broadening of the optical line.

Stoneham (1969), shows theoretically that the origin of strain broadening has an effect on the lineshapes of the broadened lines. Dislocations give rise to Gaussian lineshapes for the broadened lines, while broadening by point defects gives rise to a Lorentzian lineshape. For example, inhomogeneous strain broadening arising from randomly distributed halide ion impurities in sodium chloride crystals results in a Lorentzian contribution to the strain lineshape (arising from broadening by dislocations) of the zero phonon lines in the pure crystal (Hughes 1968). In a study of lineshapes of zero-phonon lines in diamond, many lineshapes were found to have a Lorentzian : Gaussian ratio of 0.5 (Davies 1970(a)). The lineshapes were explained as arising out of the strain field due to the nitrogen impurity present.

Stoneham (1969) used a statistical approach to derive the form of the line broadening :

The assumptions for the case of strain broadening used were :

1) Only first order terms of the strain perturbation were considered.

This allows us to write the transition energy as

$$\hbar\omega = \hbar\omega_0 + \hbar\omega_1 e \qquad \ldots 2$$

where strain, ε is

$$\varepsilon = \sum_{ij} (a_{ij} e_{ij}) \qquad \ldots 3$$

(e is the strain tensor, $\hbar\omega_1 a_{ij}$ is the coupling coefficient where the a_{ij} is determined mainly by symmetry).

Since the lineshape, which is equal to the distribution of $\hbar\omega$, is equivalent to the distribution of ε, the problem of solving for the lineshape reduces to one of solving for the distribution of ε, or determining the probability of ε lying between ε and ε+dε. This can be seen in the following way :

Noting from equation 2 that,

$$\varepsilon = \hbar(\omega - \omega_0)/\omega_1 \qquad \ldots 4$$

$$I_{obs}[\hbar(\omega-\omega_0)] = I[\varepsilon = (\omega - \omega_0)/\omega_1] \qquad \ldots 5$$

Note that the inside of the brackets on the right hand side of 5) is simply the inside of the brackets on the left hand side divided by $\hbar\omega_1$, i.e. the intensity distribution is simply the stress distribution scaled by a constant.

Since the 1.945 eV line splits under stress (Davies and Hamer, 1976), the A_1 component has transition energy

$$\hbar\omega_1 = \hbar\omega_0 + \hbar\omega_1\beta_1\varepsilon \qquad \ldots 6$$

and a fraction $f_1(\varepsilon)$ of the total intensity.

where strain, ε is

$$\varepsilon = \Sigma_{ij} (e_{ij} e_{ij}) \qquad \ldots 3$$

(e is the strain tensor, $\hbar\omega_1 a_{ij}$ is the coupling coefficient where the a_{ij} is determined mainly by symmetry).

Since the lineshape, which is equal to the distribution of $\hbar\omega_1$ is equivalent to the distribution of ε, the problem of solving for the lineshape reduces to one of solving for the distribution of ε, or determining the probability of ε lying between ε and ε+dε. This can be seen in the following way :

Noting from equation 2 that,

$$\varepsilon = \hbar(\omega - \omega_0)/\omega_1 \qquad \ldots 4$$

$$I_{\omega_1}[\hbar(\omega - \omega_0)] = I[\varepsilon = (\omega - \omega_0)/\omega_1] \qquad \ldots 5$$

Note that the inside of the brackets on the right hand side of 5) is simply the inside of the brackets on the left hand side divided by $\hbar\omega_1$, i.e. the intensity distribution is simply the stress distribution scaled by a constant.

Since the 1.945 eV line splits under stress (Davies and Hamer, 1976), the *n*th component has transition energy

$$\hbar\omega_1 = \hbar\omega_0 + \hbar\omega_1\beta_1\varepsilon \qquad \ldots 6$$

and a fraction $f_1(\varepsilon)$ of the total intensity.

And since from equation 5,

$$\varepsilon = h(\omega - \omega_0)/\omega_1 \qquad ...7$$

the intensity resulting from all components at ω is

$$I_{obs}[h(\omega - \omega_0)] = \Sigma f_i[(\omega - \omega_0)/\omega_1\beta_i]I[(\omega - \omega_0)/\omega_1\beta_i]$$

2) **The contributions of all the defects to the strain, ε, add linearly.** i.e. linear elasticity is assumed, and this is generally true for strains $<10^{-2}$.

i.e. if Z_i gives the position and any relevant variables of the ith defect, then

$$\varepsilon(Z_1, Z_2, ..., Z_N) = \Sigma^N_{i=1}\varepsilon(Z_i) \qquad ...8$$

3) **The defects which cause broadening are not correlated with one another.**

This has the consequence that $P(Z_1, Z_2 ... Z_N)$, the probability of finding a particular configuration of defects$\{Z_1, Z_2, ... Z_N\}$, can be factorised :

$$P(Z_1, ... Z_N) = p(Z_1)p(Z_2)...p(Z_N) \qquad ...9$$

where $p(Z_i)$ are the probabilities of finding the individual defects with position and internal variables as given by Z_i.

This can only be approximately true and holds in the case of low concentrations of defects only. It can be shown from the above that, in the case of $I(\varepsilon)$ symmetric about $\varepsilon = 0$,

$$I(\varepsilon) = 1/\pi \int_{-\infty}^{\infty} dx \cos(x\varepsilon) \exp[-pJ(x)] \qquad ..10$$

where

$$J(x) = \int dz p(z)\{1 - \cos[x\varepsilon(Z)]\} \qquad ..11$$

and $p = N/v$, the density of defects giving rise to the strain.

In the case of two defect types, it can be shown (Stoneham 1969) that the line shape is simply the convolution of the lineshape when species A alone causes broadening and the lineshape when B alone causes the broadening.

Since point defects and dislocations have different functions for their strain fields (ε is proportional to $1/r$ for dislocations (Stoneham 1969), and ε is proportional to $1/r^2$ for point defects (Hughes 1968)) the resultant effect on the lineshape is different, with dislocations yielding Gaussian lineshapes, and point defects yielding Lorentzian lineshapes. Of course, when both point defects and dislocations are present, the final lineshape is a convolution of Lorentzian and Gaussian, i.e. a Voigt function (Posener 1959).

In physical terms, it is expected that lineshapes of crystals with high concentrations of point defects would be Lorentzian, becoming Gaussian as the concentration is reduced, leaving only the effect of dislocations. This has been experimentally observed, for example by Hughes (1968) in the case of the ZPL of the N1 colour centre in Br-doped NaCl crystals.

In the case of high concentrations of point defects however, Davies (1971) shows that account has to be taken of the nature of crystal lattices. If a defect is closer

than a minimum distance, say *d*, from an emitting optical centre, the defect and the centre will combine to form a new optical centre. Thus the probability of finding a defect is not the same everywhere, since, for distances smaller than *d* from the emitting optical centres the probability becomes zero. Davies (1971) shows that the consequence of this for the lineshape is that a Gaussian contribution to the lineshape is observed, instead of the Lorentzian contribution to the lineshape predicted for point defects. This effect can be qualitatively explained as follows: The effect of the absence of defects closer to an emitting optical centre than *d* is seen as fewer of the large perturbations to which such nearby defects would give rise i.e. a decreased intensity in the wings of the line which results in a more Gaussian lineshape. Any changes to lineshape will naturally be less marked at low concentrations of defects, since the probability of finding a defect closer than *d* to an emitting optical centre will be small anyway, so the effect is only observed for high concentrations of defects. Davies (1970(b)) demonstrated this "near neighbour" effect in the case of the H3 centre in natural diamond with concentrations of nitrogen defects of the order 0.1 atomic %, and calculated a value for *d* of 0.85±0.2 nm. The effect is predicted to be more marked at high concentrations with defects that have low stress fields, and for cases where the optical centre and defect are such that *d* would be large (Davies (1970(a)).

This "near neighbour" effect has been explicitly addressed by Orth et al (1993) who developed a treatment of inhomogeneous broadening by point defects which takes the discrete lattice into account. Their work confirms the applicability, in the case of low defect densities, of the Stoneham (1969) elastic continuum analysis which predicts Lorentzian lineshapes for inhomogeneous broadening by point defects. In the case of high defect densities, the findings of Davies (1970(a)) that a Gaussian lineshape is obtained are also confirmed.

2. EXPERIMENTAL

2.1 Apparatus

2.1.1 Overview

The photoluminescence apparatus is schematically illustrated in figures 2.1 and 2.2 (90° arrangement) and figures 2.3 and 2.4 (180° arrangement).

2.1.2 Laser

A Spectra Physics 171 or Spectra Physics 2020 argon-ion laser was operated in the light intensity controlled mode, ensuring a consistent output power during an experiment. Nominal power outputs of 400 to 600 mW were used (based on the output power gauge of the Spectra Physics 2020 laser).

Unwanted plasma lines were minimised by first passing the laser beam through a prism and collecting the main component onto a slit, and later passing the beam through an Anaspec 300-S continuously tuneable laser filter monochromator. A quarter wave plate was used to convert the plane polarised laser light to circularly polarised light.

2.1.3 Optics

The laser beam was guided to the sample situated in a cryostat using various mirror assemblies. Two different geometries were used for the optical arrangement: in the 90° arrangement, the emitted radiation was collected through the cryostat window at 90° to the incident laser beam, the axis of the collected light making a low angle with the front of the sample; in the 180° (or "backscatter") arrangement, the incident laser beam was guided by means of a tiny mirror placed between the collecting lens and the cryostat onto the face of

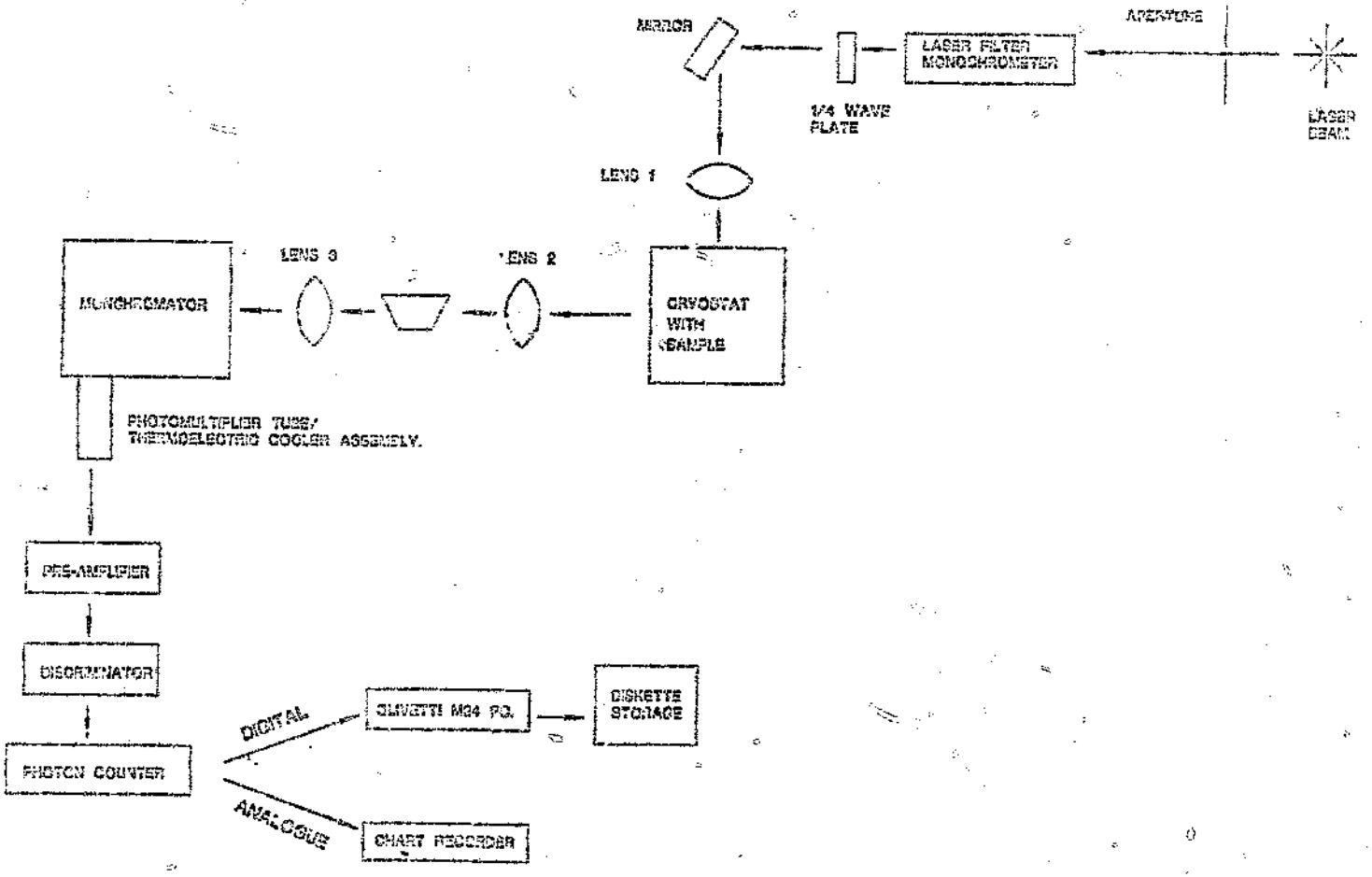

Figure 2.1 Block diagram of the experimental photoluminescence set-up (90° arrangement).The individual components are: an argon-ion laser excitation source; the means of removing unwanted plasma lines from the laser beam; a quarter wave plate for translating the linearly polarised laser light into circularly polarised light; optics to focus the laser light onto the sample; a cryostat for maintaining the sample at the correct temperature; optics to collect the emitted luminescence light and to focus it onto the entrance slit of a monochromator; a monochromator; a detector and photon counting apparatus; a personal computer (PC) for data storage on magnetic disk.

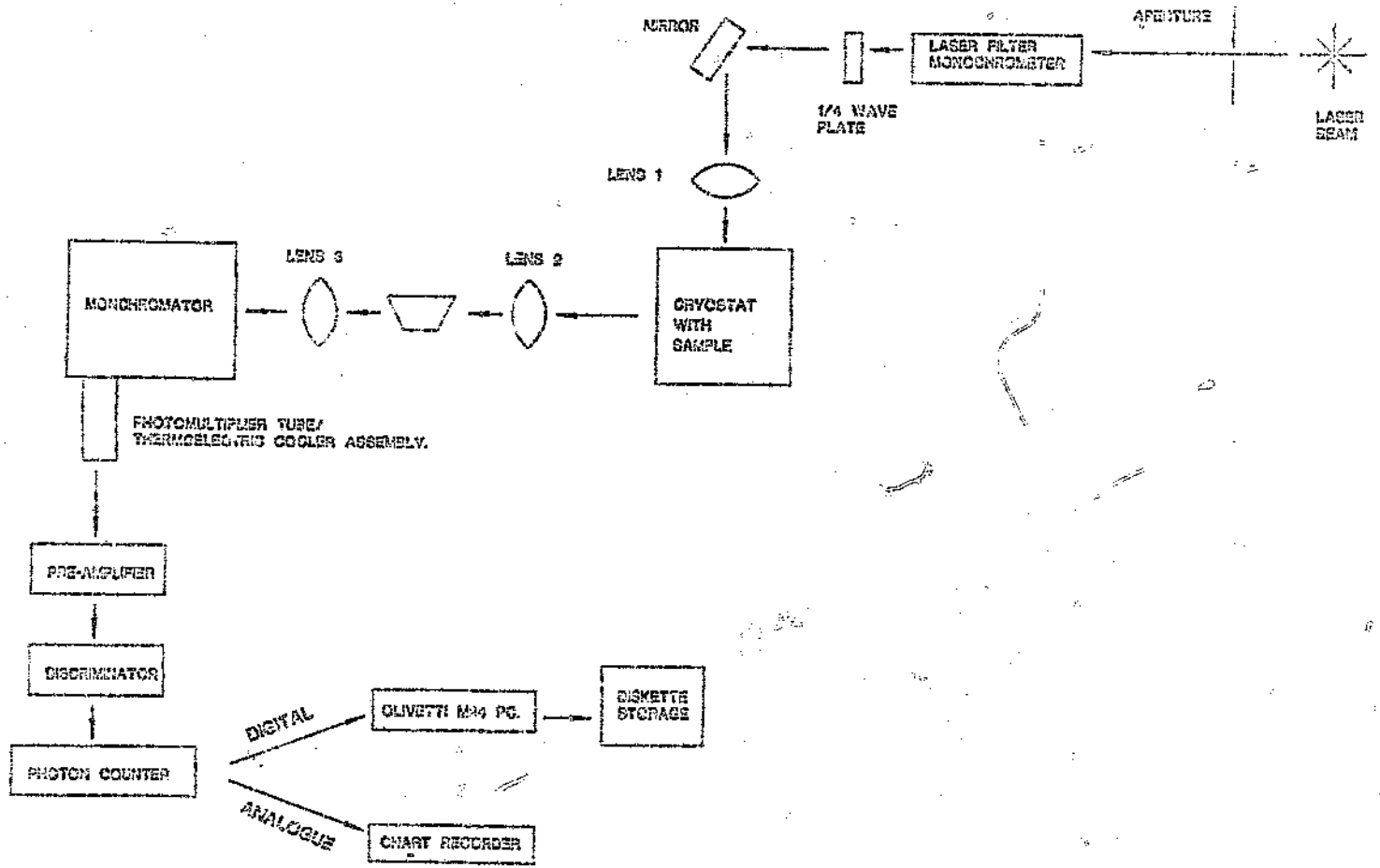

Figure 2.1 Block diagram of the experimental photoluminescence set-up (90° arrangement).The individual components are: an argon-ion laser excitation source; the means of removing unwanted plasma lines from the laser beam; a quarter wave plate for translating the linearly polarised laser light into circularly polarised light; optics to focus the laser light onto the sample; a cryostat for maintaining the sample at the correct temperature; optics to collect the emitted luminescence light and to focus it onto the entrance slit of a monochromator; a monochromator; a detector and photon counting apparatus; a personal computer (PC) for data storage on magnetic disk.

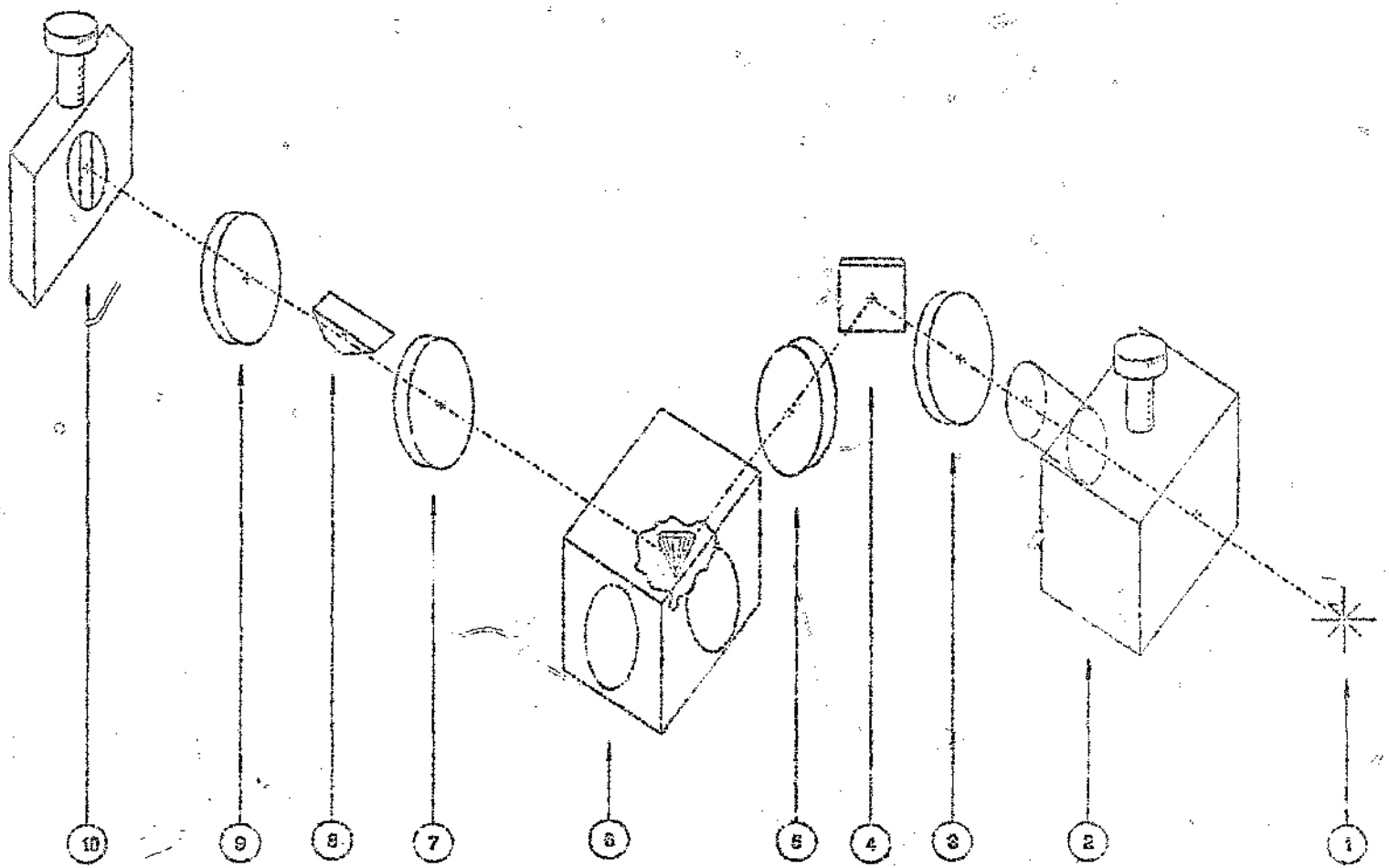

Figure 2.2 Schematic of the experimental photoluminescence set-up (90° arrangement). Laser source 1); laser monochromator 2); 1/4 wave plate 3); mirror 4); 100mm focal length lens 5); cryostat 6); 120mm focal length lens 7); dove prism 8);120mm focal length lens 9); monochromator entrance slit 10).

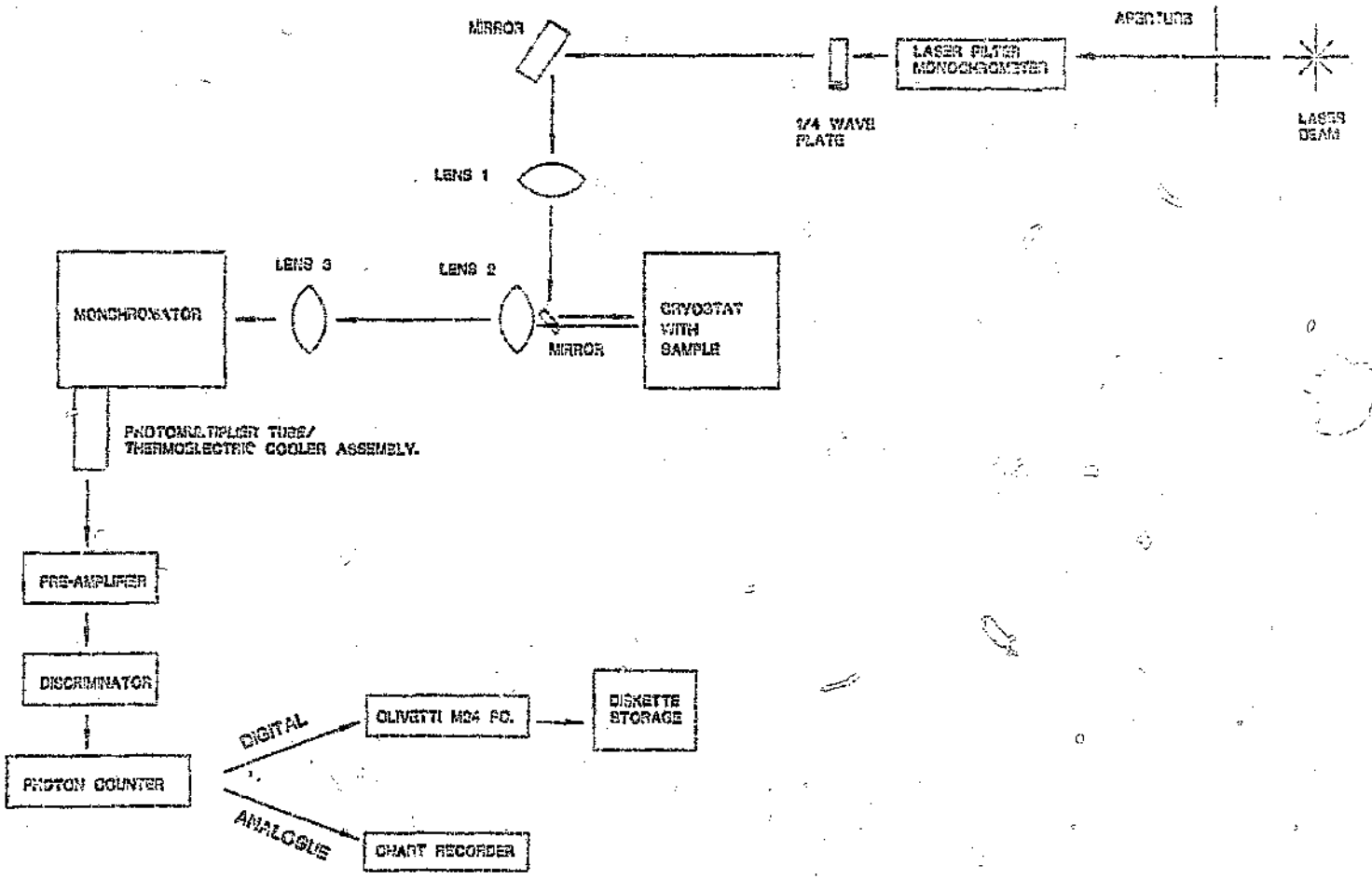

Figure 2.3 Block diagram of the experimental photoluminescence set-up (180° arrangement). The individual components are: an argon-ion laser excitation source; the means of removing unwanted plasma lines from the laser beam; a quarter wave plate for translating the linearly polarised laser light into circularly polarised light; optics to focus the laser light onto the sample; a cryostat for maintaining the sample at the correct temperature; optics to collect the emitted luminescence light and to focus it onto the entrance slit of a monochromator; a monochromator; a detector and photon counting apparatus; a personal computer (PC) for data storage on magnetic disk.

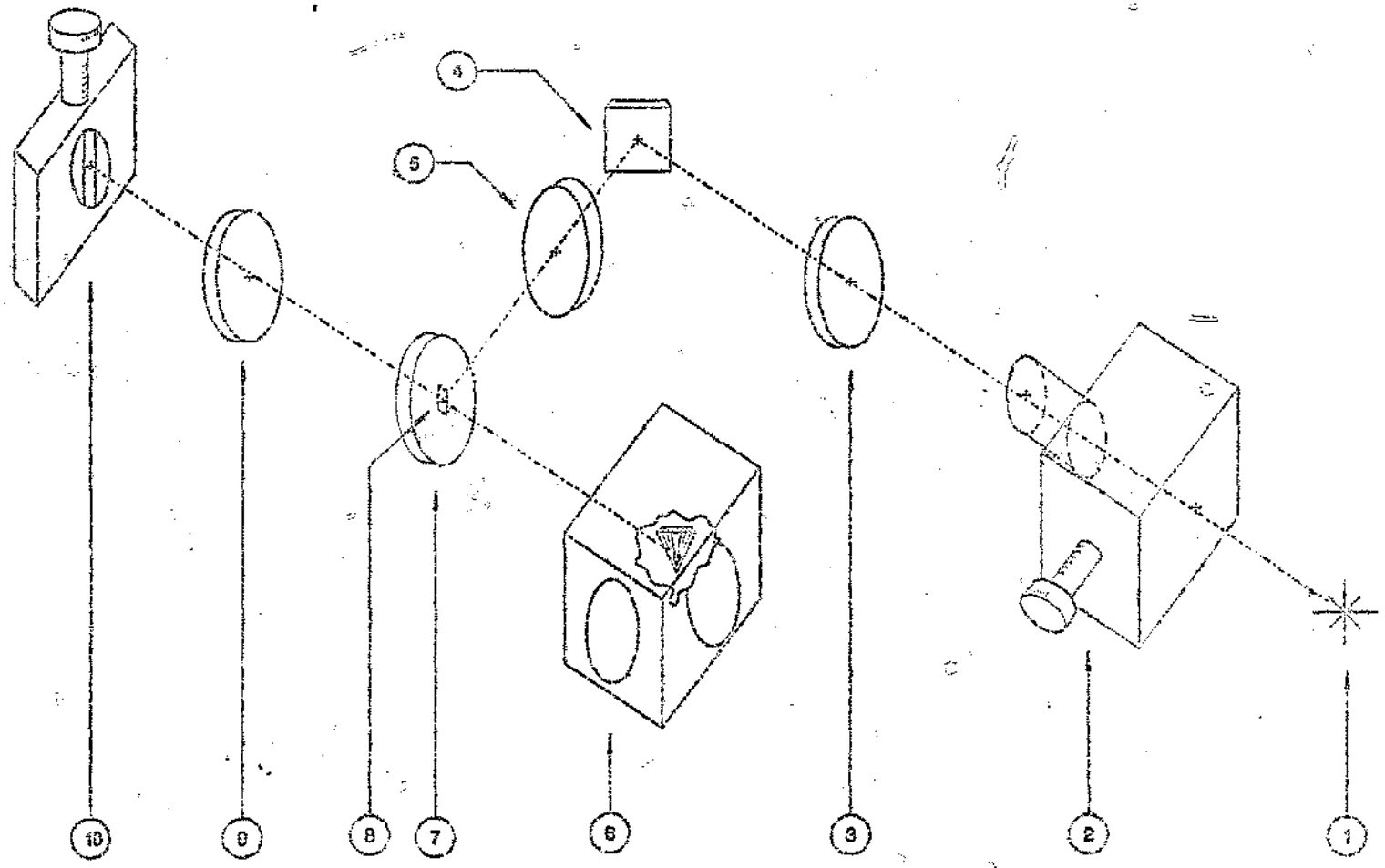

Figure 2.4 Schematic of the experimental photoluminescence set-up (180° arrangement). Laser source 1); laser monochromator 2); 1/4 wave plate 3); mirror 4); 100mm focal length lens 5); cryostat 6); 120mm focal length lens 7); mirror 8); 120mm focal length lens 9); monochromator entrance slit 10).

the sample through the same front window of the cryostat through which the emitted radiation was collected. In either arrangement, the incident beam could be focused onto the sample, using a 100 mm focal length lens. The light emitted from the sample was collected by a 120 mm focal length lens, situated such that the sample was positioned at its focal point. A second 120 mm focal length lens was used to focus the collected light onto the entrance slit of the Jarrell-Ash monochromator (discussed in detail in section 2.1.5). The collection optics resulted in a unit magnification of the sample image at the slit. In some cases, a glancing-angle illumination of the sample was employed, resulting in a line illumination of the sample rather than a spot. In these cases a dove prism was interposed between the two 120 mm lenses in the collection optics. This allowed the image of the illuminated line on the sample face to be rotated through 90° and thus to become aligned with the entrance slit, increasing the collection efficiency. In cases where the laser beam illuminated a spot on the sample surface, this was unnecessary and was usually not employed.

2.1.4 Cryostat

An Oxford Instruments continuous flow cryostat was used. It consisted of a CF1204 cryostat, a TTL200 transfer tube, a VC30 flow controller, a gas flow pump, and an ITC4 temperature controller. Vacuum in the vacuum insulation chamber and vacuum insulation sleeve of the transfer tube was maintained by a turbomolecular pump with a rotary backing pump. As temperatures of 77 K were required, liquid nitrogen was used as the coolant, while helium was used as the exchange gas within the cryostat, to be discussed below.

The continuous gas flow cryostat works as follows: the cryostat has an inner sample chamber which is filled with the exchange gas and into which the sample is suspended by a sample holder rod. The sample chamber is insulated from the ambient environment by a vacuum space between the sample chamber wall and the outer cryostat wall. The windows in the inner sample chamber wall are of silica with indium mounting rings. The outer silica windows are sealed with rubber "o" rings. The portion of the sample chamber wall just above the windows contains a heat exchanger which is cooled by a flow of liquid nitrogen, and which also contains a heater element and a rhodium/iron resistance thermometer, allowing accurate temperature control to be achieved by balancing the heating and cooling actions. The sample holder rod terminates in a massive copper thermal link which contacts the walls of the heat exchanger, and to which the copper sample holder itself is attached. The presence of the exchange gas within the sample chamber assists in heat exchange between the heat exchanger block and the sample, as well as to allow removal of radiation induce heat from the sample face. Evacuation of the outer vacuum chamber and the outer vacuum sleeve of the liquid nitrogen transfer arm ensures good thermal insulation between the cold, inner sample chamber or liquid nitrogen lines and the ambient atmosphere. Typically, a vacuum of $<5x10^{-5}$ Torr is used.

The liquid nitrogen coolant is drawn through the transfer arm from a vacuum dewar through the cryostat cooling circuit by the gas flow pump. The temperature of the heat exchanger block is maintained by a combination of controlling the liquid nitrogen flow rate via a needle valve, and by heating the heat exchanger block via a resistance heater. The ITC4 temperature controller is an intelligent microprocessor-based device which, in the configuration used for these experiments, controls the temperature measured at the heat exchanger block by the Rh/Fe resistance thermometer by adjusting the current supplied to the resistance heater located on the heat exchanger block. Best temperature control was achieved by using the proportional, integral, derivative (PID) control algorithm.

2.1.5 Monochromator

The monochromator used was a Jarrell-Ash C25-100 Czerny-Turner 1 m double grating scanning monochromator. This monochromator consists of two Czerny-Turner spectrometers mounted one above the other. This arrangement provides for an exceptionally good stray light level (at least 10^{-10} at ± 10 Angstroms from the parent line with single line emission).

The double spectrometer arrangement employs two gratings, one per monochromator. The gratings have 1180 gratings per millimeter, resulting in a first order reciprocal linear dispersion of 0.82 nm/mm.

The monochromator has bilateral entrance, exit and intermediate straight edged slits, the former two being independently focusable. The slits are adjustable by means of micrometer screws from 5 μm to 3000 μm and may be tilted for perfect azimuth adjustment. Typical slit width settings of 300 and 100 μm thus results in a nominal bandpass of 0.24 nm and 0.082 nm respectively.

Wavelength scanning between 0 and 16000 Angstroms (with a precision of 1 part in 6000) is achieved by a 12 speed electrical linear scanning drive with manual overdrive. Scanning speeds are selectable in a range from 0.5 to 2500 Angstroms per minute. A direct wavelength readout in Angstroms is provided. A digital encoder was attached to the wavelength drive, allowing for digital recording of the wavelength driven from any selected starting wavelength. This digital data, together with the digital output from the photon counting system (Section 2.1.6) was fed into an Olivetti M24 PC for digital storage and display of recorded spectra.

The operating conditions varied and are discussed in section 2.3 below.

2.1.6 Photon Counting System

The photon counting system used for these experiments consisted of a means of detecting individual photons, in this case a photomultiplier tube (PMT), a pre-amplifier, a discriminator (PAR Model 1121 amplifier/discriminator), a counter (PAR Model 1112 Photon Counter Processor), and some form of data storage such as a chart recorder for analogue output and a personal computer (Olivetti M24 PC) for digital data storage and display. The principle of operation is as follows: a photon, on striking the window of the PMT, causes the emission of photo-electrons. The emitted electron is accelerated through the dynode system of the PMT, creating an avalanche of electrons which gives rise to a current pulse at the output. An anode load resistor and output capacitor convert the current pulse to a voltage pulse. This is pre-amplified and passed on to the pulse height discriminator. The pulse height discriminator rejects pulses below a threshold level (or outside a voltage window with a minimum *and* a maximum threshold) and passes the others on to the photon counter. The photon counter converts the voltage pulses into standardised current pulses which are then passed through an averaging circuit. The count is integrated for a time interval pre-set by the operator by means of a thumb-wheel and then issued as an output signal.

The PMT used was initially an EMI 9863Q, low noise, 14-stage, photomultiplier tube with an S20 spectral response, later replaced with a Burle C31034A-02 photomultiplier tube with a GaAs photocathode (specially selected version with a dark count of 12 counts per second at -20 °C with a 60ER spectral response which is almost constant between 300 and 850 nm (33333 and 11765 cm^{-1})). The virtually constant spectral response between

those energies makes it unnecessary to correct for spectral response when this detector is used within this range.The PMT was thermo-electrically cooled using a Products For Research refrigerated chamber, model TE210RF. The typical dark-count of the Ruple PMT measured by integrating the counts over 10 seconds and dividing the total count by 10 was between 3 and 6 s^{-1}.

The photon counting system described above minimizes the errors in generating an output signal with a magnitude equal to the number of photons striking the PMT in the pre-set integration time (typically 1 second in these experiments but occasionally more).

Samples

2.2.1 Sample Type

The samples used in this study were chosen to represent the extreme range of the properties of commercial synthetic diamond produced by HPHT technology.

Large, single crystals of sizes up to a few mm are grown by the reconstitution technique at slow growth rates to produce very high quality crystals. Three such crystals were included in this study: a crystal of predominantly octahedral morphology; a crystal of cubo-octahedral morphology; and a crystal of predominantly cubic morphology. These crystals were abbreviated Oh, CO, and Cu and can be seen in Figures 2.5, 2.6 and 2.7 respectively.

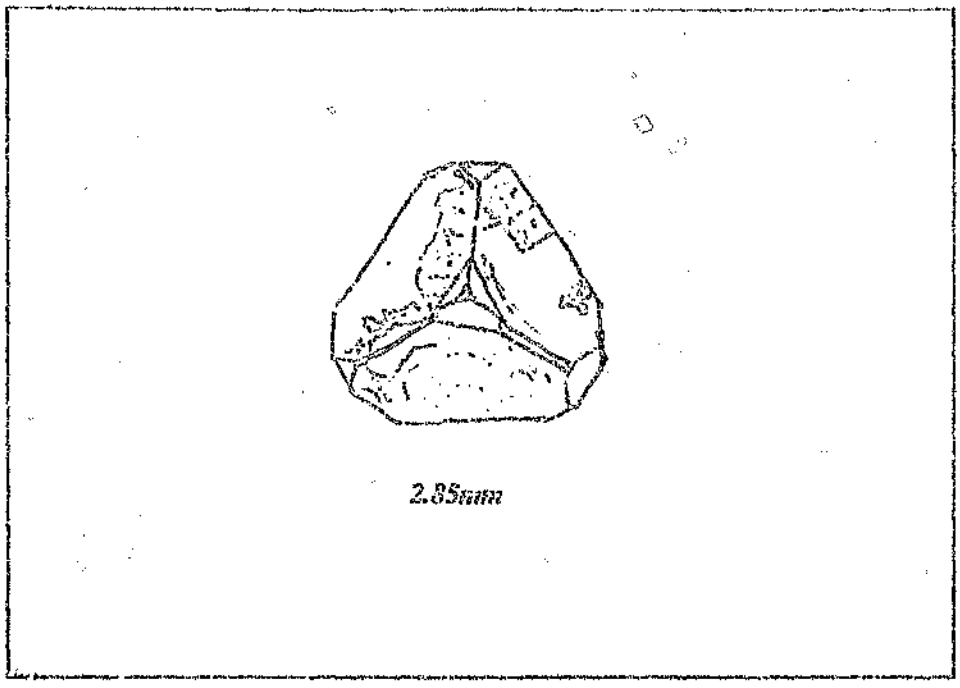

Figure 2.5 Octahedral single crystal, identified as Oh. The face measured is the bottom face in the illustration.

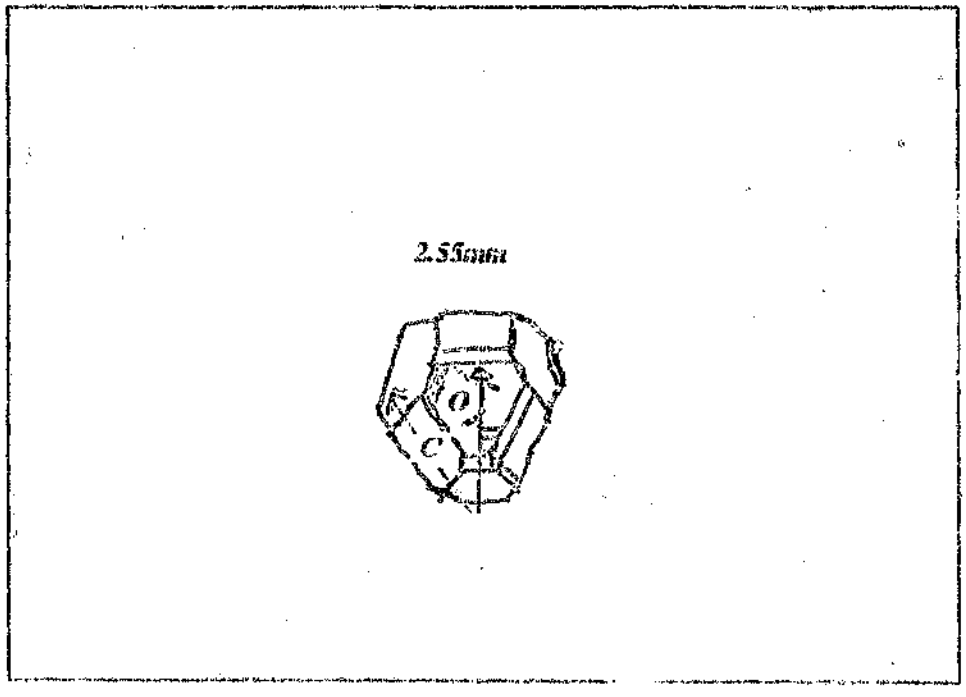

Figure 2.6 Cubo-octahedral single crystal, identified as CO. The {100} and {111} faces measured are marked as "C" and "O" respectively.

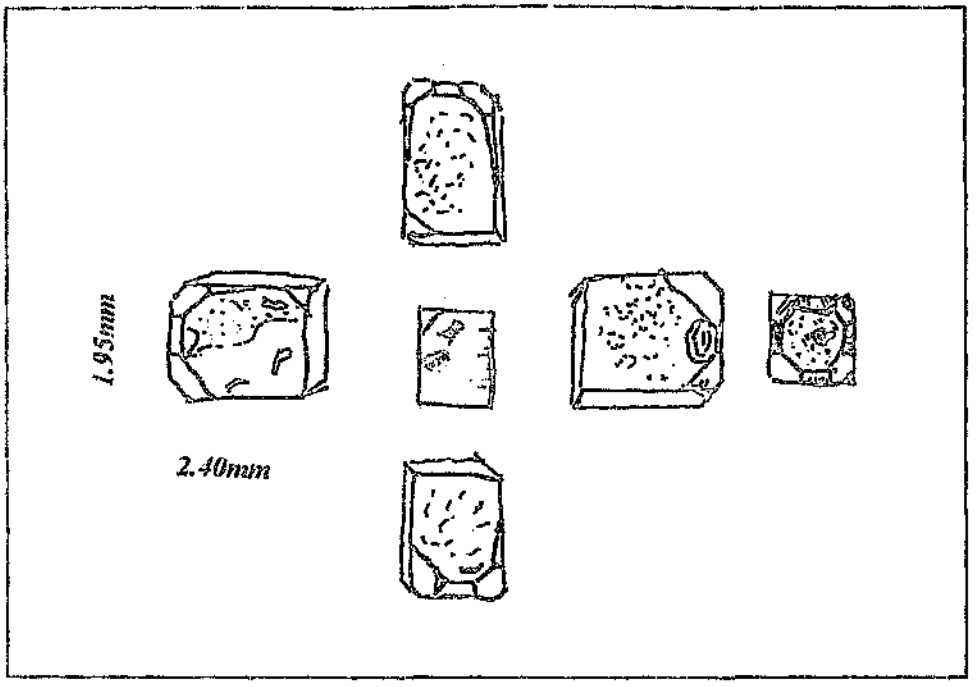

Figure 2.7 Cubic single crystal, identified as Cu. The face depicted in the centre was the face chosen for measurement. Notice the two metal inclusions in the centre of this face.

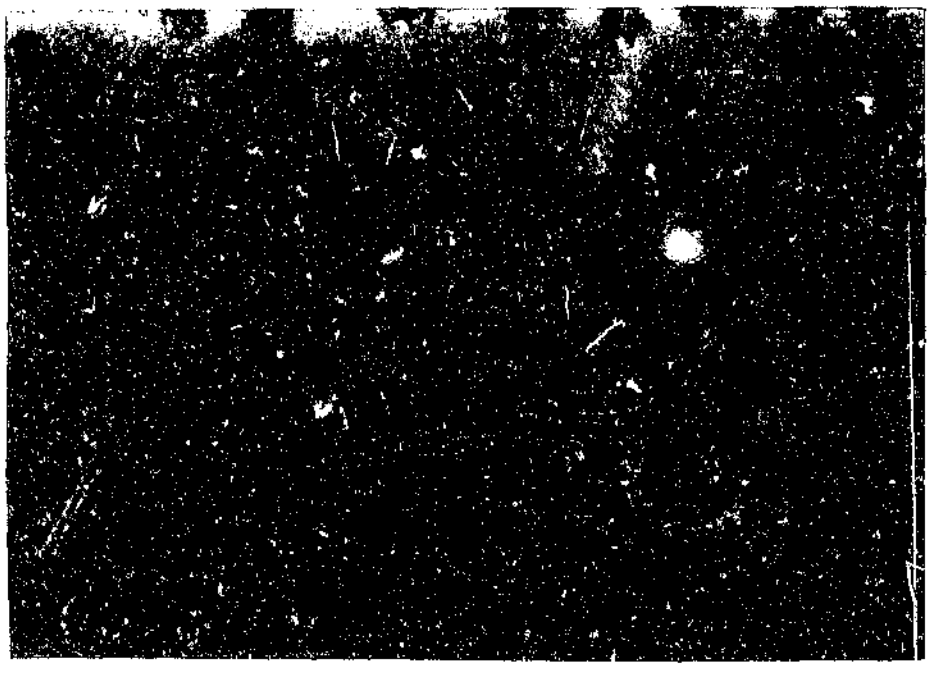

Figure 2.8 CDA 140/170 # powder sample.

Friable, irregularly shaped crystals in sizes generally smaller than 80 US mesh (80 #) are required for use in resin bonded grinding wheels. This probably represents the opposite extreme to the almost perfectly crystalline material mentioned in the preceding paragraph. To represent this type of material, a sample of CDA of size 140/170 # was chosen. This sample is designated as CDA and can be seen in figure 2.8.

A type of diamond abrasive representing diamond qualities intermediate between the above cases is Saw Diamond Abrasive (SDA). This is used primarily for sawing stone and concrete. This type of diamond is usually incorporated into a sintered metal saw segment prior to use, and is thus exposed to high temperatures prior to use. A sample of SDA of size 40/45 # was used in this study and was designated S11. It can be seen in figure 2.9. A sample (of a similar, but not identical batch) was heat treated at 1120 °C for 40 minutes under a flow of high purity argon. This sample is designated HT11 and is illustrated in figure 2.10.

2.2.2 Sectioned SDA Samples

To obtain plane surfaces well oriented with respect to the external crystal morphology and the optical axis of the exciting radiation and the monochromator, some crystals from the SDA sample S11 were incorporated into sintered segments made from a low temperature braze and then polished on a scaife. For each sample, a set was prepared polished on the {100} and on the {111} faces. These sets were designated C11 and O11. For the measurement of photoluminescence, the metal segments containing the diamond were simply mounted on the cryostat sample holder.

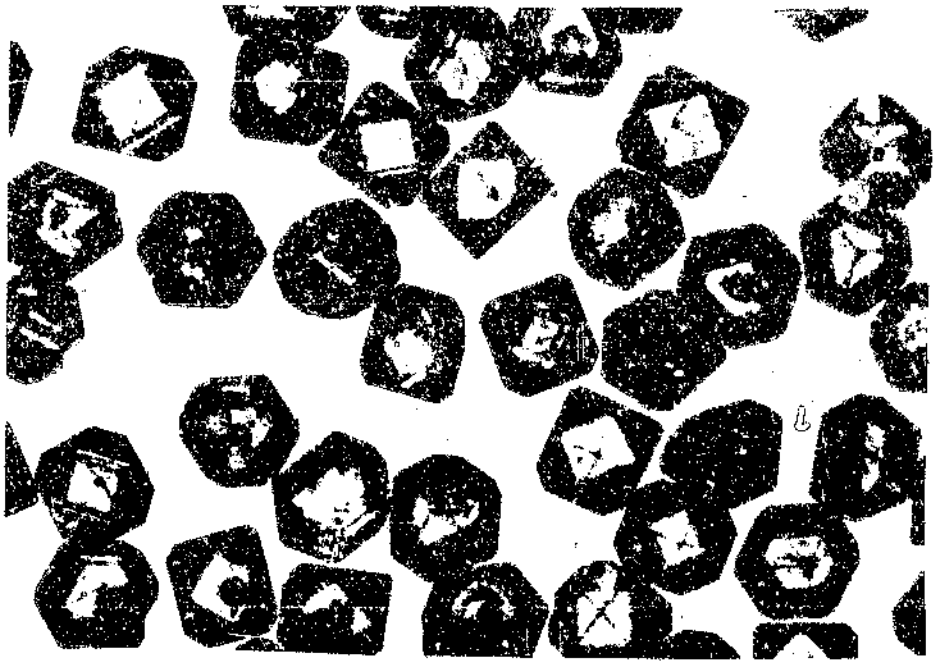

Figure 2.9 SDA 40/45 # powder sample, identified as S11.



Figure 2.10 SDA 40/45 # powder, heat treated under argon for 40 minutes at 1120 °C. This sample is designated as HT11.

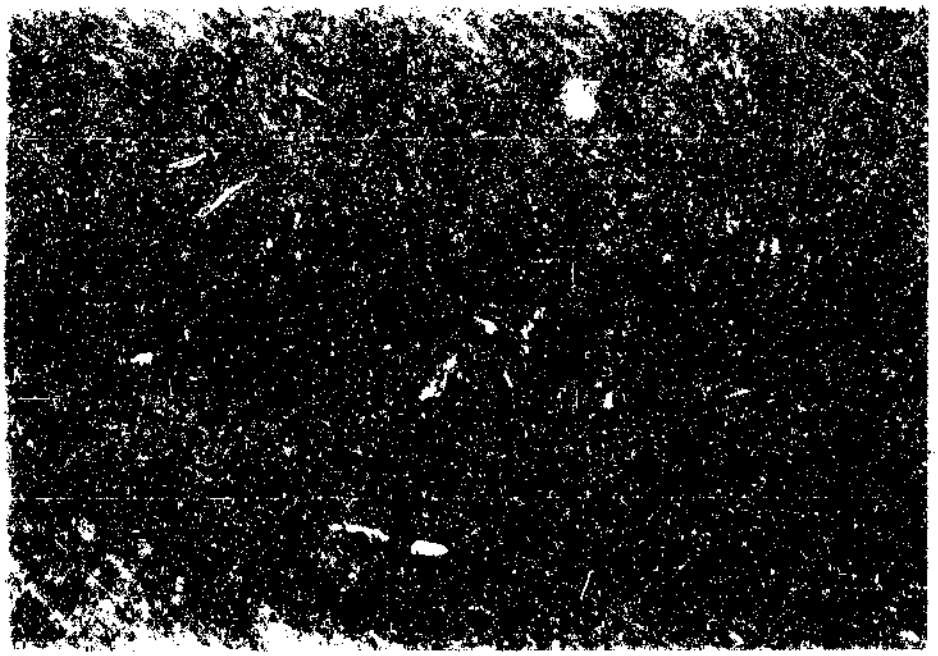

Figure 2.11 Sectioned SDA mounted in a low temperature braze matrix with {111} polished faces exposed. Notice the cracked crystal (the coloured crystal - cracks radiate from top left).

Examination of these sectioned crystals after measurement of the photoluminescence, however, revealed that some of the crystals had cracked (see figure 2.11). As the crystals were not cracked prior to measurement, it appears that cracking occurred during measurement. It is quite likely that cooling to 77 K was responsible, as diamond has a relatively low coefficient of thermal expansion compared to most metals (linear coefficient of expansion for diamond: 0.8 ± 0.1 K 10^{-6} at 293 K (Field, 1992). The diamond thus contracts only a small amount on cooling from 293 K to 77 K, while the surrounding metal contracts to a much greater extent. This would have had the consequence that the diamonds cooled to 77 K would perhaps have been sufficiently stressed to result in the cracking of one of the diamonds.

2.2.3 Powder Samples

A particular problem posed by the study of synthetic diamond abrasive grits is the inhomogeneity of any sample as particles may range in size from 1 mm down to a few microns, depending on the product. Even material from a single synthesis run is highly inhomogeneous, containing particles spanning a variety of sizes and degrees of perfection. This is a consequence, firstly of the unavoidable statistical nature of the nucleation of the crystals, and secondly, of the inevitable temperature and pressure gradients which occur in high pressure cells. If one wishes to relate the photoluminescent properties to product type, or even to specific synthesis runs, single crystal photoluminescence is not very helpful, even though it is quite within the capabilities of the technique. Some means of obtaining an average photoluminescence response from a representative ensemble of crystals is required. The approach finally adopted here was to measure photoluminescence over a relatively large area of the powder sample by using a laser spot size larger than the grain size of the powder.

An alternative approach is to confront the statistical nature of a diamond powder sample "head on", and to measure sufficient single crystals so as to be able to apply statistical analysis to the results. This approach yields a further dimension of information, in that one can obtain a measure of the variation of results within a sample type.

2.2.3.1 Large Area Luminescence

In order to measure the photoluminescence over a large area on the powders, a special sample cell was devised. It consisted of a flat quartz cell made from a standard 1 mm path-length quartz cuvette for UV-visible spectrometry. As the standard cuvettes are 10 mm wide, and several 10's of mm high, it was necessary to saw the cuvette down to a suitable size (5 mm high). This was then fitted into a modified holder for the Oxford Instruments cryostat. (See figure 2.12).

2.2.3.2 Small Area Luminescence

During the course of refining and developing the application of the photoluminescence technique to powder samples, spectra were collected for a large number of diamond powder samples in which the photoluminescence was excited with a laser spot of diameter comparable with, or smaller than the grain size of the powders. Further differences existed between the measurement of these samples and those above. These included the quartz sample cell used, the excitation conditions, and the photomultiplier type.

The sample cell was simply a quartz U-tube, which was filled with the sample powder and mounted in the sample holder for the cryostat (see figure 2.13). The major disadvantage of this sample cell was the presence of a curved, rather than plane quartz surface between the sample and the incident beam and collecting optics. As it was not always possible to ensure that the laser beam was incident on the quartz surface at an appropriate angle to minimise reflection, this led to additional uncertainties in the effectiveness of sample illumination.

The excitation conditions differed in that the laser powers used were higher than those adopted later, and the laser beam was focused (as opposed to an unfocused laser beam used later). The net result was probably a higher effective excitation energy per unit volume of the sample. The major problem with this arrangement was, however, in the use of a focused laser beam. The spot size was focused down to less than .02 mm diameter, smaller than the typical grain size of the powders. This led to large sampling problems, the resulting spectra being appropriate to single crystals rather than to spectra averaged over an ensemble of particles within the sample.

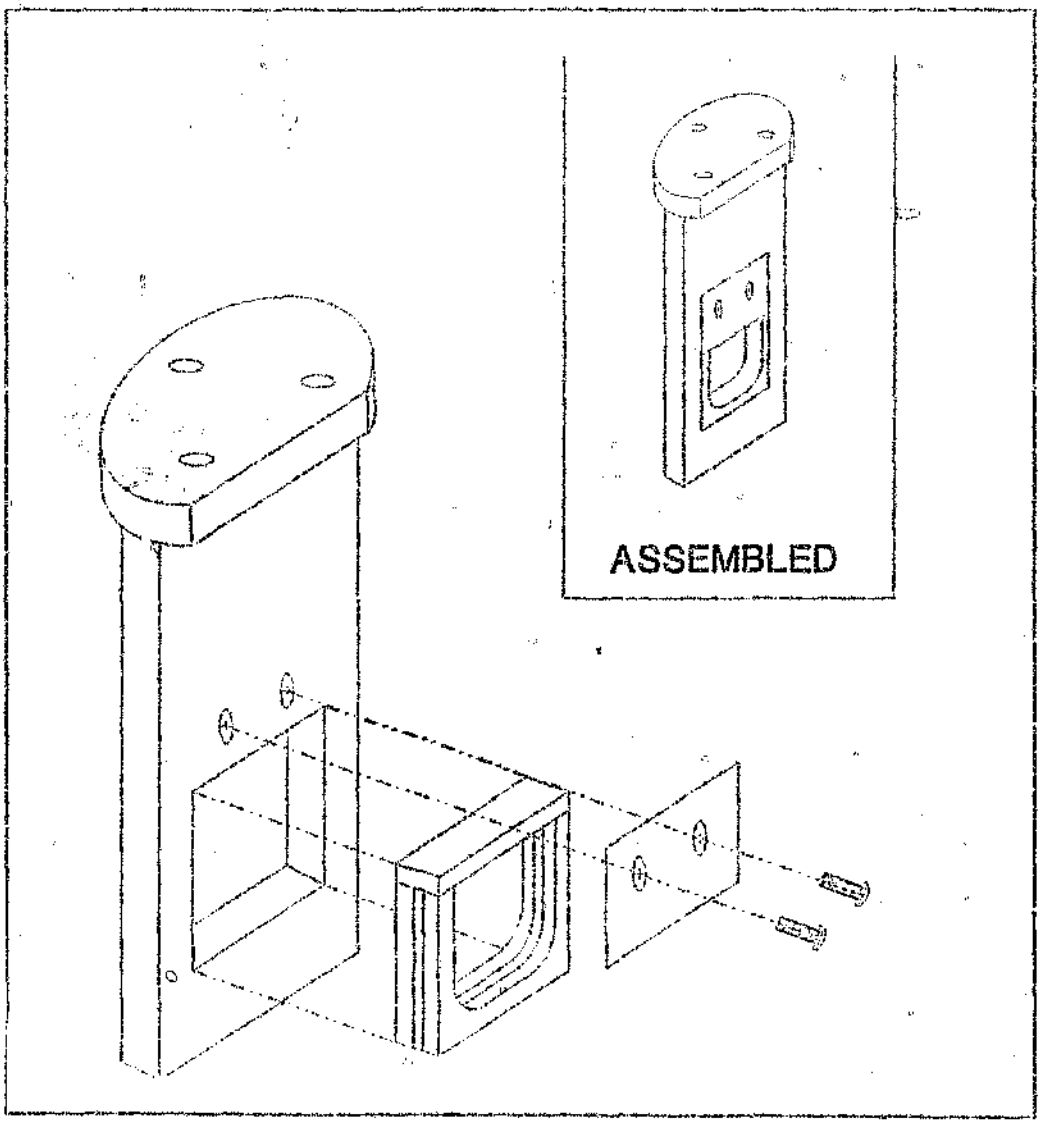

Figure 2.12 Modified sample holder for the Oxford Instruments CF1204 Cryostat used for large sample luminescence. The sample cell is a shortened 1 mm path-length quartz cuvette used for UV-visible spectroscopy.

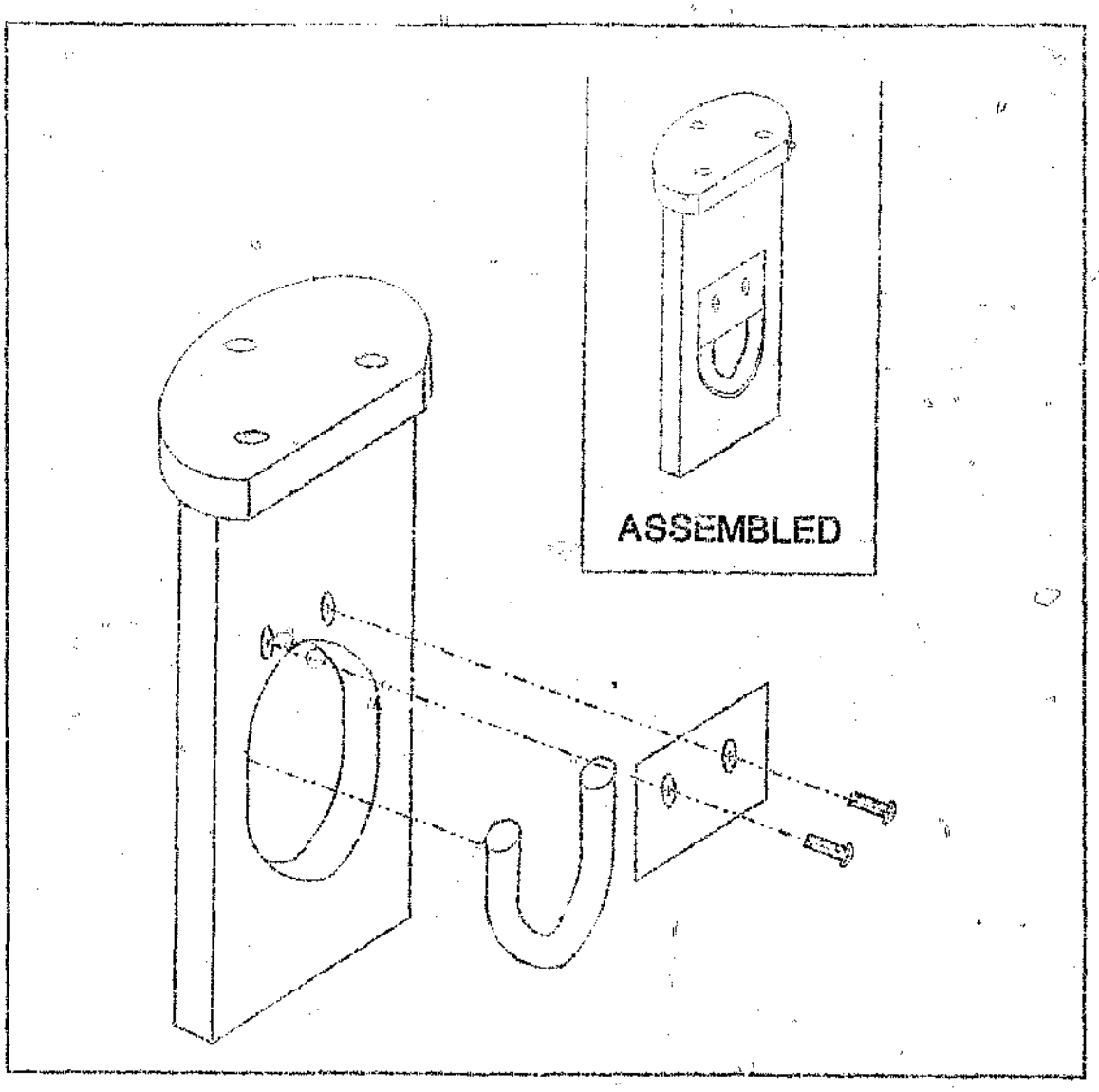

Figure 2.13 Sample holder for the Oxford Instruments CF1204 Cryostat used for small sample luminescence. The sample cell is a quartz U-tube.

While the sampling problems mentioned above precluded the use of these measurements to relate the features of the photoluminescent spectrum of a sample to the sample origin, they are still valid data for the investigation of trends if analysed as distributions of results obtained on sub-samples of each sample. In addition these data are quite acceptable for the investigation of correlations between photoluminescent features WITHIN individual sub-samples.

The samples examined by this approach were all of the SDA or CDA type. They are differentiated on the basis of the particle size within each sample in US mesh sizes. As mentioned above, conditions within any synthesis cell are not homogeneous, the resulting diamond crystals have distributions of properties. One of the most obvious distributions is the size distribution. The samples chosen here represented the peak of the size distribution (40/45 #) and a fraction well below this peak (50/60 #).

2.2.4 Large Crystals

The large diamond crystals were pressed into a hole drilled in a brass disc where the diamond was held in place with indium metal. These discs were simply mounted in the same sample holder in the cryostat. Both the {100} and the {111} faces of one cubo-octahedral crystal CO were examined, and were designated COO and COC respectively to differentiate the two faces.

2.3 Measurement Conditions

For both the small and the large area luminescence measurements, the following measurement conditions were applied :

For general scans refer to table 2.1.

For zero-phonon line scans refer to table 2.2.

Table 2.1

Integration time	1 second
Range (λ_{exc} = 488 nm)	20202 to 11765 cm^{-1}
Range (λ_{exc} = 514 nm)	19231 to 11765 cm^{-1}
Slitwidth	300 µm (effectively 6 cm^{-1} at 637.4 nm)
Scan Rate	25 nm/min
Nominal laser power	400 mW

Measurement conditions used for general scans

Table 2.2

Integration time	1or 2 second
Slitwidth	100 µm (effectively 2 cm^{-1} at 637.4 nm)
Range (λ_{exc} = 514 nm)	15848 to 15564 cm^{-1}
Scan Rate	0.5 or 25 nm/min
Nominal laser power	400 mW

Measurement conditions used for zero-phonon line scans

2.3.1 Choice of Laser Line

Of the several lines available from an argon ion laser, both the 488 nm and the 514 nm lines were used. As the three defects which dominate the photoluminescence of synthetic diamond accessible with these excitation wavelengths are the H3, the 575 nm, and the 1.945 eV centres, at 503.2 nm, 575 nm, and 637.4 nm respectively, the 488 nm excitation is particularly useful, as all three centres are simultaneously excited. In most cases, however, the H3 luminescence dominated. Excitation by 514 nm was also used to advantage as it does not excite the H3, but yields more efficient luminescence from the other two. In general, spectra were taken under both excitation conditions. Spectra of the 1.945 eV ZPL, specifically, were taken using 514 nm excitation as this reduced the slope of the baseline which arises from the tail of the H3 luminescence.

In an attempt to reduce all differences in the experiment between samples, the exact slit widths and laser powers were retained as far as possible. Retaining constant slit widths ensured that the degree of broadening of the sharper lines in the spectrum was kept constant from sample to sample. This allows a direct qualitative comparison of the degree of line broadening between spectra, even in the case of the general spectra. Retaining the laser powers constant reduced the likelihood of different degrees of laser induced warming of the samples.

2.3.2 Temperature

All spectra were recorded at 77 K controlled to within the limits of the Oxford Instruments ITC4 temperature controller (typically ±0.1 °C).

2.4 Normalisation of the Spectra

The intensity recorded for photoluminescence in experiments such as these, is dependent on several uncontrollable factors such as the excitation volume, collection efficiency, laser beam penetration depth and the exact geometry of the experiment. All of the above are highly dependent on the nature of the sample: in the case of powder samples, because of the random orientation of the particles, varying amounts of light may be reflected from the surface and light penetrating the samples may be internally reflected by the diamond surfaces (this is exacerbated by the high refractive index for diamond). The luminescent light may be subject to the same phenomena. In the case of single crystal samples, while surface reflection may be controlled to a degree by illuminating flat surfaces with the laser beam, the unpredictable nature of the excitation and luminescent light inside the sample remains the same. To allow even semi-quantitative comparison of luminescent intensities, the practice of normalising the spectra was adopted in all cases except for the ZPL spectra. The approach adopted was that reported by Evans et al (1984). Normalisation is achieved by dividing the intensity recorded at each wavelength point on the spectrum by the integrated intensity of the first order Raman peak measured under identical excitation, collection and geometric conditions. As the Raman effect is a bulk diamond effect excited by the same incident laser beam, and is subject to the same excitation and geometrical arrangement as during the spectrum measurement, a reasonable compensation for the uncontrollable factors can be achieved. Despite this, the technique can be at best considered as semi-quantitative .

3. RESULTS

This chapter is broken up into four parts: the first (section 3.1) part compares the results obtained in this work with results of other authors; the second (sections 3.2 to 3.4) deals with the differences in the concentration of different point defects in the different types of synthetic diamond studied as revealed by the photoluminescent intensity; the third part (3.5) covers the statistical analysis of the results, examining the distribution of the measured photoluminescence intensities for the different centres, and also the correlations between the intensities of the different centres within the same sample; the fourth section (section 3.6) deals with the difference in the lineshapes of the 1.945 eV ZPL as a function of the different sample types.

3.1 Comparison with Previous Work

Because of the numerous uncontrolled factors influencing the relationship between the concentration of a luminescent defect and the intensity of the photoluminescence actually detected, most published photoluminescence spectra give the intensity in terms of "arbitrary units". The practice adopted in this work, of normalising the spectra (described in section 2.4 above), helps to compensate for these unknowns to a large degree, allowing comparison of intensities from one spectrum to another. In order to obtain a quantitative comparison of the intensities in this work with those in other works, it is necessary that the other authors also used the procedure of normalisation. Fortunately this practice was followed by Robertson (1984) and Dodge (1986), allowing quantitative comparison of their photoluminescence spectra with those determined in the present work.

A photoluminescence spectrum of polycrystalline diamond (Syndite, manufactured by De Beers), measured in this work, at room temperature, shows the same overall features as those measured by Robertson (1984) on commercial polycrystalline diamond compacts and on binderless compacts of synthetic diamond. These features can be seen in figure 3.1: three peaks indicate the presence of substantial concentrations of H3, 575 nm and 1.945 eV defects.

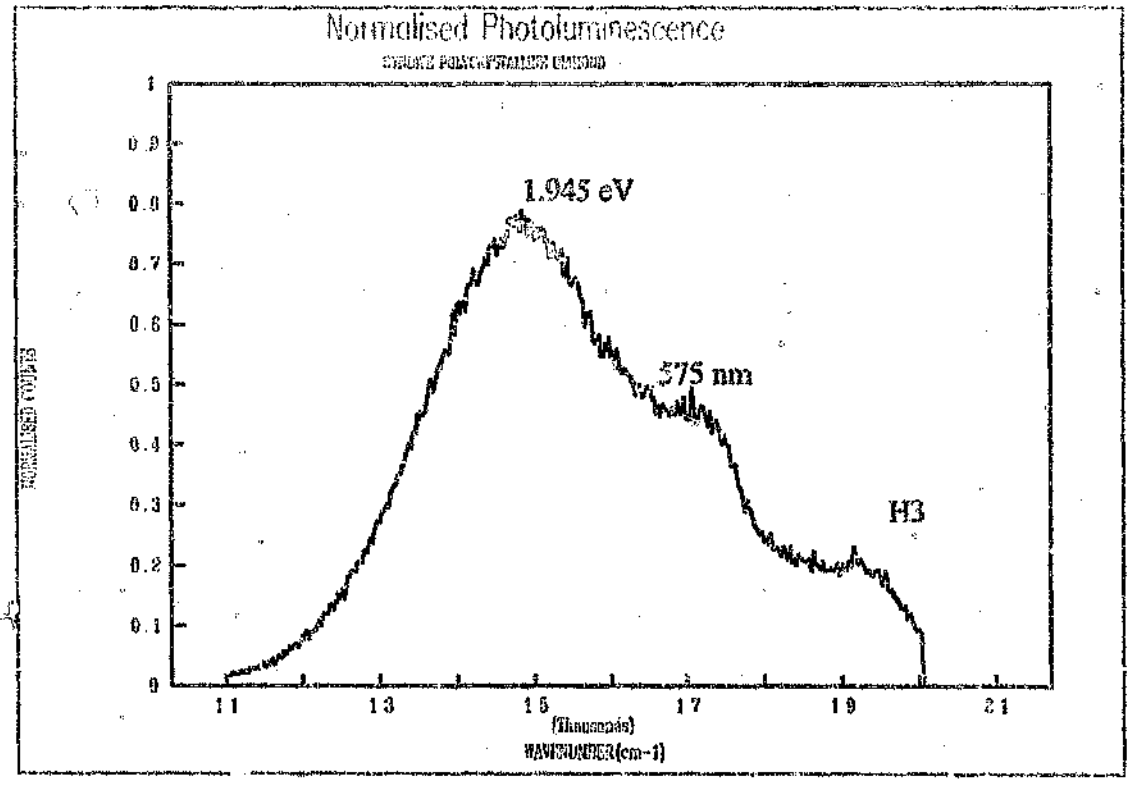

Figure 3.1 Room temperature photoluminescence spectrum of polycrystalline diamond, SYNDITE, showing the same features as spectra measured by Robertson (1984).

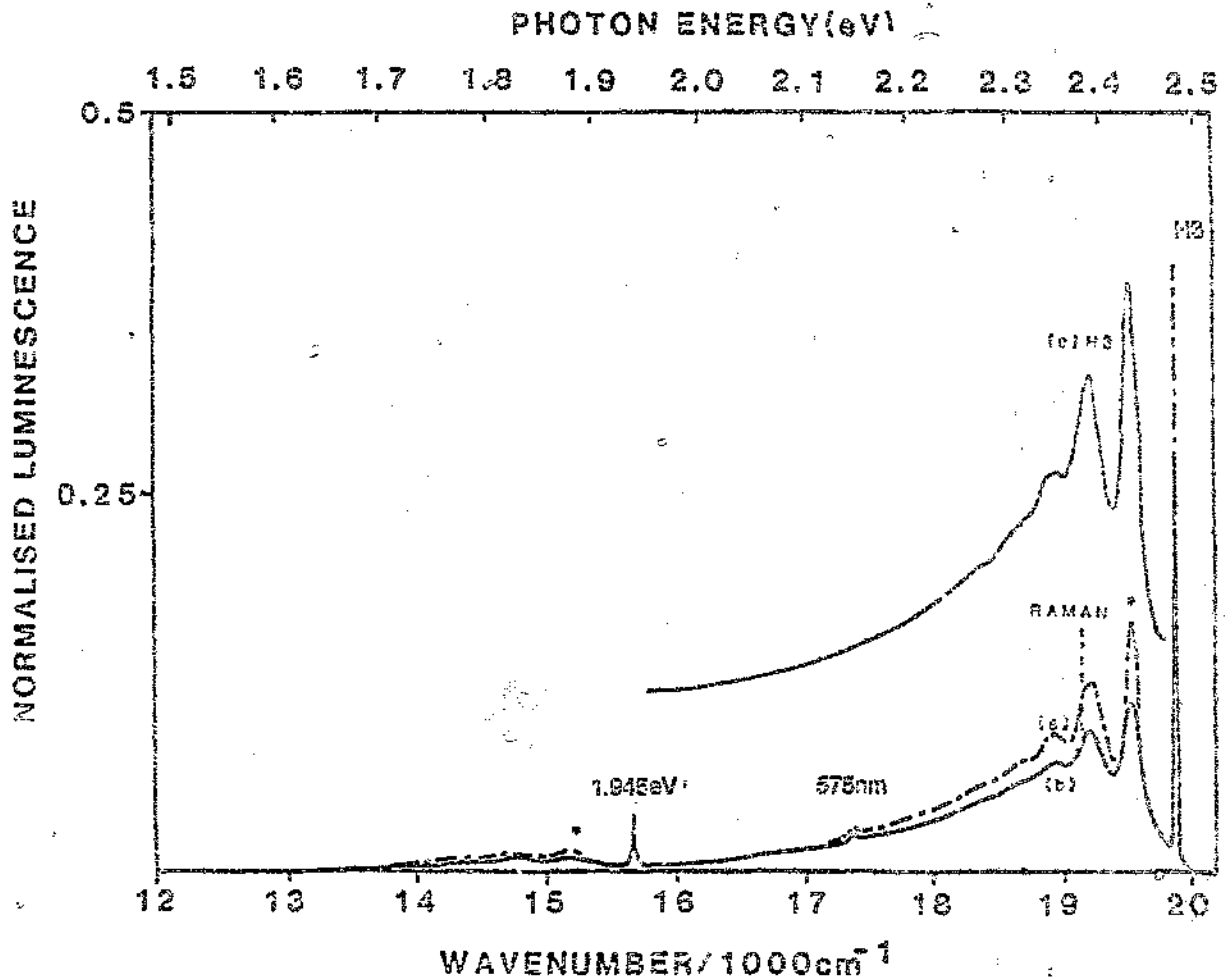

Figure 3.2 Example SDA photoluminescence spectra (labelled a) and b)) from Dodge (1986) . The H3, 575 nm and 1.945 eV ZPLs are indicated. One-phonon lines for the H3 and 1.945 eV luminescence systems are marked with an asterisk. Graph a) is an example of a pure H3 spectrum.

The work of Dodge (1986) contains normalised spectra of SDA crystals and MDA powder (MDA is synthetic diamond abrasive similar to SDA, but of much smaller particle size). An example spectrum from, Dodge (1986) is given as figure 3.2. In both cases, the spectra consist of H3 luminescence and traces of 1.945 eV luminescence as observed for the samples in this work. The normalised intensities, given in table 3.1 below, indicate a reasonable agreement between the measurements of Dodge and those of this work.

Table 3.1

Normalised Intensities			
Sample	**Reference**	**H3 1-phonon**	**1.945 eV 1-phonon**
MDA	Dodge 1986	0.138	0.034
SDA	Dodge 1986	0.124	0.005
SDA	Dodge 1986	0.161	0.014
SDA: Range	Dodge 1986	0.1-0.8	
Type Ia: Range	Dodge 1986	0.01-0.08	
Fine SDA	This Work	0.086-0.376	0.003-0.006
Coarse SDA	This Work	0.108-0.213	0.005-0.031

Reasonable agreement between the normalised intensities measured by Dodge (1986) and those measured in this work are indicated.
Note: "Fine" refers to 50/60 # "Coarse" refers to +50 #.

Summary: Comparison with previous work.

- The normalised photoluminescence spectra of various diamond sample types measured in this work yield intensities comparable with those measured by other authors on similar samples.

3.2 Intensities due to Different Defects

In general the scans covering the three expected luminescent spectra show only the H3 and the 1.945 eV centres. (The 575 nm centre was observed under the standard measurement conditions (given in table 2.1) only in the case of the spectrum from the {100} face of the cubo-octahedral large crystal COC. This luminescence was also observed for the powder sample CDA, but not under the standard measurement conditions chosen for the comparison. In all small area luminescence measurements made on the SDA and CDA samples, luminescence from all of H3, 1.945 eV and 575 nm was observed. This will be discussed later in sections 3.5.1.2 and 3.5.2.4.)

A very weak broad luminescence line centred around 840nm (11905 cm^{-1}) was detected in those luminescence spectra where the background luminescence from the 1.945 eV centre was sufficiently low in this area to allow this weak peak to be detected (*viz.* the 514 nm excited luminescence spectra for S11 , HT11, O11, C11, and Oh, shown in figures 3.10 b), 3.11 b), 3.12 b), 3.13 b) and 3.14 b) repectively). It should be noted that the position of this peak is very close to the lowest energy limit of the detector used in these experiments. The detector sensitivity decays very rapidly to zero in this region and this might result in distortion of the shape of this broad peak. The position given for this peak is thus open to question. No other reference to this luminescence system is known to this author.

The spectra from the different samples differed mainly in the strength and the degree of broadening observed for the luminescence detected from the specific centres discussed above.

3.3 Reproducibility of Measurements on Powder

The success of the approach adopted for the measurement of the powder samples (powder sample in a quartz cell, unfocused laser beam) can be judged from figures 3.3 (CDA), 3.4 (SDA grit, S11), and 3.5 (heat treated SDA grit, HT11) which show three spectra plotted on the same graph for each of the three grit types (spectra obtained

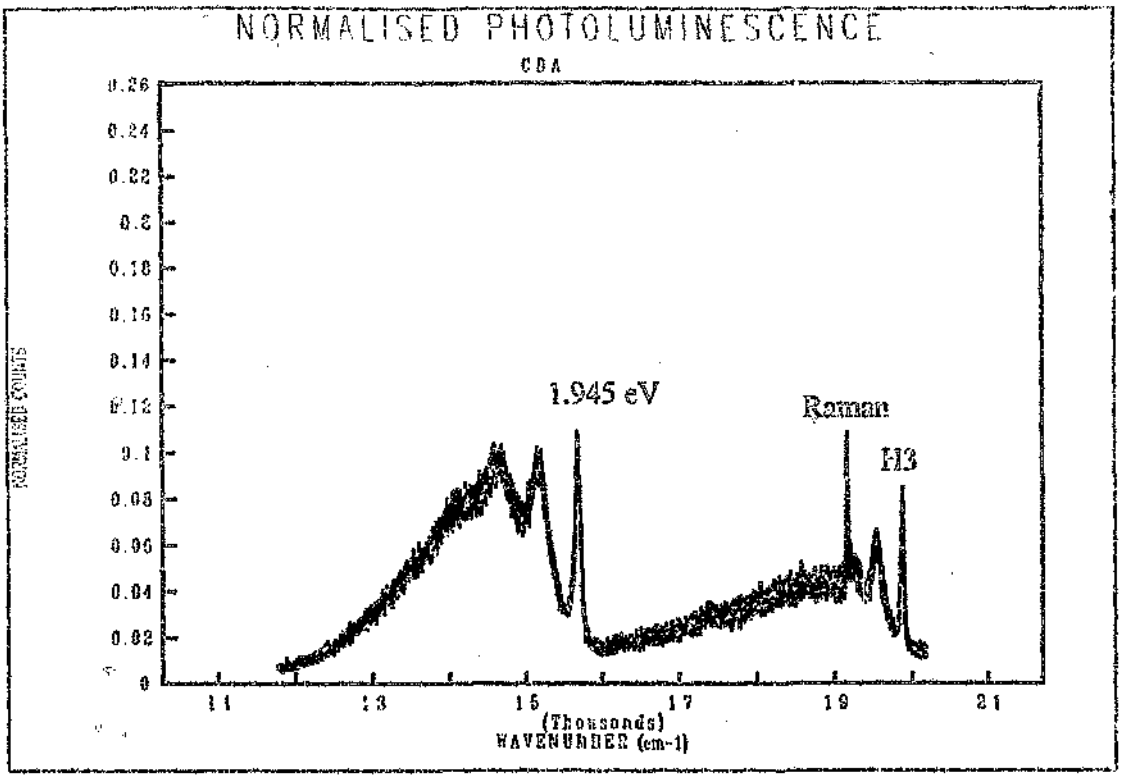

Figure 3.3 a) Replicate spectra of powder sample of CDA. λ_{exc}=488 nm

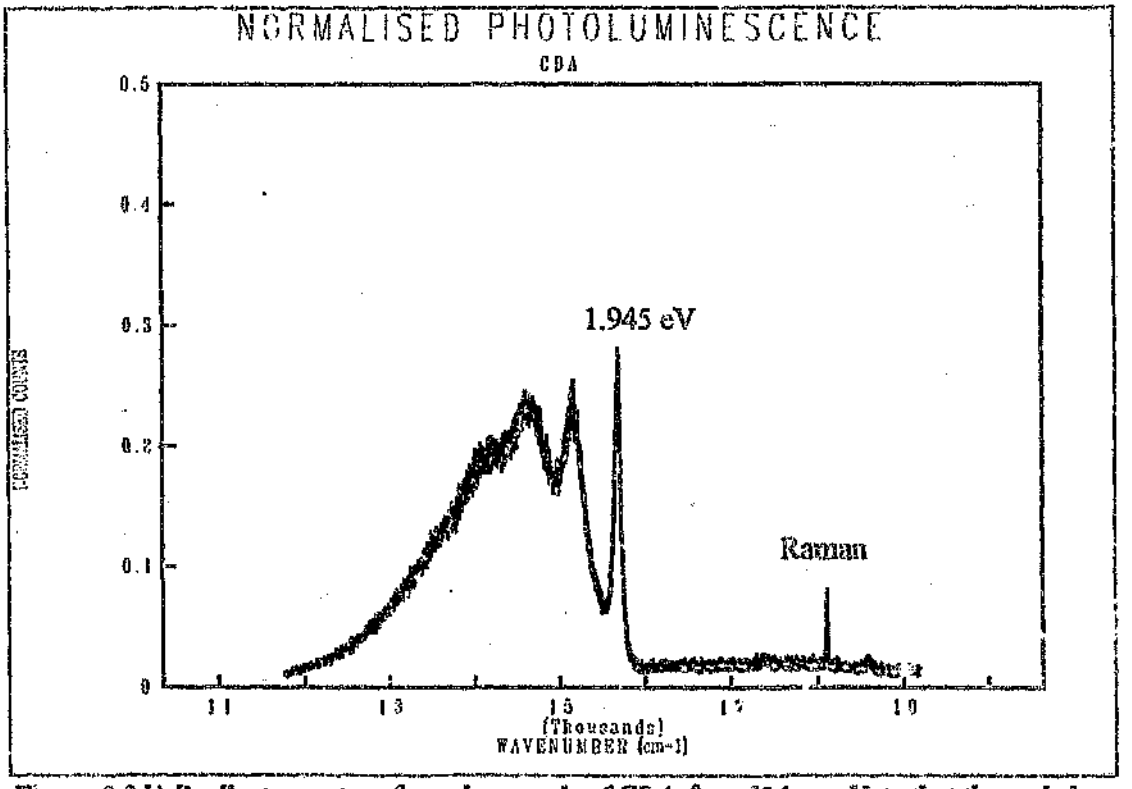

Figure 3.3 b) Replicate spectra of powder sample of CDA. λ_{exc}=514 nm. Note that the scale has been reduced by 5x in order to accomodate the high 1.945 eV intensity.

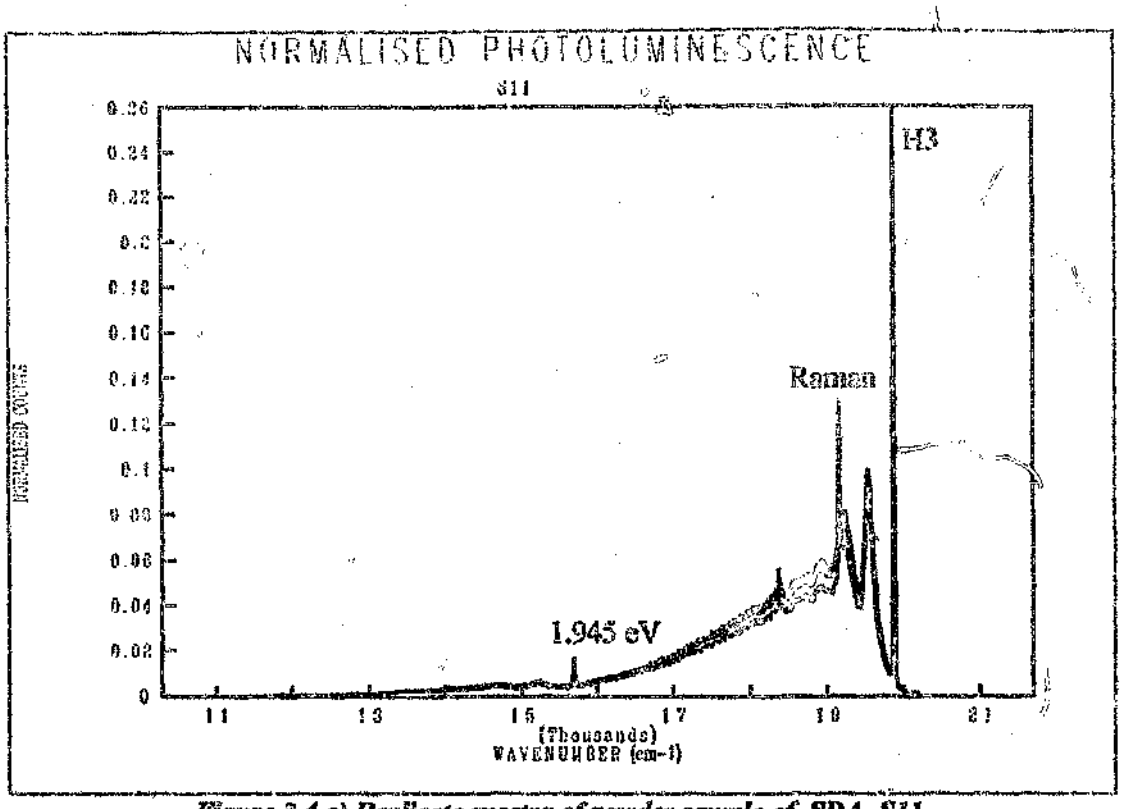

Figure 3.4 a) Replicate spectra of powder sample of SDA, S11.
λ_{exc}=488 nm

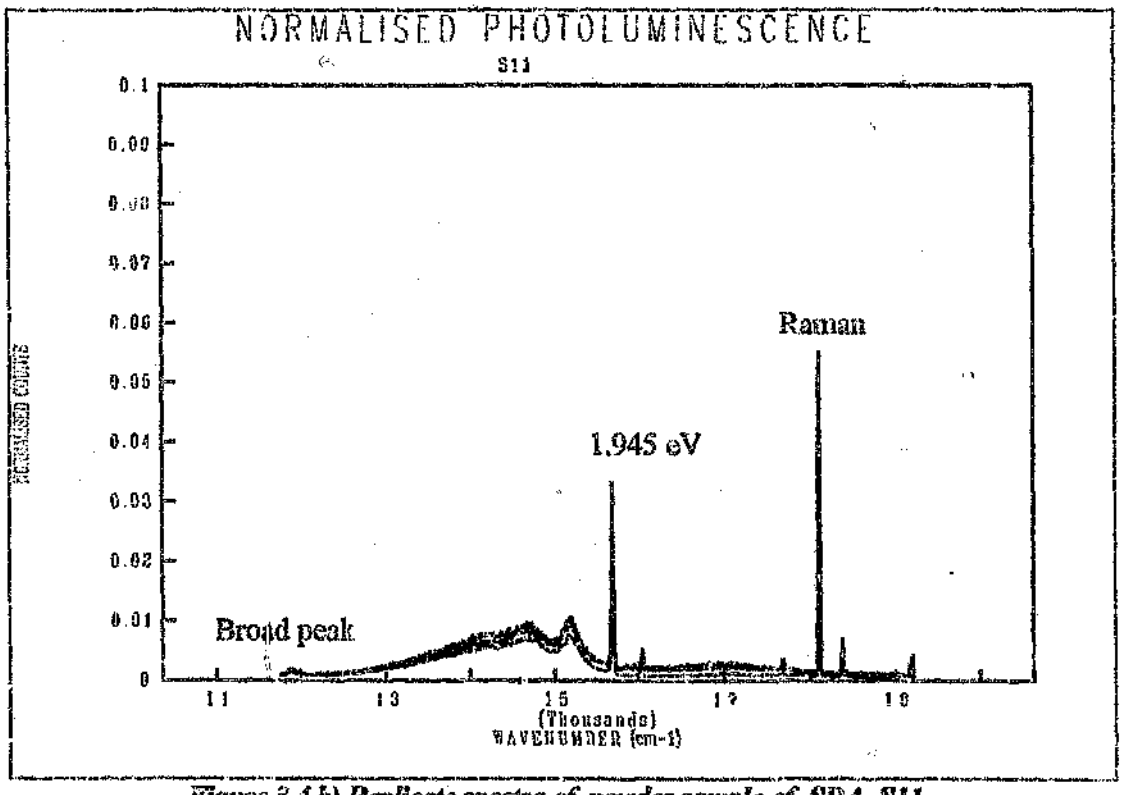

Figure 3.4 b) Replicate spectra of powder sample of SDA, S11.
λ_{exc}=514 nm

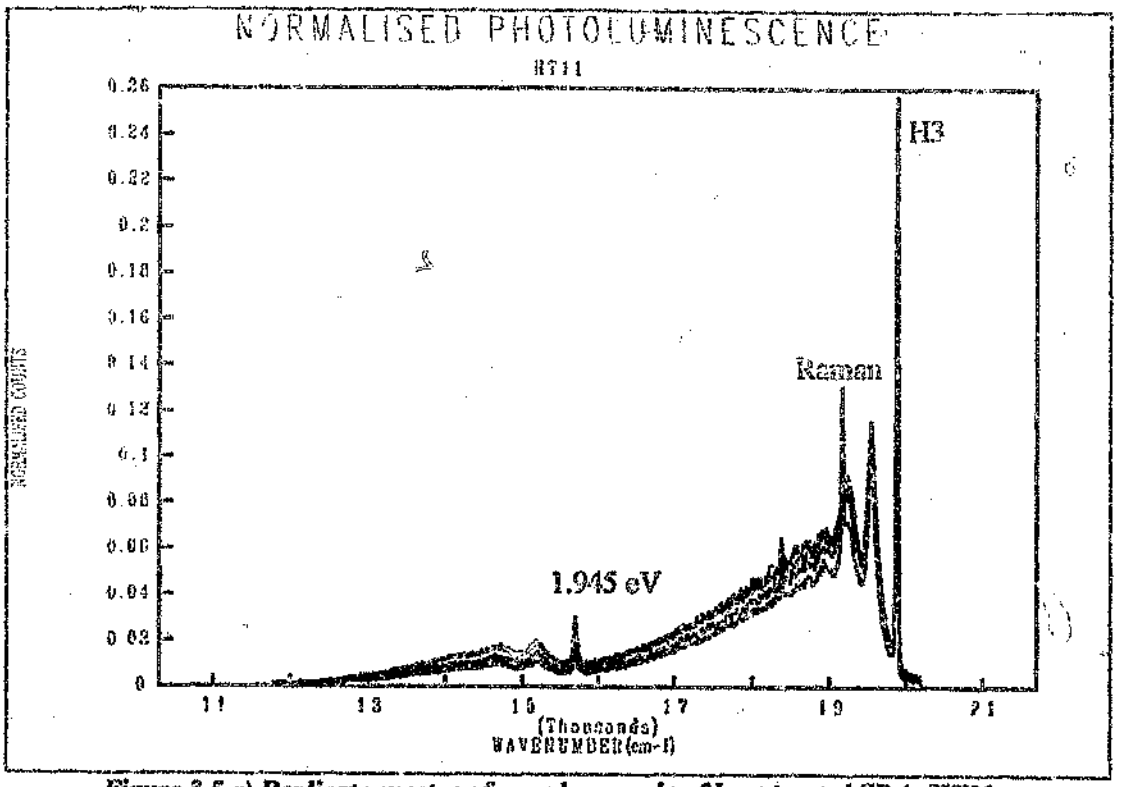

Figure 3.5 a) Replicate spectra of powder sample of heat treated SDA, HT11.
λ_{exc}=488 nm

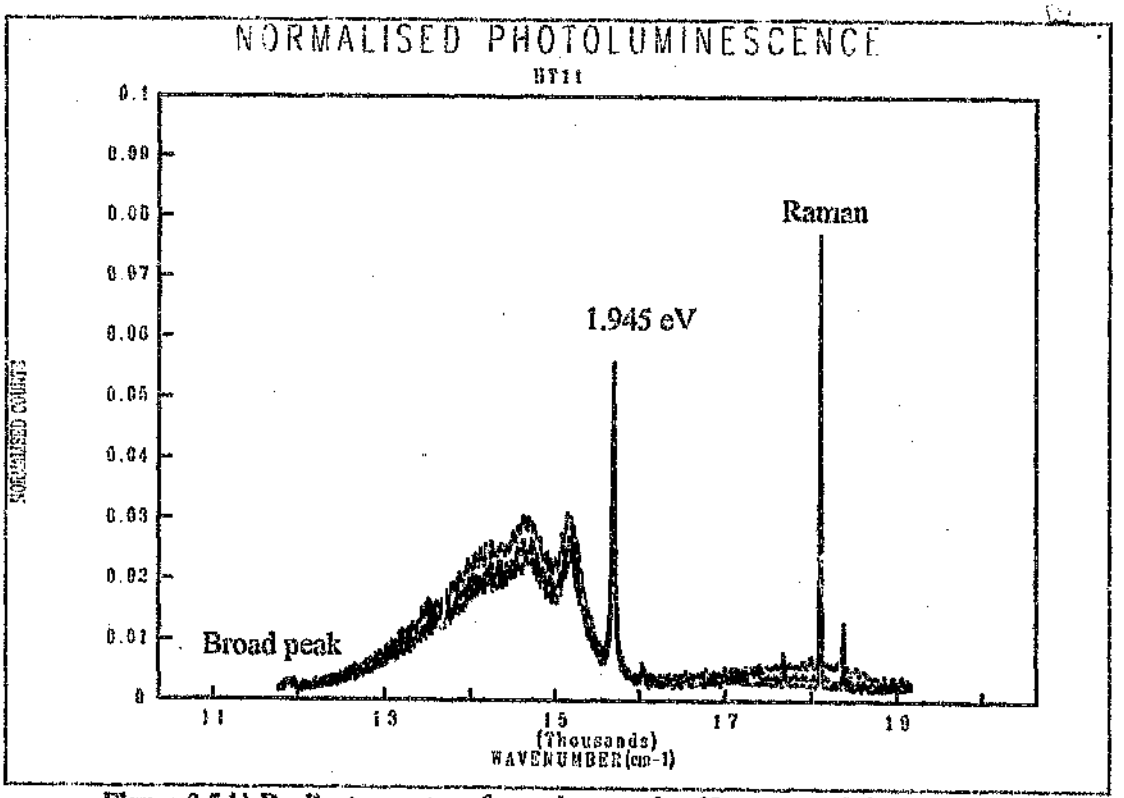

Figure 3.5 b) Replicate spectra of powder sample of heat treated SDA, HT11.
λ_{exc}=514 nm.

from 514 nm and 488 nm excitation are given as a) and b) respectively). While not identical, the scatter within the replicate spectra is virtually negligible compared to the differences between sample types. This can quantified by performing an analysis of variance (ANOVA). This test allows one to compare means of several samples in order to assess whether any difference between the means is significant or not at a chosen confidence level. It does this by comparing the variability between measurements on different samples ("factor variability") with the variability between repeat measurements (or "replicates") on the same sample ("random" or "error variability"). The test uses the relative size of the factor and error variability to calculate the probability of observing the differences between the means of the different samples (or "factors") purely by chance - low probabilities for the ANOVA indicate that the differences between samples are unlikely to be simply the result of random scatter in the results. This probability is calculated by expressing factor and error variability as an F-ratio and using a knowledge of the distribution of this ratio, the F-distribution, to read off the probability of observing this ratio purely by chance (Spiegel 1988).

A series of ANOVA's performed on the one-phonon peak intensities for the H3 and 1.945 eV luminescence for the three powder types: Untreated SDA (S11); heat treated SDA (HT11); and CDA (CDA). A single factor, the effect of different sample type was analysed. (These analyses are termed "one way ANOVA's".) Three replicate measurements of each sample type were used. The response variables were: the normalised luminescence for the 1.945 eV one-phonon sideband; the normalised luminescence for the H3 one-phonon sideband; and the FWHH of the 1.945 eV ZPL. The results are given as tables 3.2, 3.3 and 3.4 respectively. The analyses show the differences between the sample means to be significant at better than the 99.9 % confidence level (significance level <0.001) for all three response variables. The graphical comparison of the scatter about the means (a "means plot") of the 1.945 eV one-phonon sideband intensities in figure 3.6 has error bars indicating the 95 % confidence limits. As these do not overlap, the mean intensities for the 1.945 eV one phonon side bands of all three sample types can be said to be significantly different at the 95 % level. A similar interpretation of the means plot of the H3 one-phonon sideband intensities in figure 3.7 shows that the average intensities of the one phonon

side bands of the H3 centre for CDA differs significantly from those of S11 and HT11 at the 95 % confidence level. The latter two intensities, however, can not be distinguished at the 95 % confidence level. In the case of the 1.945 eV ZPL FWHHs in figure 3.8, it can be seen that the 95 % error bars for CDA S11 and HT11 do not overlap with each other, indicating significantly different 1.945 eV ZPL FWHH at the 95 % confidence level.

Table 3.2

One way analysis of variance for 1-phonon sideband intensity of 1.945 eV					
Factors : Powder sample type-S11, HT11, CDA, Replicates = 3.					
Source of Variation	**Sum of Squares**	**d.f.**	**Mean Square**	**F-ratio**	**Sig. Level**
Between groups	.0890272	2	.0445136	1695.398	.0000
Within groups	.0001575	6	.0000263		
Total (corrected)	.0891848	8			

One way ANOVA for the 1.945 eV one-phonon sideband normalised luminescence. The abbreviations have the following meanings: d.f. = degrees of freedom, Sig. Level = significance level. The significance level given here indicates the extremely low probability of observing the ratio of factor variability to error variability, as expressed by the F-ratio, purely by chance, indicating that the differences between the means of the intensities are significant.

Table 3.3

One way analysis of variance for 1-phonon sideband intensity of H3 centre					
Factors : Powder sample type -S11, FT11, CDA. Replicates = 3.					
Source of Variation	Sum of Squares	d.f.	Mean Square	F-ratio	Sig. Level
Between groups	.0049989	2	.0024995	33.289	.0006
Within groups	.0004505	6	.0000751		
Total (corrected)	.0054494	8			

One way ANOVA for the H3 one-phonon sideband normalised luminescence. The abbreviations have the following meanings: d.f. = degrees of freedom, Sig. Level = significance level. The significance level given here indicates the extremely low probability of observing the ratio of factor variability to error variability, as expressed by the F-ratio, purely by chance, indicating that the differences between the means of the intensities are significant.

Table 3.4

One way analysis of variance for the FWHH of the 1.945 eV ZPL line (measured off the spectra)					
Factors : Powder sample type -S11, FT11, CDA. Replicates = 3					
Source of Variation	Sum of Squares	d.f.	Mean Square	F-ratio	Sig. Level
Between groups	8097.8867	2	4048.94	397.1	.0000
Within groups	91.7200	9	10.1911		
Total (corrected)	8189.61	11			

One way ANOVA for the 1.945 eV ZPL FWHH. The abbreviations have the following meanings: d.f. = degrees of freedom, Sig. Level = significance level. The significance level given here indicates the extremely low probability of observing the ratio of factor variability to error variability, as expressed by the F-ratio, purely by chance, indicating that the differences between the means of the FWHH are significant.

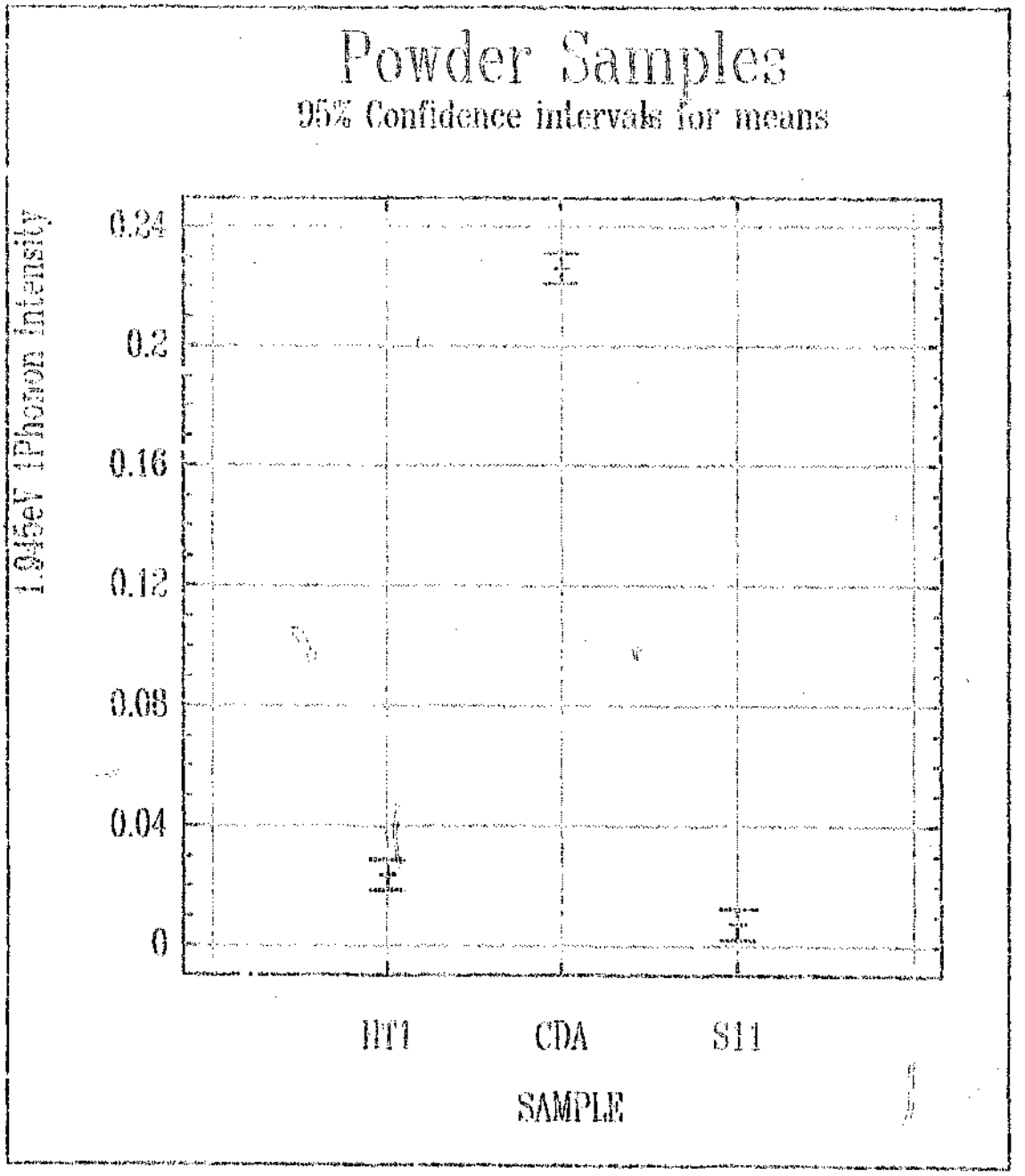

Figure 3.6 Plot of means of the 1.935 eV 1-phonon luminescence intensity for the powder samples. Error bars indicate 95 % confidence intervals.

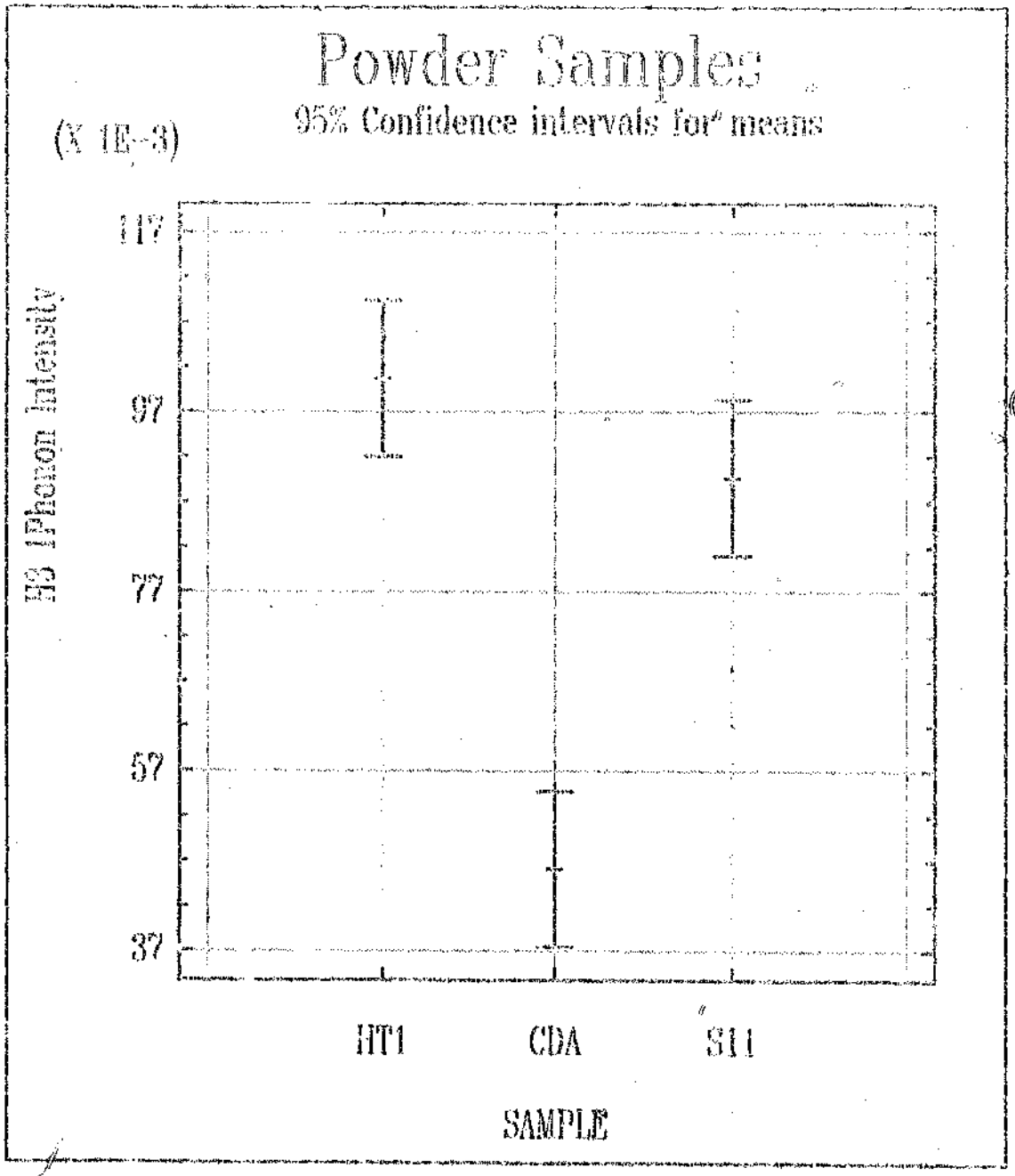

Figure 3.7 Plot of means of the H3 1-phonon luminescence intensity for the powder samples. Error bars indicate 95 % confidence intervals.

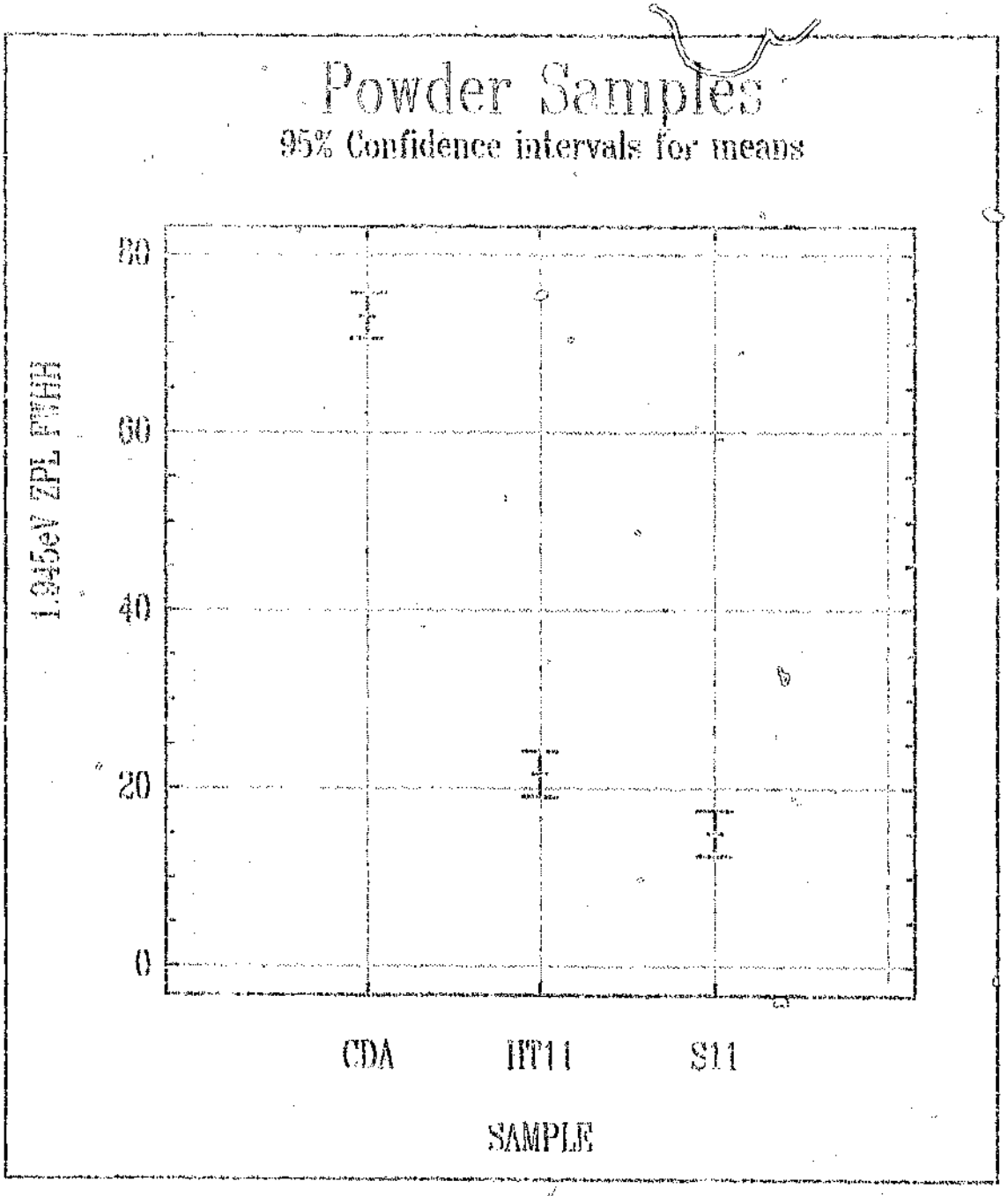

Figure 5.8 Plot of means of the 1.945 eV ZPL FWHH for the powder samples. Error bars indicate 95 % confidence intervals.

3.4 Comparison of Representative Spectra

Having established that the differences observed for the means of the different powder sample luminescence spectra are significant, the photoluminescence spectra for each of the powder sample types is henceforth represented by the average spectrum obtained by averaging each point on the spectrum over the three replicate spectra measured for each powder sample type. Representative spectra of all sample types are given as tabulated below in table 3.5. Table 3.6 summarises the results by listing the peak intensities of the normalised luminescence spectra for the various sample types.

Table 3.5

Designation	Sample	Type	Figure
CDA	CDA Poorly crystalline, highly defective, fine grain	Powder	3.9
S11	SDA-type material - crystalline, medium grain	Powder	3.10
HT11	SDA-type after heat treatment at 1120 °C	Powder	3.11
O11	SDA (S11) sectioned parallel to octahedral face	Sections	3.12
C11	SDA (S11) sectioned parallel to cubic face	Sections	3.13
Oh	Octahedral morphology crystal	Crystal	3.14
COO	Octahedral face of Cubo-octahedral crystal	Crystal	3.15
COC	Cubic face of cubo-octahedral crystal	Crystal	3.16
Cu	Cubic morphology crystal	Crystal	3.17

Reference table for sample labelling and identity. The spectra presented for powders are averages of the three recorded. The spectra for sections are as-recorded single spectra. The spectra for single crystals are as-recorded single spectra. The data is summarised in table 3.6 below. Spectra taken using 488 nm excitation are labelled a). Spectra taken using 514 nm excitation are labelled b).

Table 3.6

Luminescence	S11	HT11	CDA	O11	C11	Oh	COO	COC	Cu
488 nm Excitation									
H3 ZPL	0.23	0.24	0.06	0.14	0.24	0.09	0.02	0.23	0.60
H3 1Ph	0.09	0.10	0.05	0.11	0.14	0.03	0.01	0.10	0.47
1.948 eV ZPL	0.01	0.01	0.09	0	0.01	0	0.02	0.03	0.03
1.948 eV 1Ph	0.01	0.01	0.08	0.01	0.01	0	0.01	0.02	0.02
514 nm Excitation									
575 nm ZPL									
575 nm 1Ph									
1.945 eV ZPL	0.01	0.05	0.24	0.01	0 03	0.01	0.05	0.07	0.09
1.945 eV 1Ph	0.01	0.02	0.23	0.01	0.01	0	0.03	0.04	0.08

Table summarising the normalised luminescence peak intensities for the representative spectra of the different sample types listed in table 3.5 and illustrated in figures 3.9 to 3.17 and summarised in figures 3.18 and 3.19. The table is given for reference to the numerical data "1Ph" indicates that the value given for the intensity refers to the one-phonon sideband.

The variation in the intensity of the H3 and 1.945 eV luminescence is summarised graphically in figure 3.18 (Graph of ZPL and one-phonon sideband intensity of H3) and figure 3.19 (Graph of ZPL and one-phonon sideband intensity of 1.954 eV) respectively. The strength of the luminescence is strictly equal to the area under the entire luminescence system, but can be roughly estimated from the height of the one phonon band (significant variations in the ZPL height resulting from strain broadening which varies from sample to sample, as well as the difficulties in obtaining an accurate spectrum of such a narrow peak, make the height of the broader one phonon line height a less unreliable indicator than the ZPL height itself). (Temperature broadening can be ignored as all spectra were taken at 77 K.)

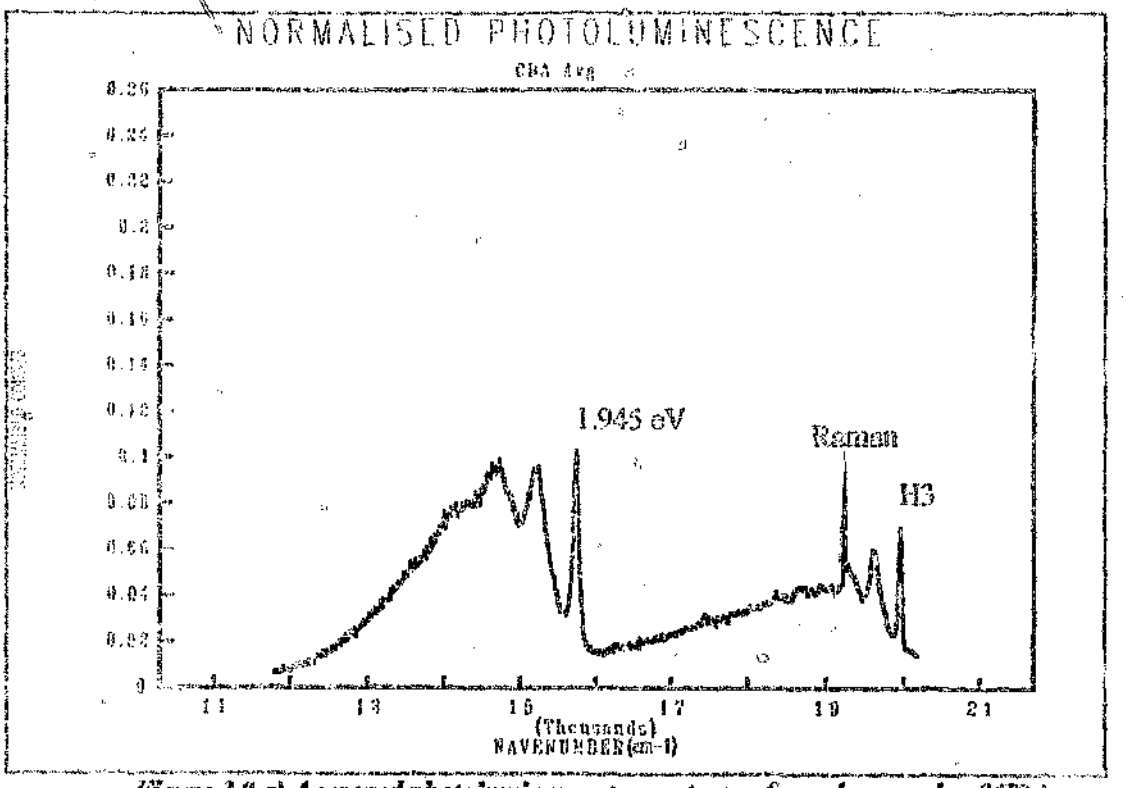

Figure 3.9 a) Averaged photoluminescence spectrum of powder sample of CDA. λ_{exc}=488 nm

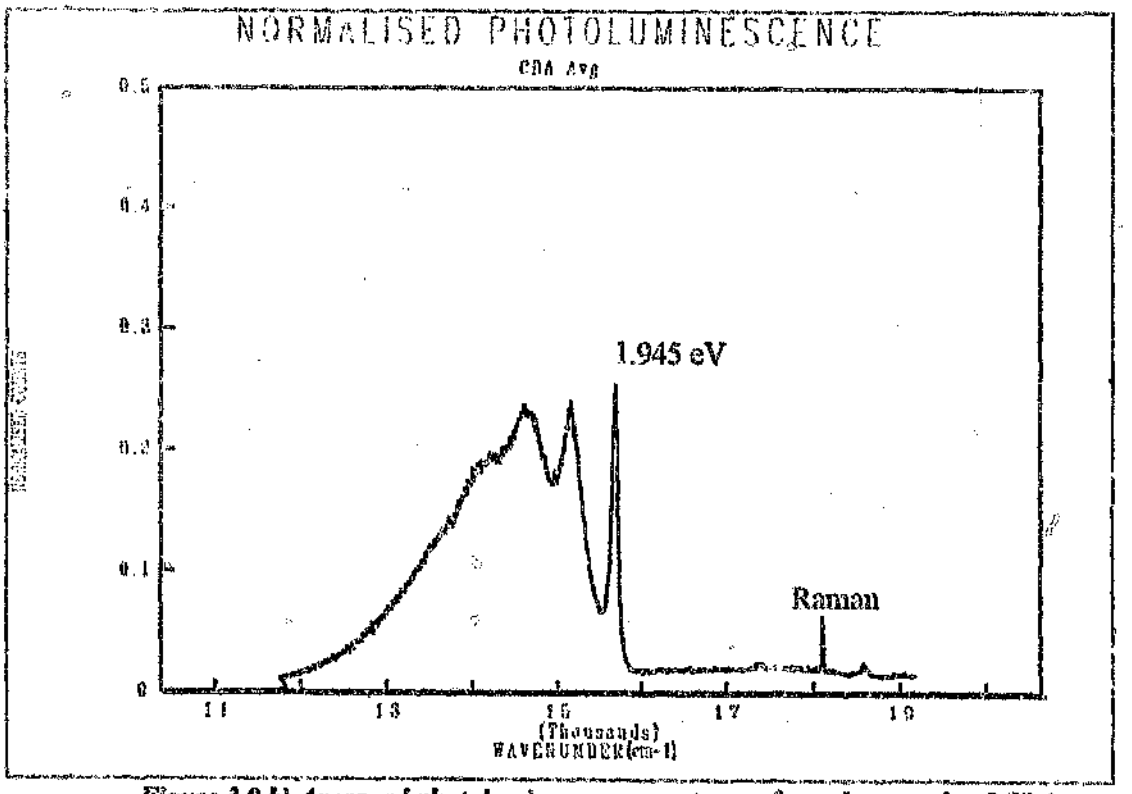

Figure 3.9 b) Averaged photoluminescence spectrum of powder sample of CDA. λ_{exc}=514 nm Note the 5x reduced scale to accomodate the high luminescence intensity.

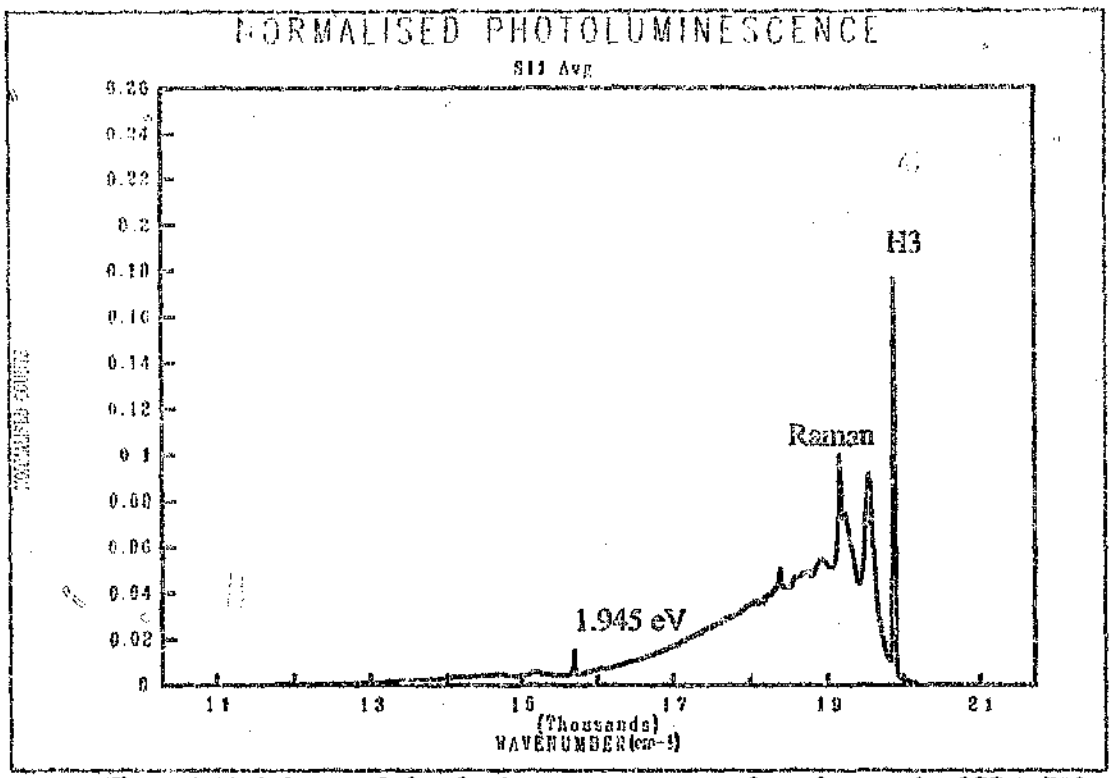

Figure 3.10 a) Averaged photoluminescence spectrum of powder sample of SDA, S11. λ_{exc}*=488 nm*

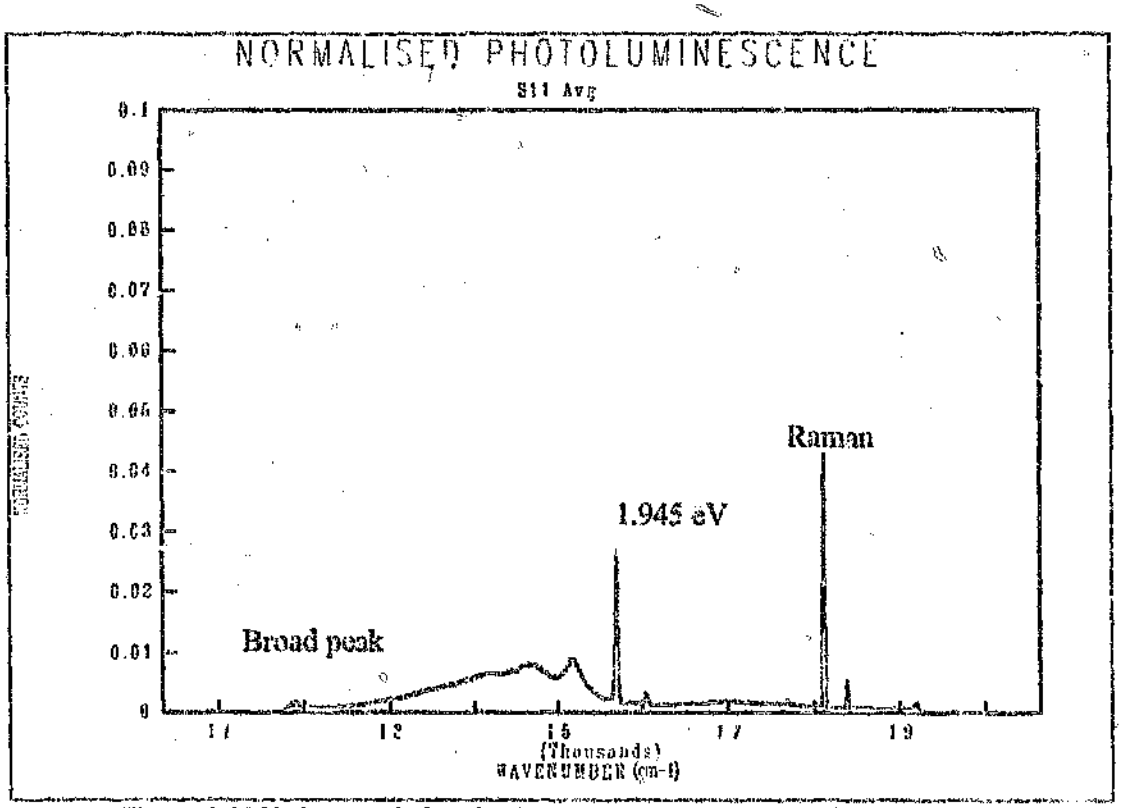

Figure 3.10 b) Averaged photoluminescence spectrum of powder sample of SDA, S11. λ_{exc}*=514 nm*

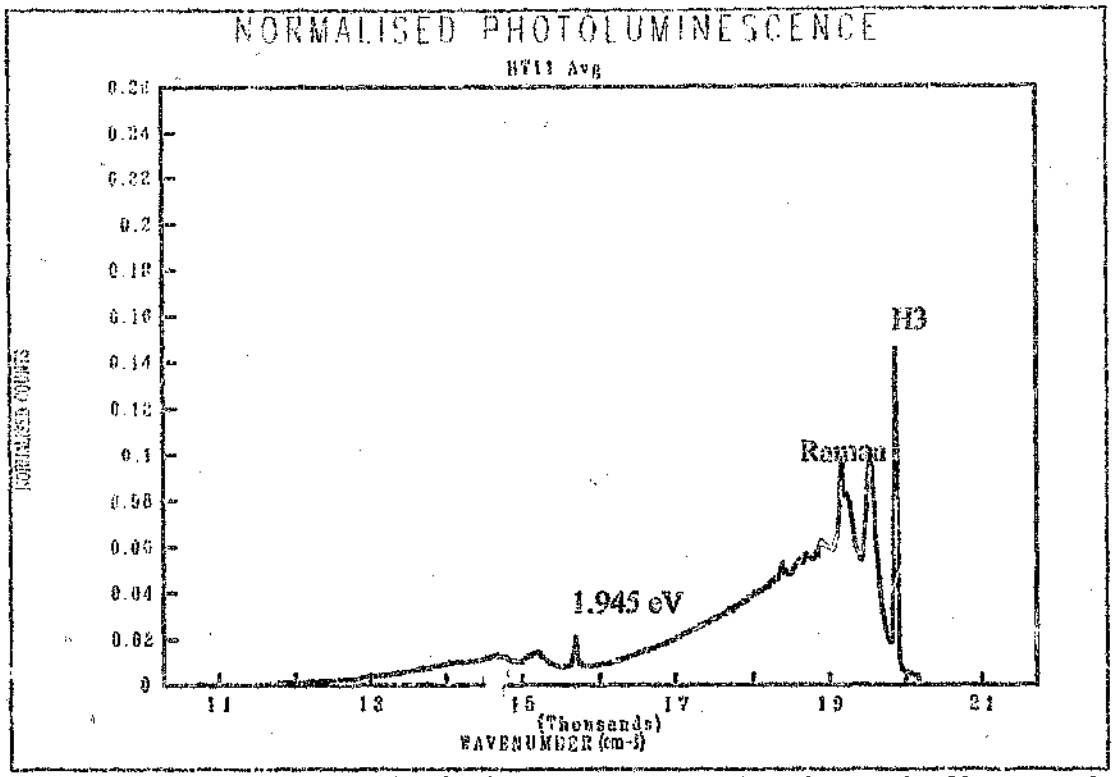

Figure 3.11 a) Average photoluminescence spectrum of powder sample of heat treated SDA, HT11. λ_{exc}=488 nm.

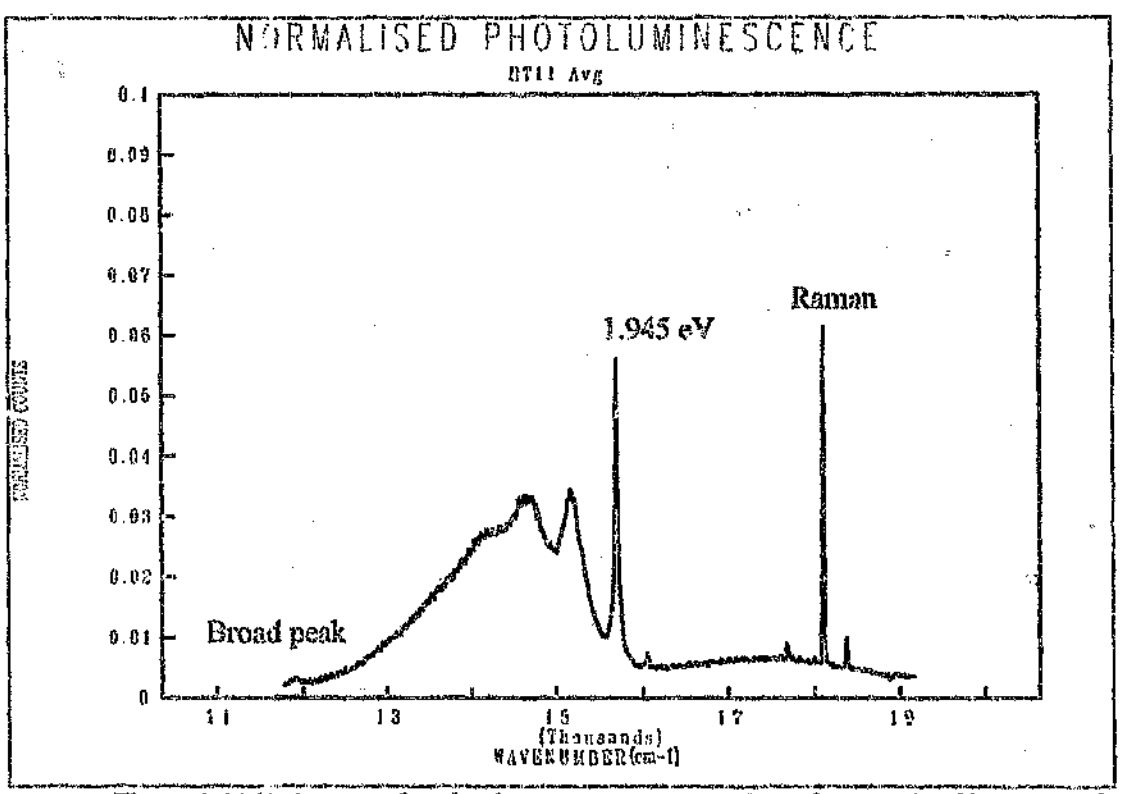

Figure 3.11 b) Average photoluminescence spectrum of powder sample of heat treated SDA, HT11. λ_{exc}=514 nm.

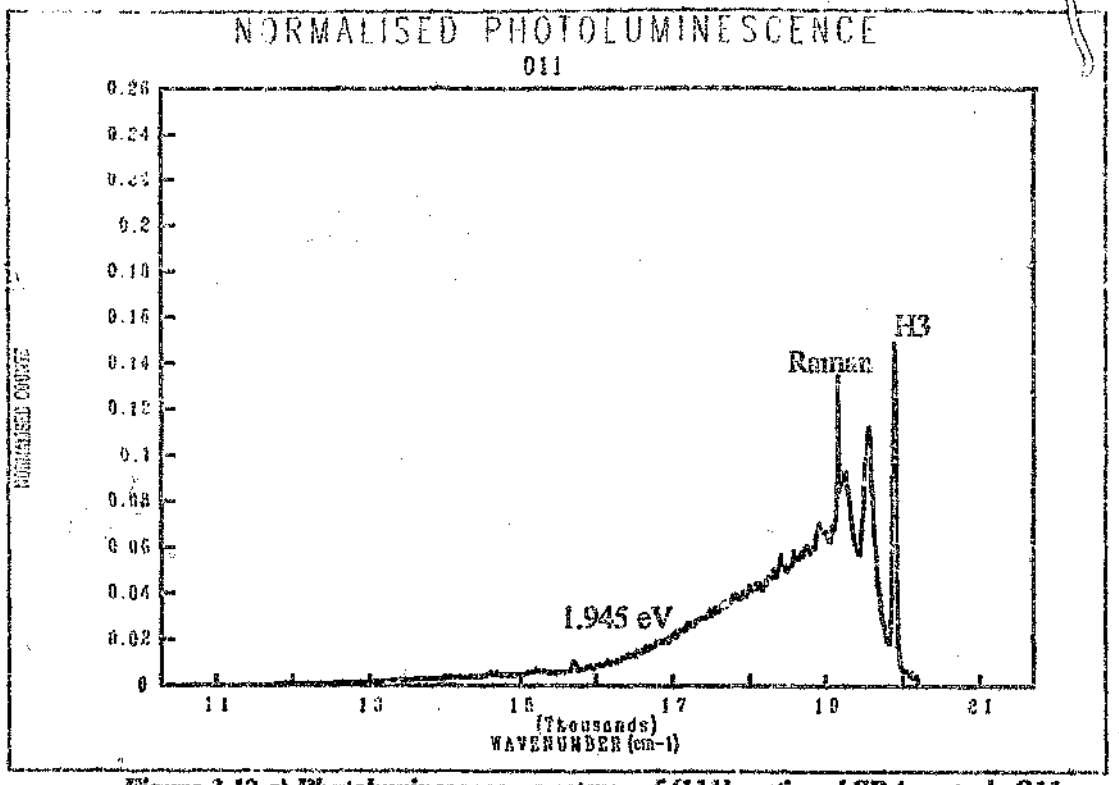

Figure 3.12 a) Photoluminescence spectrum of {111} sectioned SDA: sample O11. λ_{exc}=488 nm.

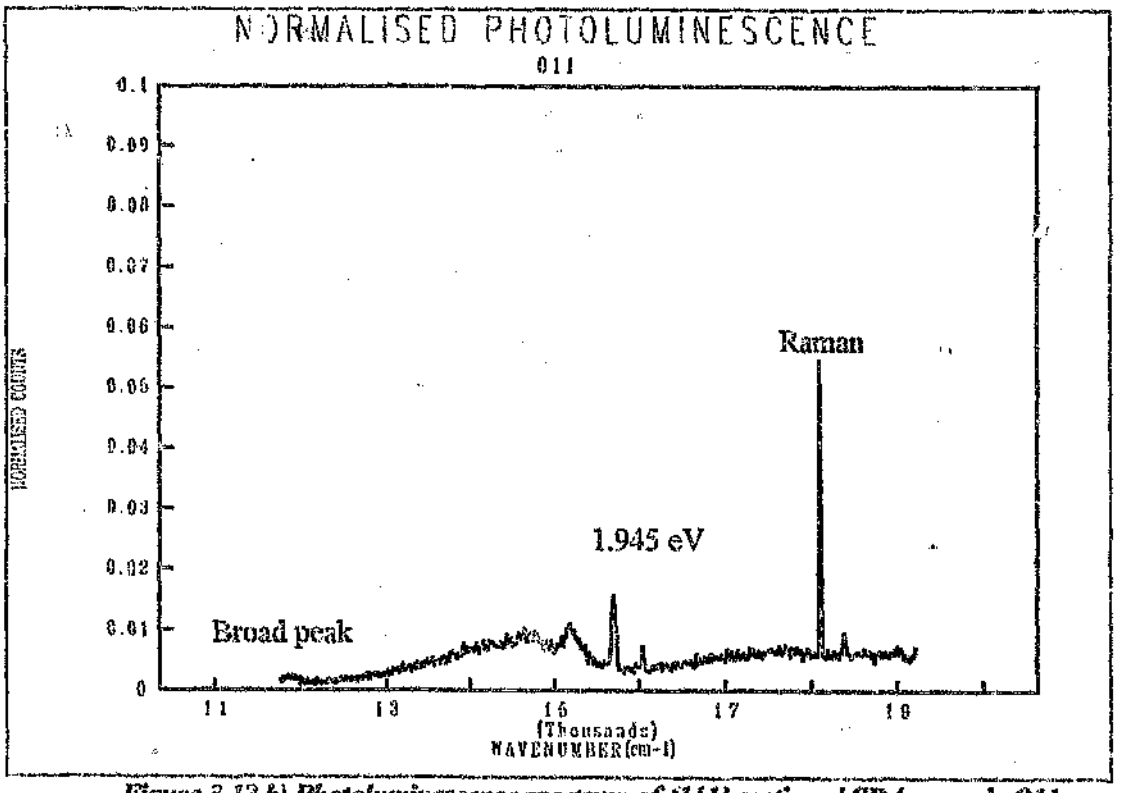

Figure 3.12 b) Photoluminescence spectrum of {111} sectioned SDA: sample O11. λ_{exc}=514 nm.

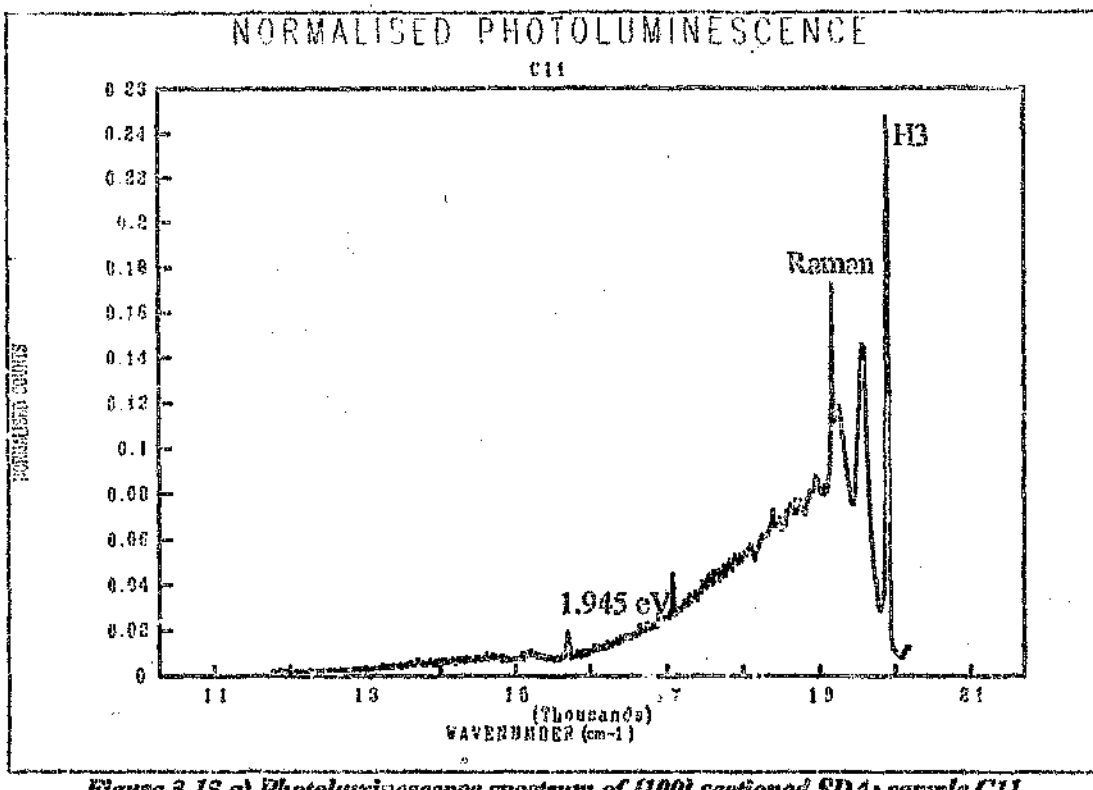

Figure 3.13 a) Photoluminescence spectrum of {100} sectioned SDA: sample C11. λ_{exc}=488 nm.

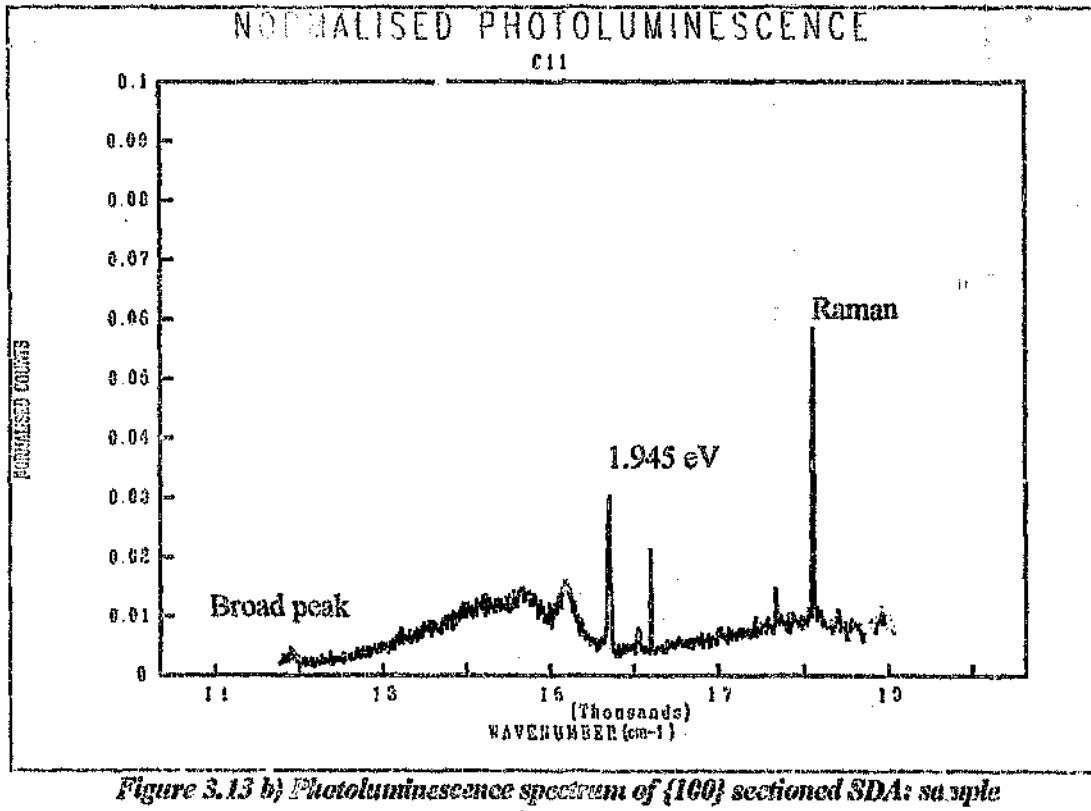

Figure 3.13 b) Photoluminescence spectrum of {100} sectioned SDA: sample C11. λ_{exc}=514 nm.

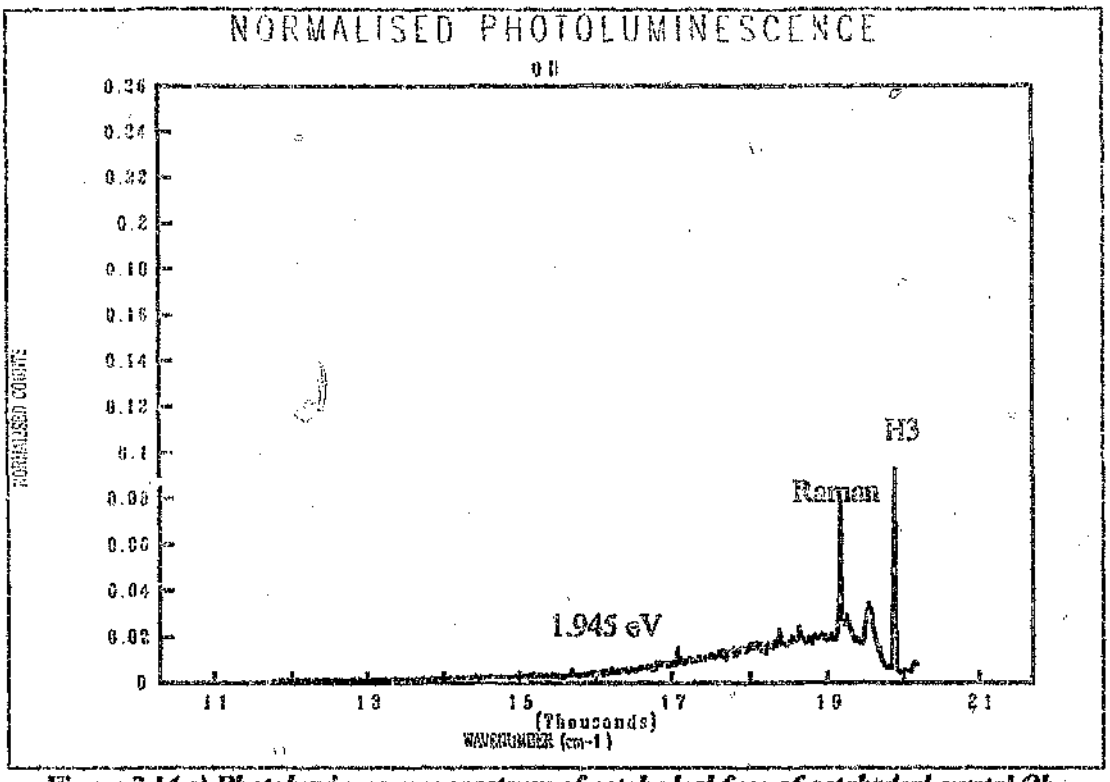

Figure 3.14 a) Photoluminescence spectrum of octahedral face of octahedral crystal Oh. λ_{exc}=488 nm.

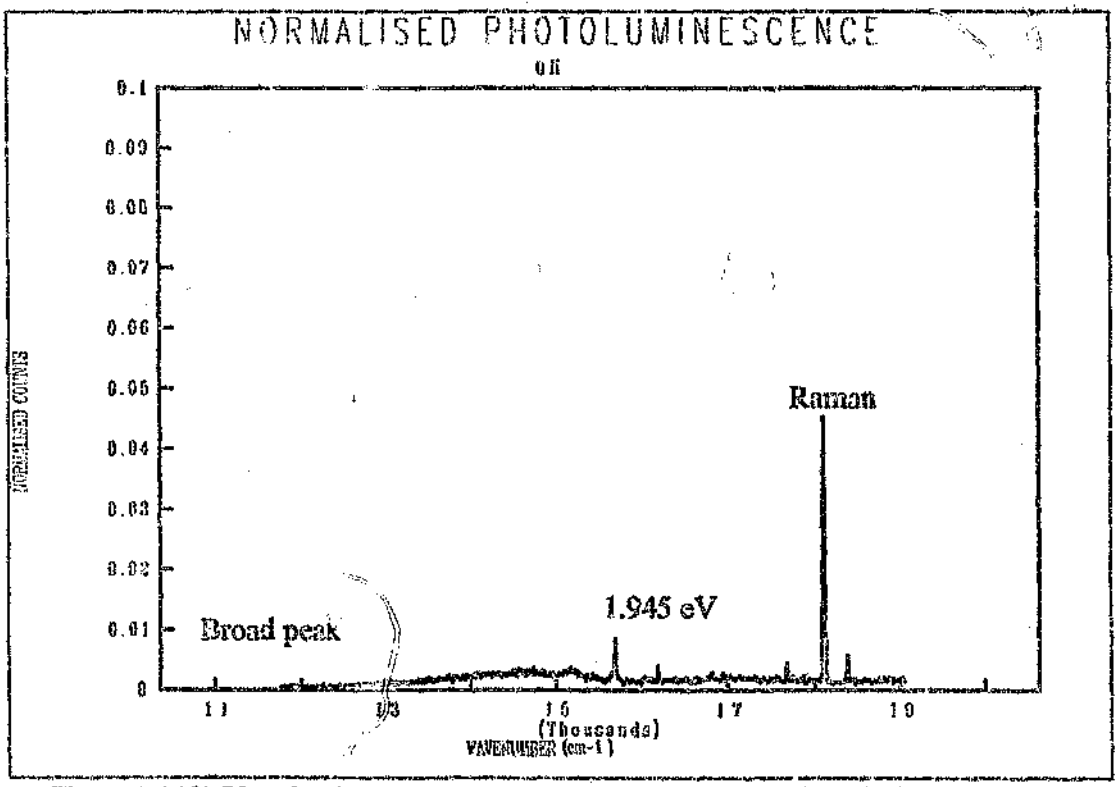

Figure 3.14 b) Photoluminescence spectrum of octahedral face of octahedral crystal Oh. λ_{exc}=514 nm.

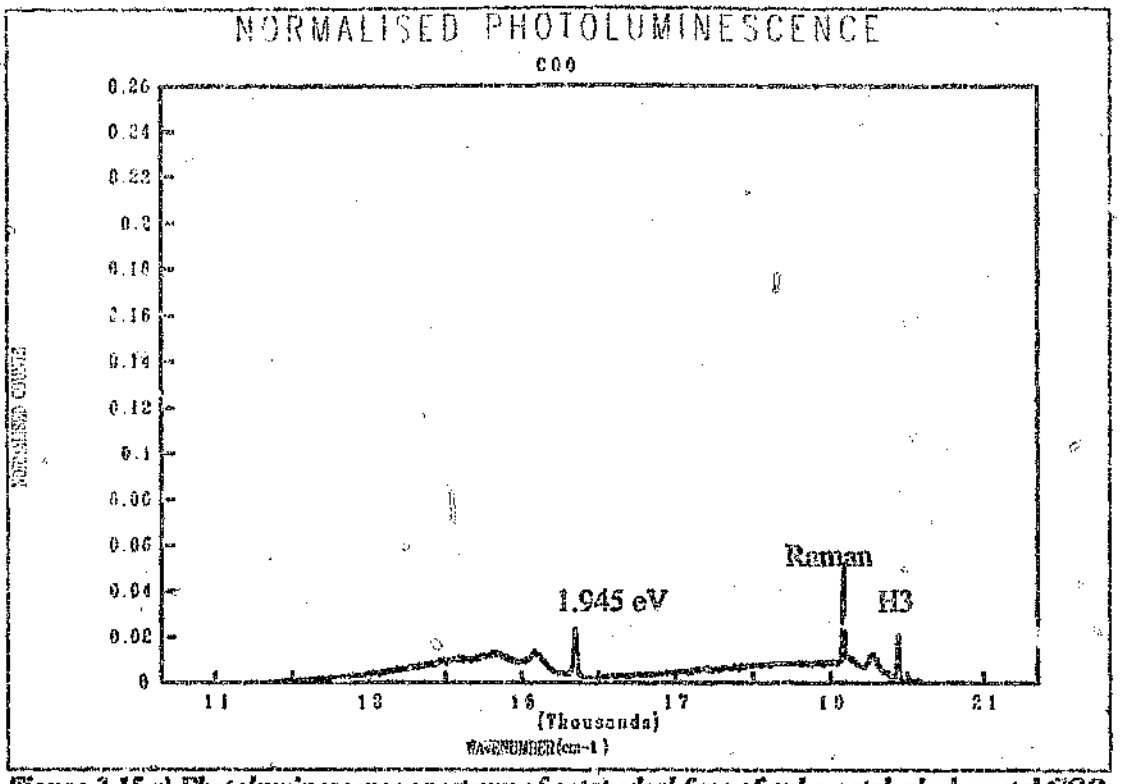

Figure 3.15 a) Photoluminescence spectrum of octahedral face of cubo-octahedral crystal COO. λ_{exc}=488 nm.

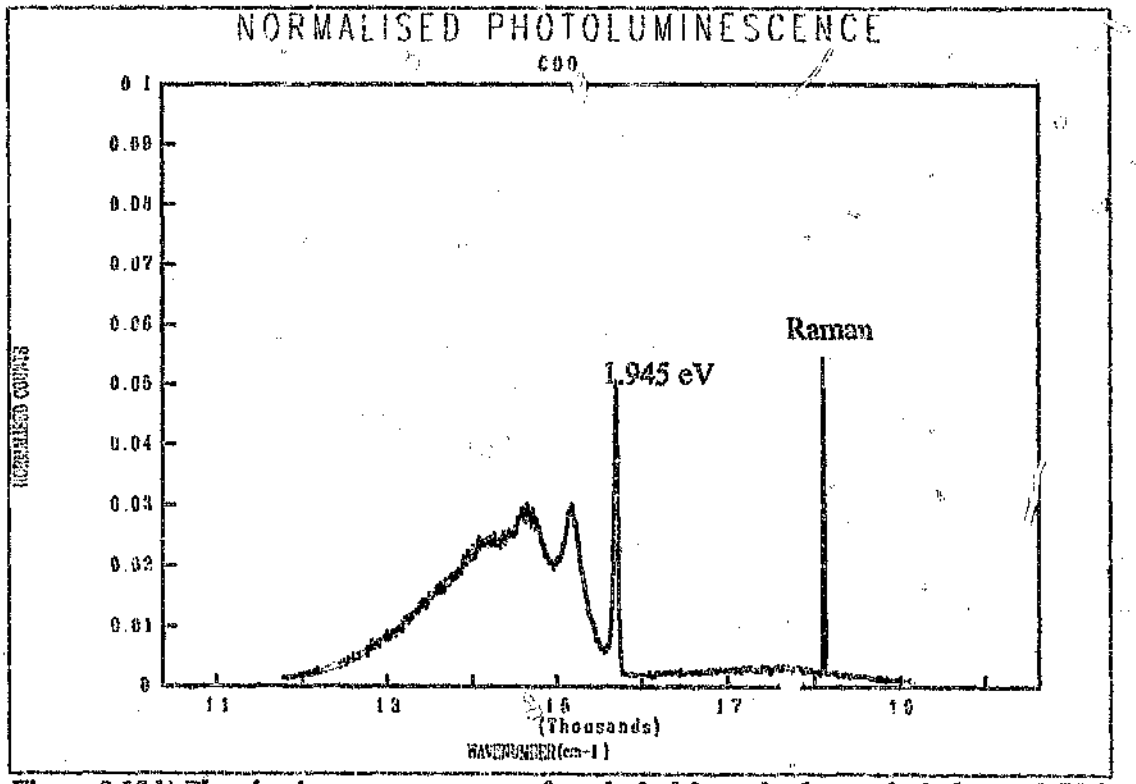

Figure 3.15 b) Photoluminescence spectrum of octahedral face of cubo-octahedral crystal COO. λ_{exc}=514 nm.

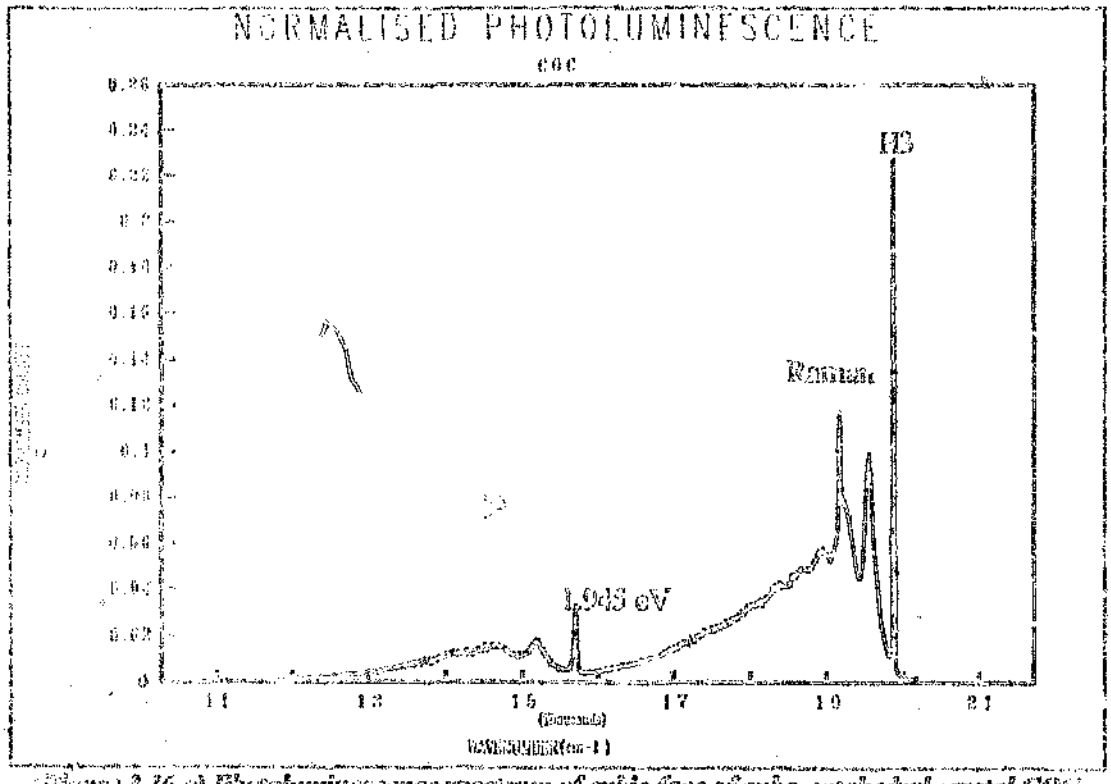

Figure 3.16 a) Photoluminescence spectrum of cubic face of cube-octahedral crystal CC6. λ_{exc}=488 nm.

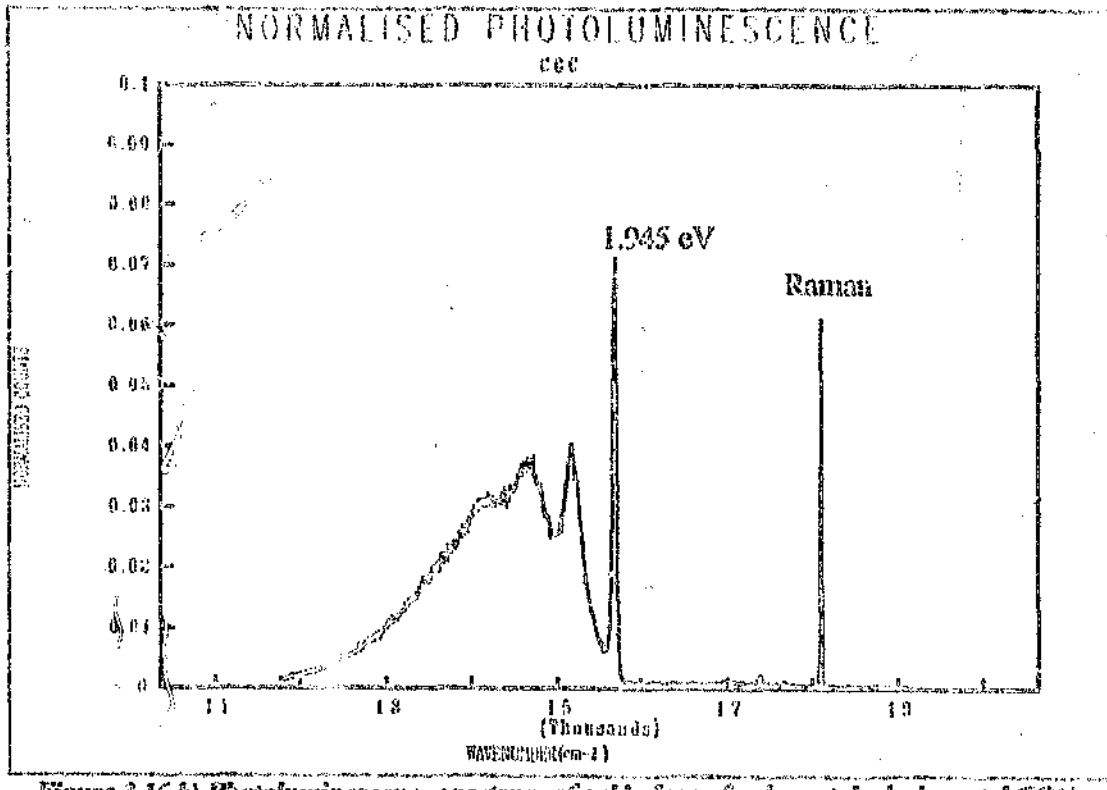

Figure 3.16 b) Photoluminescence spectrum of cubic face of cube-octahedral crystal CC6. λ_{exc}=514 nm.

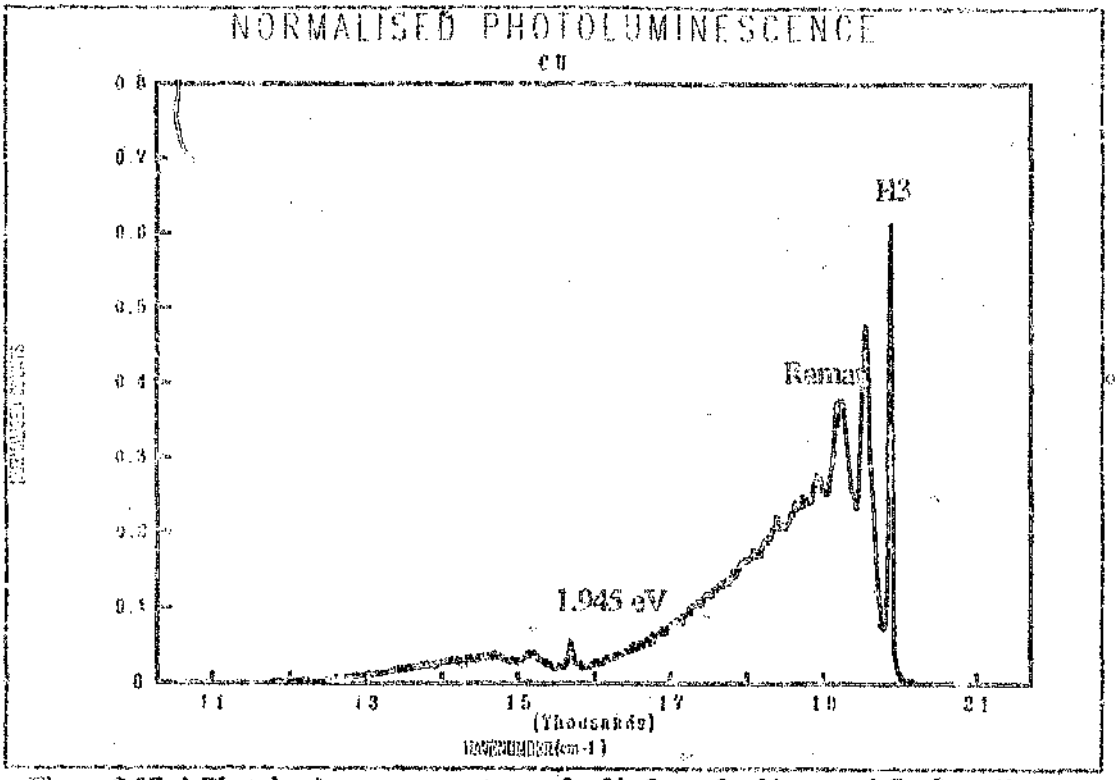

Figure 3.17 a) Photoluminescence spectrum of cubic face of cubic crystal Cu. λ_{exc}=488 nm Note the reduced scale to accomodate the high luminescence intensity.

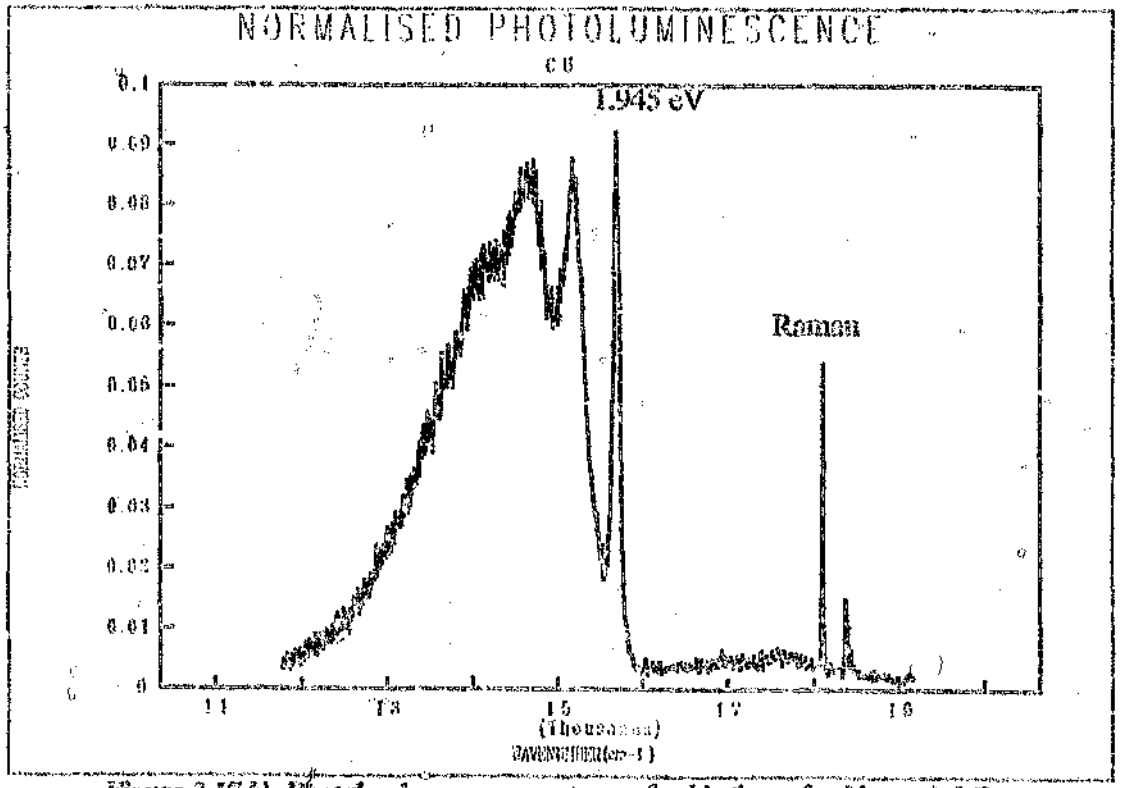

Figure 3.17 b) Photoluminescence spectrum of cubic face of cubic crystal Cu. λ_{exc}=514 nm

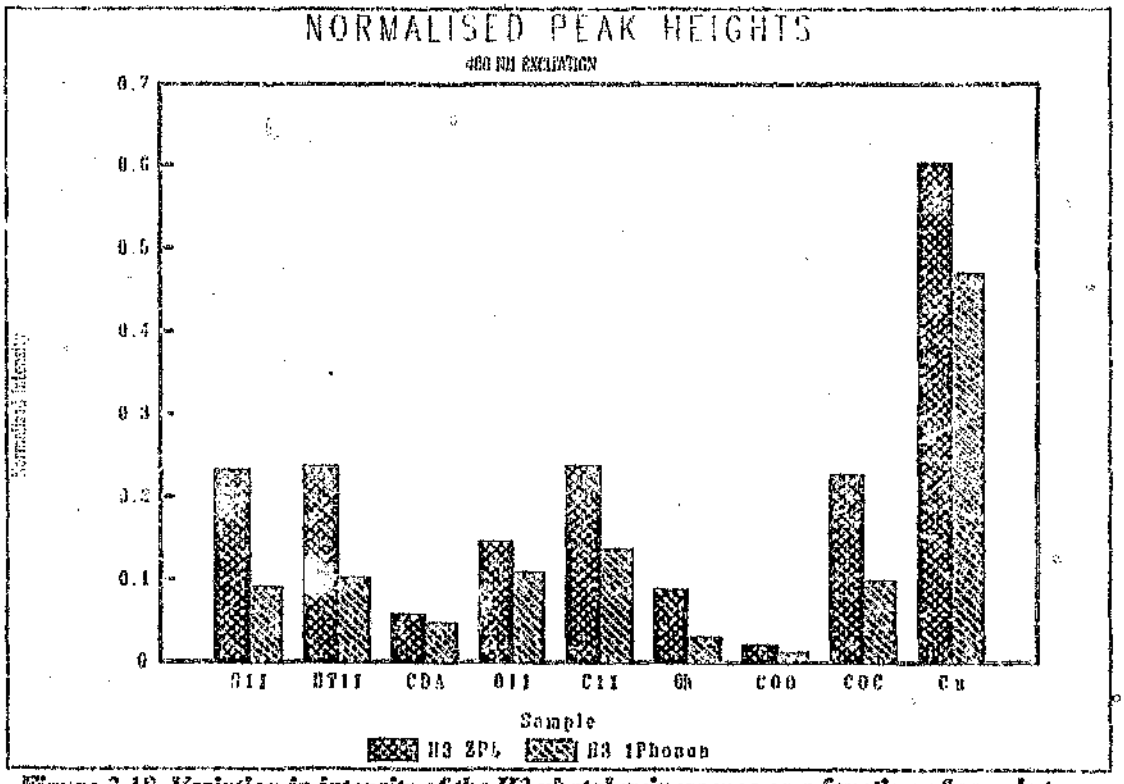

Figure 3.18 Variation in intensity of the H3 photoluminescence as a function of sample type.

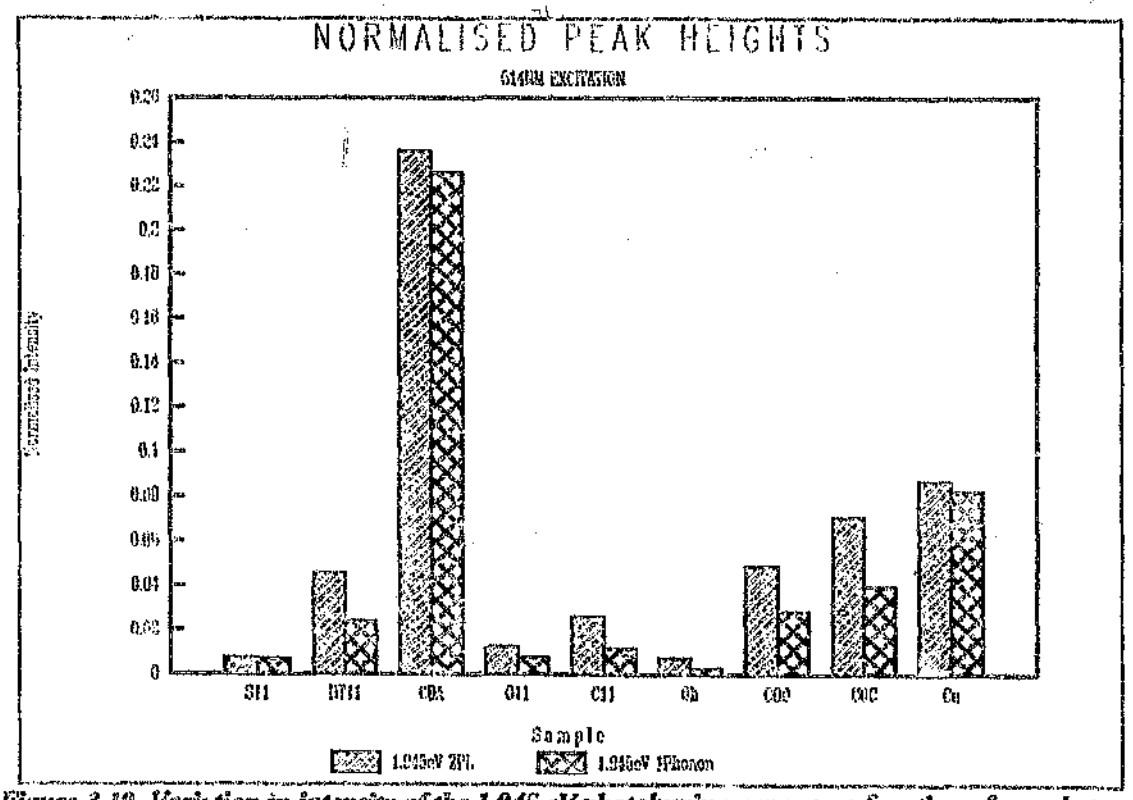

Figure 3.19 Variation in intensity of the 1.945 eV photoluminescence as a function of sample type.

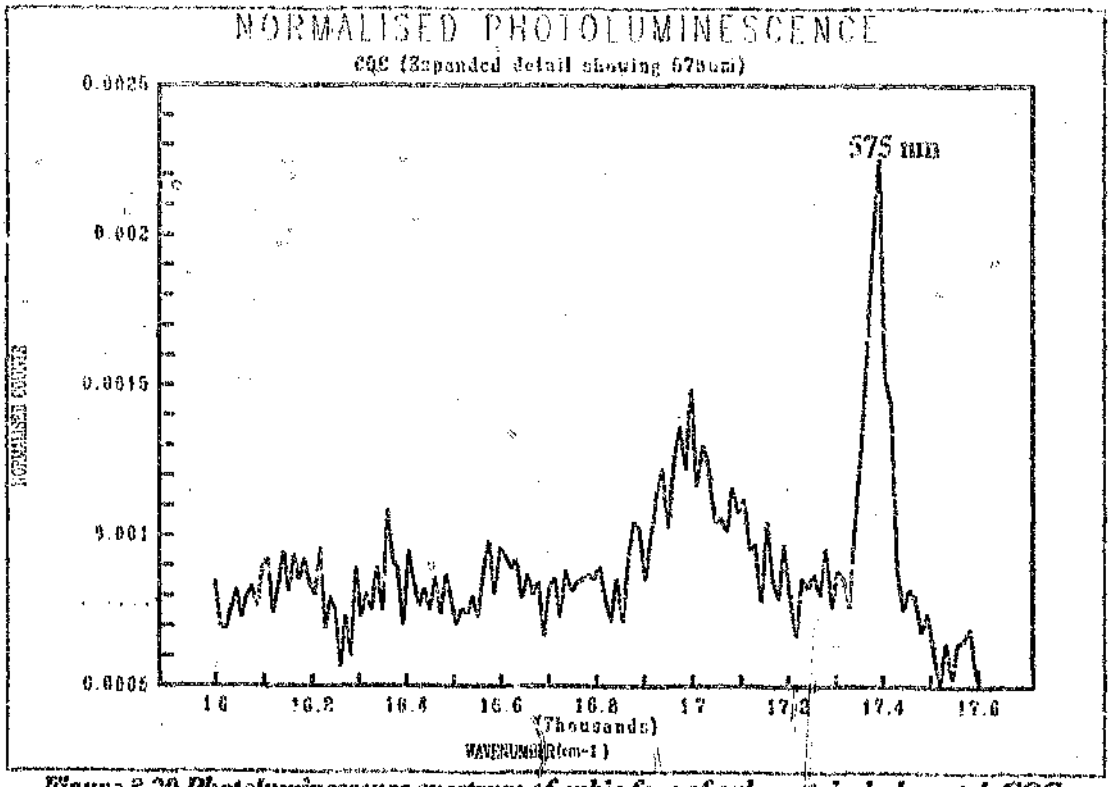

Figure 3.20 Photoluminescence spectrum of cubic face of cubo-octahedral crystal, COC, showing the 575 nm luminescence. λ_{exc}=514 nm.

3.4.1 The H3 Centre

The one phonon intensities may be seen to vary (figure 3.18): Cu >> S11, HT11, C11, O11, COC > CDA > Oh > COO. The diamond type (CDA, SDA or the various types of single crystal) appears to play a major role, as does the morphology or growth zone (of course these two factors are interrelated as the different types of diamond differ not only in their growth history, but also in their morphology). By comparing the intensities of the H3 one phonon line for the {100} and the {111} sections of SDA (C11 and O11), for the {100} and {111} faces of the cubo-octahedral crystal (COC and COO), and for the cubic and the octahedral crystals (Cu and Oh), it is apparent that a higher intensity is favoured in the case of the more cubic growth zones. The cubic crystal, Cu, displays a vastly higher intensity of H3 luminescence than any of the other sample types.

3.4.2 The 1.945 eV Centre

The intensities appear to follow the order (figure 3.19): CDA >> Cu >> COC, COO, HT11 > C11, O11, S11, Oh.

In a similar fashion to the H3 intensity, the intensity of the 1.945 eV one phonon line appears stronger in the case of the more cubic growth zones. Two other cases are notable: the intensity in the case of CDA far exceeds that of any of the other samples; and the intensity in the case of the heat treated SDA powder, HT11 is significantly greater than that of the untreated SDA powder, S11.

The 1.945 eV ZPL broadening is discussed in section 3.6.2.

As all the luminescence centres observed are believed to involve nitrogen atoms, it might be reasonable to suspect that the variation in intensities of all centres are simply the result of the different overall nitrogen concentrations in

the different samples. If this were the major effect, both the 1.945 eV and the H3 centres would correlate with the nitrogen concentration, and could thus be expected to correlate with one another. Figure 3.21 shows that the ratio of the intensity of the one-phonon lines for H3 and 1.945 eV centres do not, in fact correlate very well. Evidently other factors are at work. This representation, however, allows one to easily identify extremes of intensity types: the octahedral crystal, Oh, displays both extremely low H3 and 1.945 eV intensity. The CDA powder sample displays by far the highest 1.945 eV intensity but a low H3 intensity, while the cubic single crystal, Cu, displays a very high H3 intensity and a considerable 1.945 eV intensity.

3.4.3 The 575 nm Centre

In this suite of samples (listed in table 3.5) a very small signal was detected for this centre in the case of COC (figure 3.16). An expanded region of the same spectrum is given in figure 3.20 which shows the zero-phonon line and a few multi-phonon lines.

Summary: Comparison of representative spectra.

- The luminescent defects observed are the H3, the 1.945 eV and in the case of COC the 575 nm vibronic systems as well as an unidentified broad band at about 840 nm (11905 cm^{-1}).

- The powder sample measurement technique results in replicate spectra which are reproducible in terms of the luminescence of the main defect centres.

- The intensity of the both the H3 and the 1.945 eV one-phonon band tends to be higher for more cubic crystals, or in luminescence from {100} faces.

- The cubic crystal, Cu, displayed the highest H3 intensity.

- The CDA powder sample displayed the highest 1.945 eV intensity.
- The 1.945 eV intensity for the heat treated SDA, HT11 is greater than that of the untreated powder sample, S11.
- There is no clear correlation between the H3 and 1.945 eV intensities in the samples discussed in this section.
- The measurement made on the cubic face of the cubo-octahedral crystal, COC, displayed a detectable amount of 575 nm luminescence.

3.5 Statistical Analysis

3.5.1 Correlations between Different Defects within Samples

All the photoluminescent centres discussed in this work have two features in common: nitrogen impurity atoms and vacancies. This might be grounds for expecting correlations to exist between the concentrations of these centres in the same crystals - conditions favouring formation of one type of centre comprised of nitrogen and vacancies might be expected to favour the formation of a different centre containing these same component defects. Statistically, such a scenario can be identified by performing correlation analyses.

3.5.1.1 Large Area Luminescence

A correlation analysis was performed on the intensity of the one phonon peak of the two centres occurring in these samples: the H3 and the 1.945 eV centres. No statistically significant correlation was found (figure 3.21).

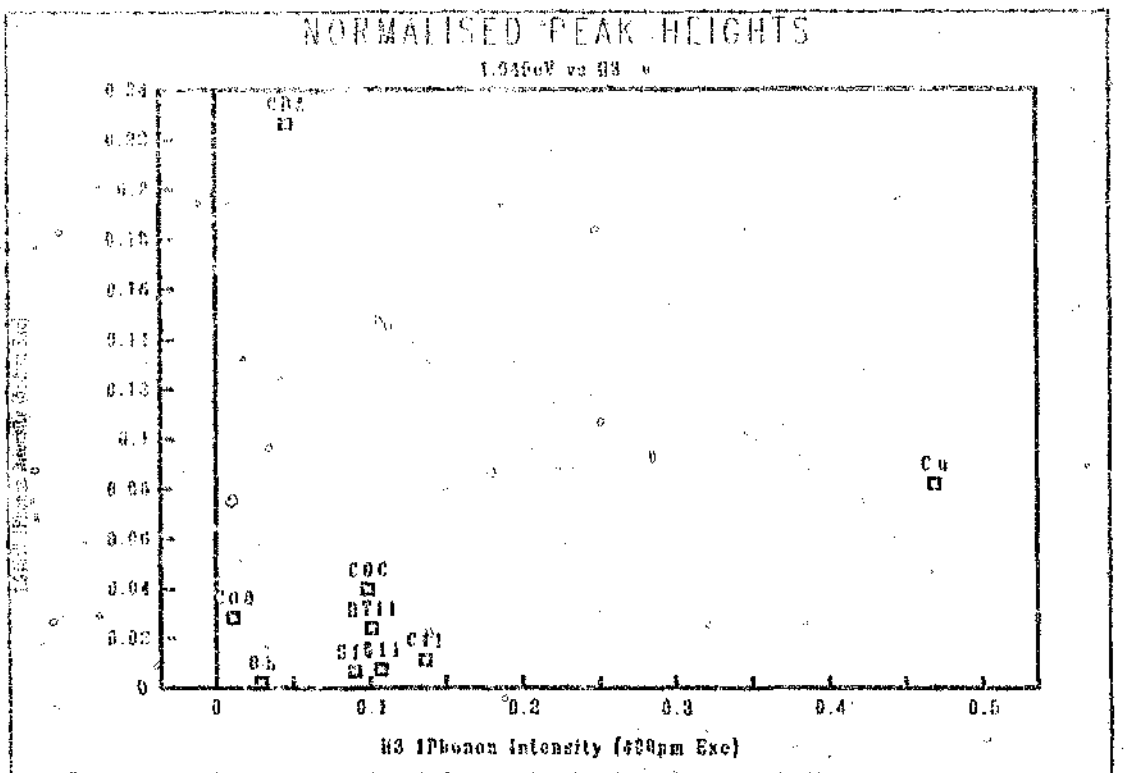

Figure 3.21 Scattergraph showing the evident lack of correlation between the luminescence due to the 1.945 eV and the H3 centres.

3.5.1.2 Small Area Luminescence

This section addresses the powder samples on which the luminescence was collected from a tightly focussed laser spot, effectively sampling very few crystals. These results yielded a wide scatter in the intensities observed for the same sample type (see the section on distributions of intensities: section 3.5.2). This is attributed to the fact that the laser spot size used was at most of similar size to single particles in the powder samples. These results, therefore, approximate those that might be obtained on single crystals. The following analysis explores the correlation between the intensities of the different luminescent centres within the same sample. In this context, the scatter in luminescent intensities observed for the same sample type is of little consequence. On each sample, a measurement was made using both 488 nm and 514 nm excitation wavelengths. The 1.945 eV luminescence is detected in both cases although it occurs on the tail of the phonon sideband of the H3 luminescence in the case of 488 nm excitation. As a rough check on the comparability of these two measurements, the peak height of the zero-phonon line measured in each case is compared in figure 3.22. There is reasonable correlation as indicated by a regression analysis which gives an r^2 value of 89.83 %. The r^2 value is the square of the correlation coefficient explained in the following paragraph, and indicates the percentage of the variation in the measure of the intensity from the 488 nm excitation that can be accounted for by the proposed linear correlation with the intensity from the 514 nm excitation. The value of 89.83 % suggests that no major changes in the position of the laser spot or in the experimental geometry have occurred in changing from one excitation wavelength to the other. The different symbols used in figure 3.22 indicate different sample types. The magnitude of the intensity of the 1.945 eV luminescence appears to vary as a function

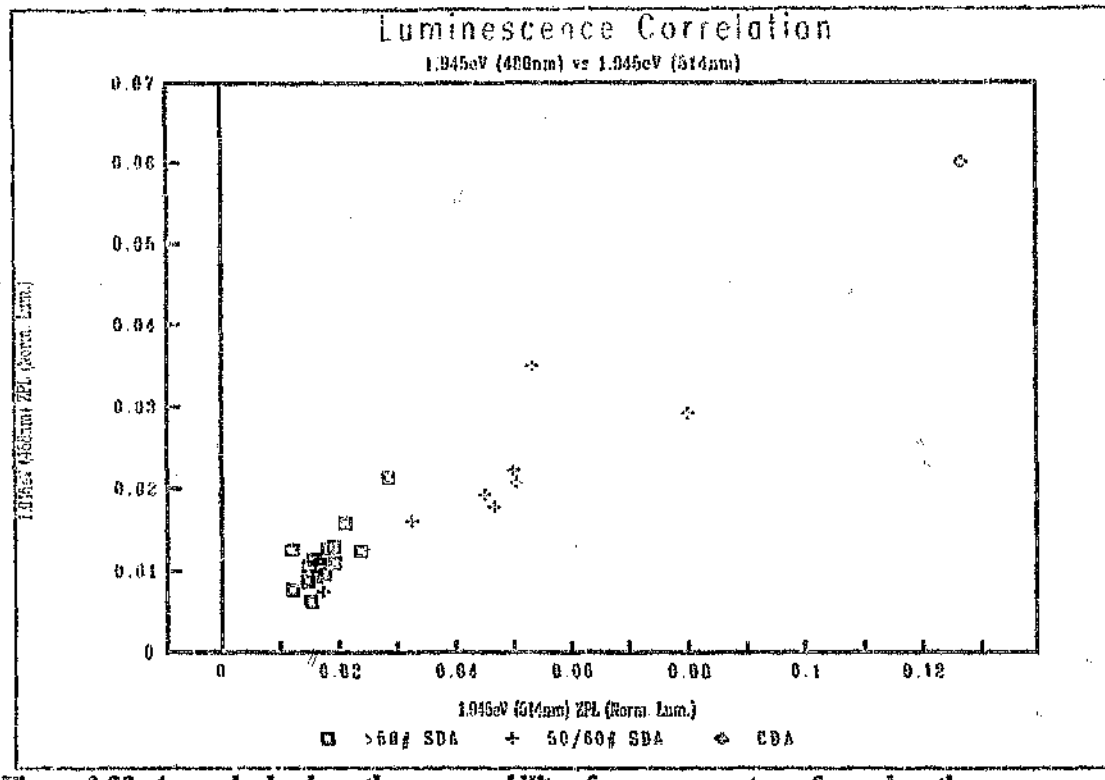

Figure 3.22 A rough check on the comparability of measurements performed on the same samples, using different excitation wavelengths. A reasonable correlation is indicated (r^2 = 89.83 %).

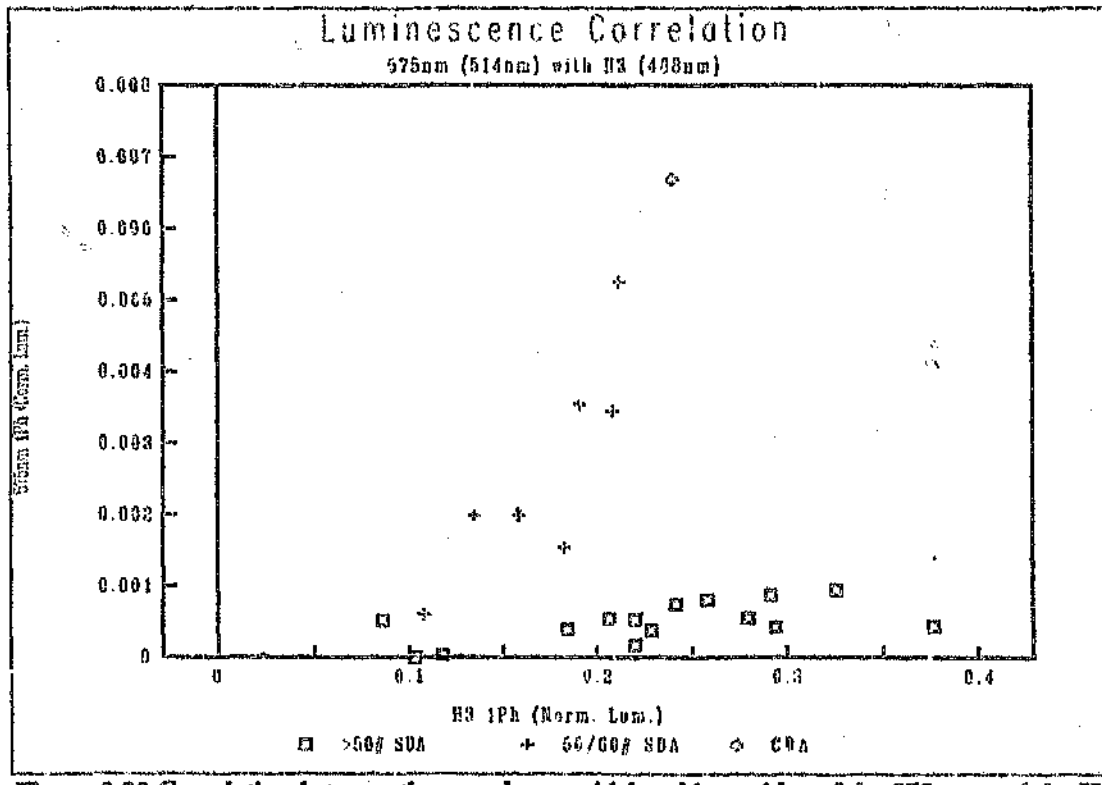

Figure 3.23 Correlation between the one phonon sideband intensities of the 575 nm and the H3 centre. While little correlation is indicated for >50 # SDA samples, a significant correlation might exist for the finer 50/60 # samples.

of the sample type: finer SDA (50/60 #) appears to display a higher level of 1.945 eV intensity than do coarser SDA samples (>50 #). The single point for the much finer CDA grit (140/170 #) displays a still higher intensity.

It is possible to statistically analyse the spectra measured here to see whether there are any correlations between the luminescent intensities of the different defects within the same crystal. This is done by means of a correlation analysis, the results of which are given in table 3.7. The top figure in each block of the matrix in the table gives the correlation coefficient for the correlation between the sample type for that row and the sample type for that column. The correlation coefficient, r, is defined as the square root of the ratio of the explained variation in the data $\Sigma(Y_{est}-Y_{avg})^2$, which is the variation not explained by the model being evaluated (linear correlation in this case), to the total variation $\Sigma(Y-Y_{avg})^2$ (Spiegel 1988). A correlation coefficient of 1 in this case would suggest that a positive linear relationship between the two defect types explains all of the variation (a value of -1 would suggest a negative linear correlation). (Note that the square of the correlation coefficient, which is always positive, is the r^2 referred to above.) The bottom figure in each block gives the significance level (This is the probability that the correlation observed would occur purely by chance. The percentage confidence level of the correlation is given by $(1 - p) \times 100$, where p is the significance level.) The correlation matrix is necessarily symmetrical about the diagonal. In table 3.7, only the correlation between the one-phonon intensities of the 575 nm centre and the 1.945 eV centre are significant (with a confidence level of 99.99 %), with a correlation coefficient of 0.8921.

The correlation between the height of the one phonon sidebands of the 575 nm and the H3 centre is shown in figure 3.23, that between the 575

nm and the 1.945 eV centres is shown in figure 3.24, and that between the 1.945 eV and the H3 centres is shown as figure 3.25.

Table 3.7

Correlation of intensity of one phonon lines for all small area luminescence samples (n=37)			
Correlation matrix			
Centre	H3	1.945 eV	575 nm
H3	1.000 .0000	.0934 .6432	.1259 .5314
1.945 eV	.0934 .6432	1.000 .0000	.8921 .0000
575 nm	.1259 .5314	.8921 .0000	1.000 .0000

Only the correlation between the intensity of the 575 nm and the 1.945 eV centres is significant at the 95 % level.

The multiple correlation analysis in table 3.7 indicated that the correlation between the 575 nm one-phonon intensity and that of H3 was insignificant. If one examines the data in the content of the sample type as indicated by the different symbols used in figure 3.23, it appears that while there appears to be little correlation between the 575 nm luminescence intensity and that of H3 for SDA samples with grit size coarser than 50 #, there could well be a significant correlation for the samples of the finer 50/60 # grit size. The correlation between 1.945 eV luminescence intensity (as measured by the height of the one phonon line of the luminescence excited by 514 nm laser illumination) and that of H3 (excited by 488 nm laser illumination) displays no apparent correlation, either in table 3.7, or in figure 3.25. However, the data appears to be grouped by the sample grit size, with the finer grit

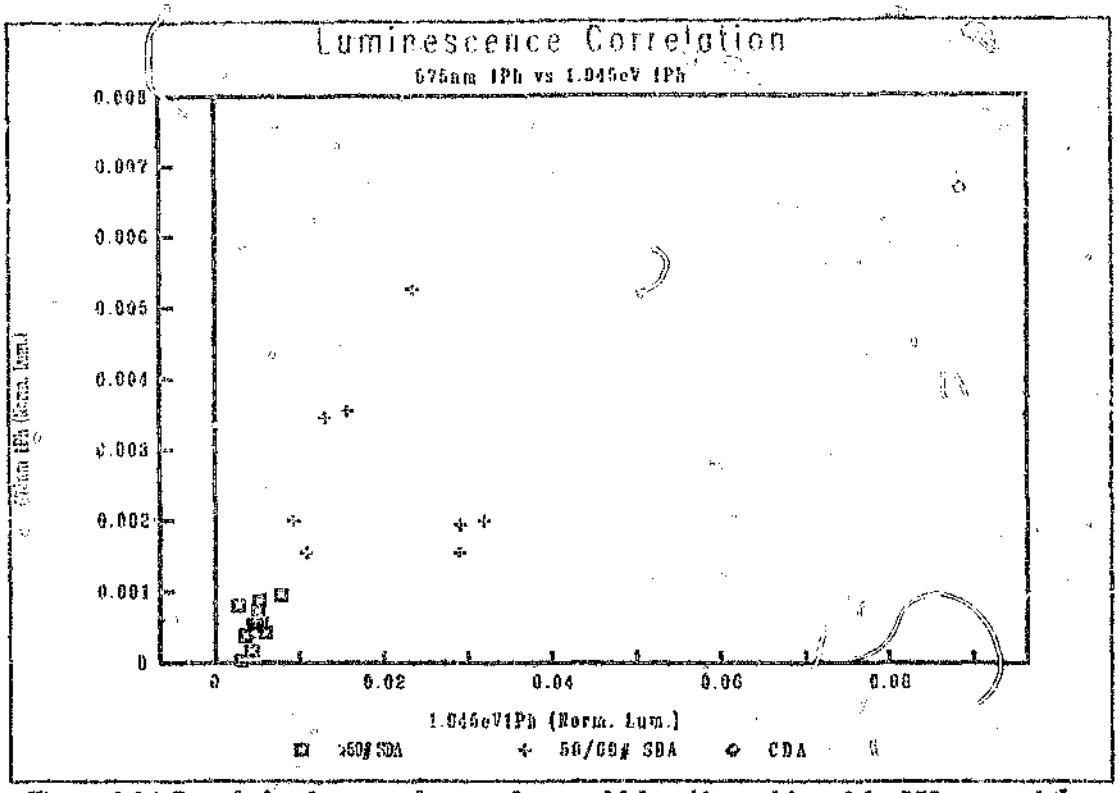

Figure 3.24 Correlation between the one phonon sideband intensities of the 575 nm and the 1.945 eV centres. A significant correlation can be seen to exist.

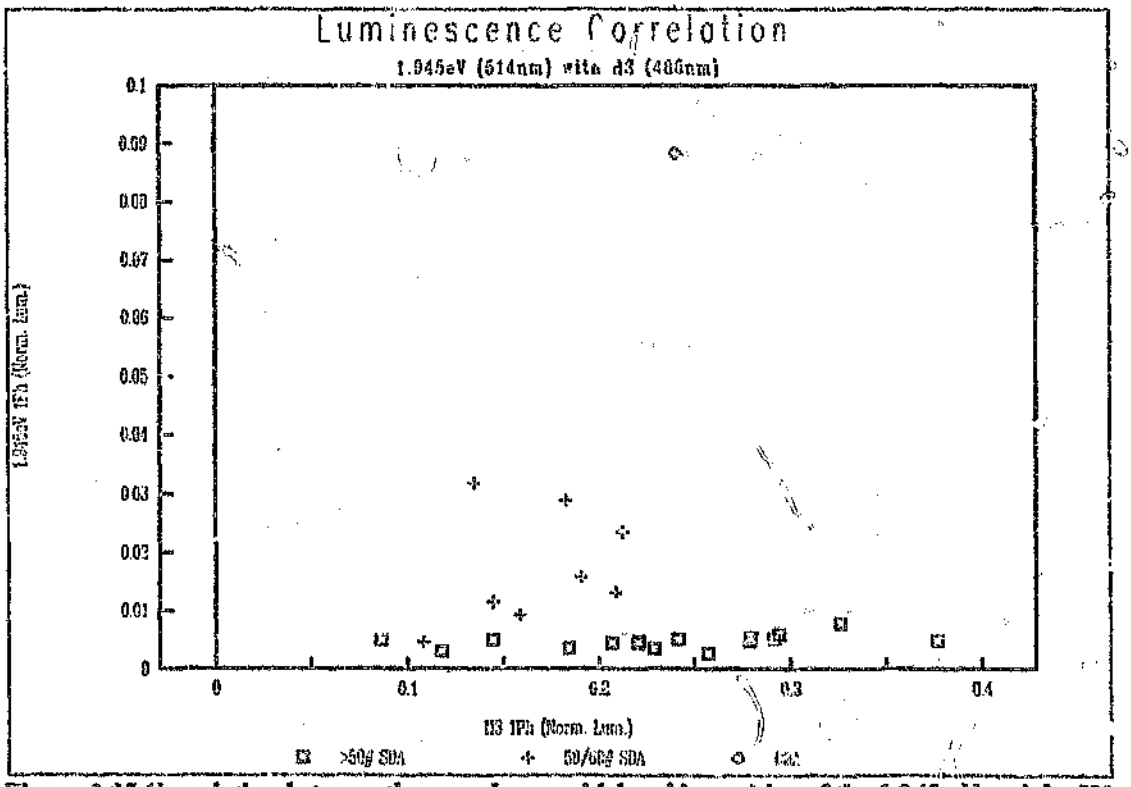

Figure 3.25 Correlation between the one phonon sideband intensities of the 1.945 eV and the H3 centres. No significant correlation appears to exist.

(50/60 #) displaying higher 1.945 eV intensities than the coarser grits. The grouping of the intensities of the luminescence from the different luminescent centres as a function of the sample type and grit size (for SDA samples) will be examined in the following section (section 3.5.2) in more detail.

As a means of testing the apparent correlation between the intensity of the one phonon line for 575 nm luminescence and that of H3 as a function of the sample type for 50/60 # samples only, a multiple correlation analysis was performed on samples of 50/60 # and again on samples coarser than this. Table 3.8 gives the results for grits coarser than 50 #, and table 3.9 for grits of 50/60 #. The correlation between the intensity of the 575 nm centre and that of the 1.945 eV centre, which was noted above, is again evident for both grit size groups. However, for the 50/60 # grit size only, the correlation between the intensities of the 575 nm centre and the H3 centre is also significant at the 99 % level.

Table 3.8

Correlation of intensity of one-phonon lines for >50 # samples (n=17)			
Correlation matrix			
Centre	**H3**	**1.945 eV**	**575 nm**
H3	1.000	-.0631	.1907
	.0000	.8099	.4635
1.945 eV	-.0631	1.000	.7796
	.8099	.0000	.0002
575 nm	.1907	.7796	1.000
	.4635	.0002	.0000

Only the correlation between the intensities of the 575 nm and the 1.945 eV centres is significant at the 95 % level.

Table 3.2

Correlation of intensity of one phonon lines for 50/60 # samples (n=9)			
Correlation matrix			
Centre	H3	1.945 eV	575 nm
H3	1.000	.6172	.8805
	.0000	.0766	.0017
1.945 eV	.6172	1.000	.7766
	.0766	.0000	.0138
575 nm	.8805	.7766	1.000
	.0017	.0138	.0000

Only the correlation between the intensities of the 575 nm and the 1.945 eV and H3 centres is significant at the 95 % level.

Summary : Correlations between Defect Intensities

- A general correlation between the intensity of the one phonon lines of the 575 nm defect and that of the 1.945 eV defect exists where both these defects exist in the same sample, irrespective of sample grit size.

- For 50/60 #, there appears to be an additional correlation between the intensity of the 575 nm and the H3 one phonon line intensities.

3.5.2 Frequency Distributions

3.5.2.1 Introduction

In the case of the small area luminescence measurements, many measurements were made on samples of similar type. In this section, these results are analysed as replicate measurements on two sizes of SDA grit : SDA 40/45 #, and SDA 50/60 #. Clearly, in view of the very small laser spot size, each measurement can be considered as the measurement of a single crystal, or of a sample of very few crystals. One consequently expects to obtain a distribution of results for each sample type. The results are plotted as frequency distributions of the peak height of the luminescent intensity of the different luminescent systems.

The differences observed for the distributions of intensities could be of two types: differences in the range of intensities measured for a grit size (i.e. of the variance); or differences in the value of the mean value about which the results are scattered. Differences in the variance can be tested for significance using the F-test. Differences in the mean can be tested for significance using the "Student's t" test. In the case of unequal variance in the two means, however, an approximate t-test must be used. This does not pool variances, but adjusts the degrees of freedom (Underhill, 1985).

3.5.2.2 The 1.945 eV Centre

The frequency distribution shown in figure 3.26 shows a very sharp distribution for the 1.945 eV peak heights for the 13 samples of 40/45 # grit, while the distribution for the 8 samples of 50/60 # grit is broad and shifted to higher intensities. The 1.945 eV luminescence intensities for 40/45 # grit are lower than that of the 50/60 # grit and scatter over

a much narrower range. The distribution for the 1.945 eV luminescence of the 40/45 # grit is displayed in figure 3.27. Both the differences in the variance and the mean test significant at the 95 % confidence level.

3.5.2.3 The H3 Centre

There are only small differences in the frequency distribution for the two grit sizes: a slight broadening of the distribution and a shift to higher intensities for the 13 samples of 40/45 # grit (figure 3.28). The differences in both the variance and the mean test significant at the 95 % confidence level.

3.5.2.4 The 575 nm Centre

The frequency distribution for the 575 nm intensities is shown in figures 3.29 and 3.30. The 13 samples of 40/45 # grit display a narrow distribution of intensities, generally of lower intensity than that observed for the 8 samples of 50/60 # grit. Both the ratio of the variance and the differences between the means test significant at the 95 % confidence level.

Summary : Luminescence Intensity Frequency Distributions

The data are summarised in table 3.10 below.

- The foregoing analysis suggests that systematic differences between the intensity of the luminescence for the two grit sizes are probable for all defect centres.
- These differences would be small for H3 (slightly lower and less variable for 50/60 # than for 40/45 #), and more pronounced for 1.945 eV and 575 nm defects.

- The intensity for the 1.945 eV luminescence in the 50/60 # grit would be far more variable, and generally higher than that for the 40/45 # grit.

- A similar situation would exist for the 575 nm luminescence.

Table 3.10

Grit Size	40/45 #	50/60 #	40/45 #	50/60 #	40/45 #	50/60 #
Centre	H3	H3	1.945 eV	1.945 eV	575 nm	575 nm
Average	0.235	0.168	0.0048	0.0173	0.0004	0.0024
Std Dev	0.081	0.035	0.0012	0.0091	0.0003	0.0014

Section 3.5.2, an analysis of the frequency distributions of the intensities of the luminescence of the different centres, is summarised in this table by giving the average and standard deviation of the luminescence intensity for the different luminescent centres for both the >50/60 # and the 40/45 # sizes.

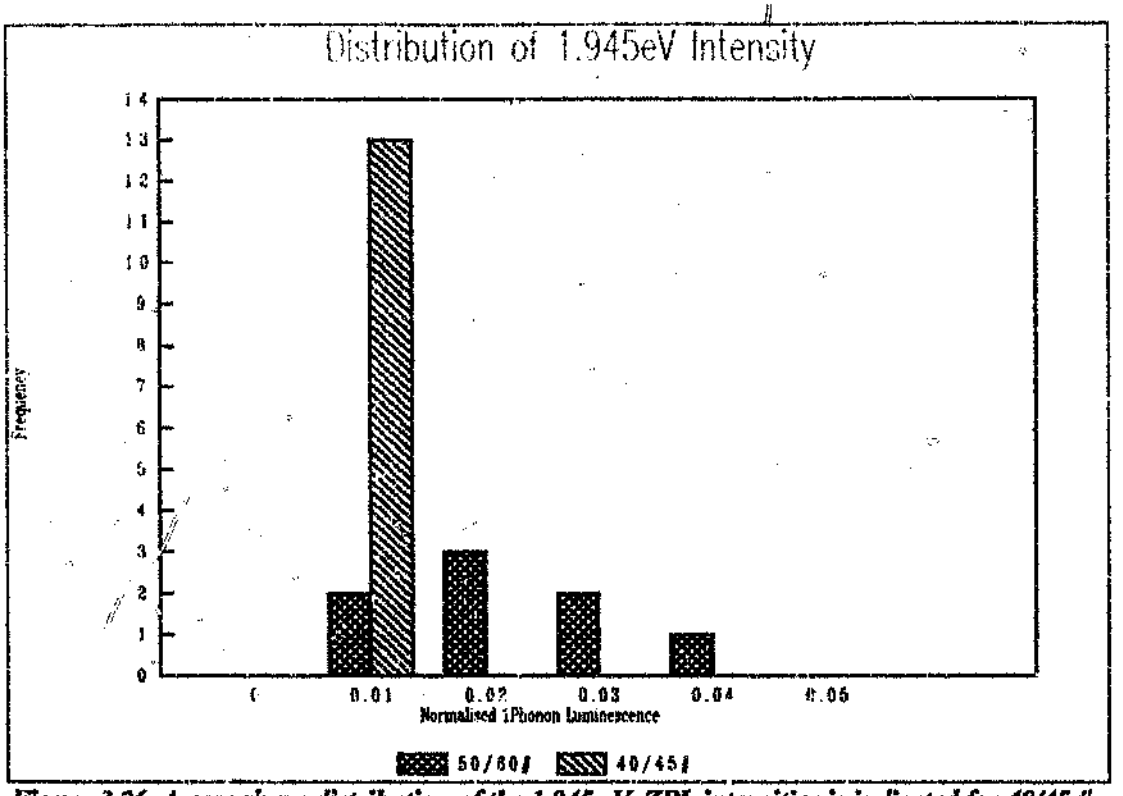

Figure 3.26 A very sharp distribution of the 1.945 eV ZPL intensities is indicated for 40/45 # SDA grit, while the distribution for 50/60 # grit is broader and shifted to higher intensities.

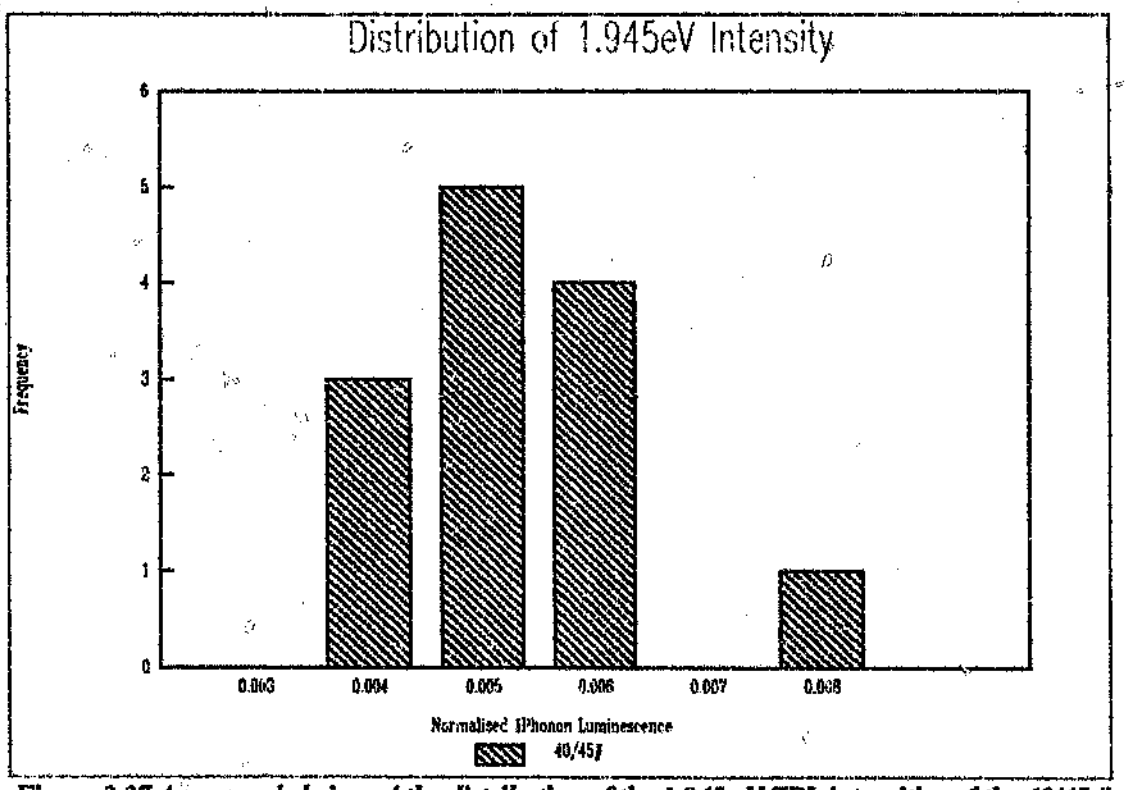

Figure 3.27 An expanded view of the distribution of the 1.945 eV ZPL intensities of the 40/45 # SDA grit from figure 3.26 above. Differences in both the variance and mean are significant at 95 %.

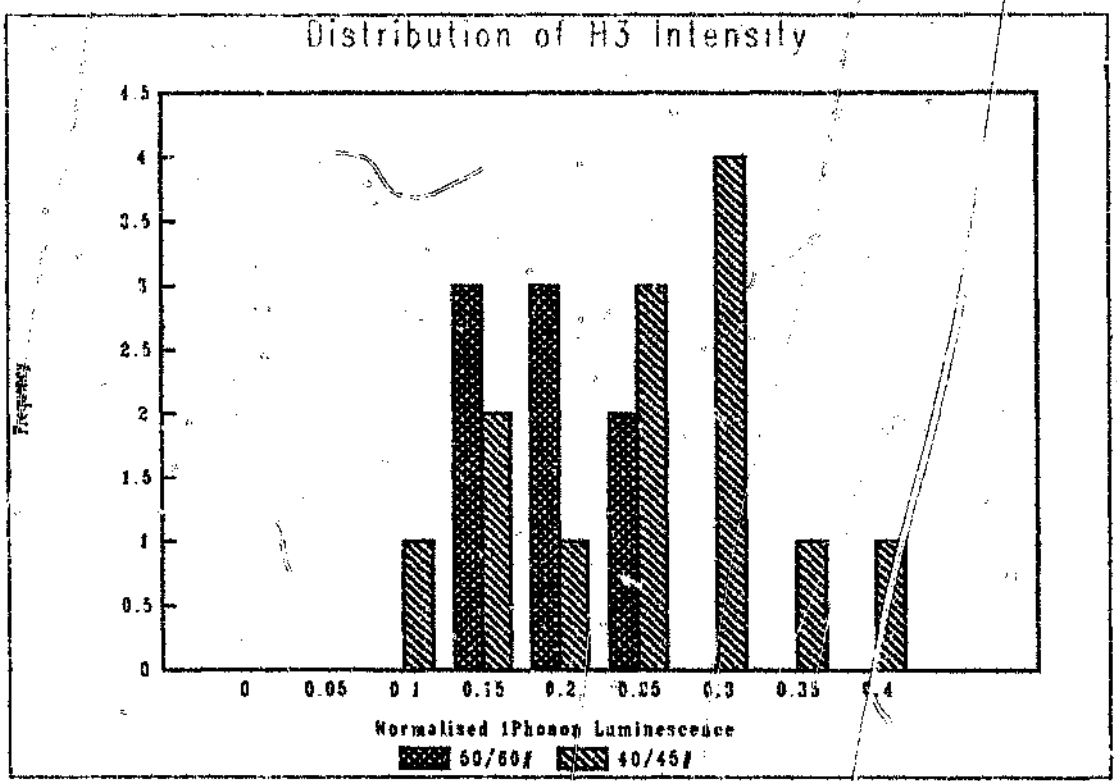

Figure 3.28 The distribution of the H3 ZPL intensities of 40/45 # SDA grit is slightly broadened and shifted to higher intensities compared to that of the 50/60 # grit. Differences in both the variance and mean are significant at 95 %.

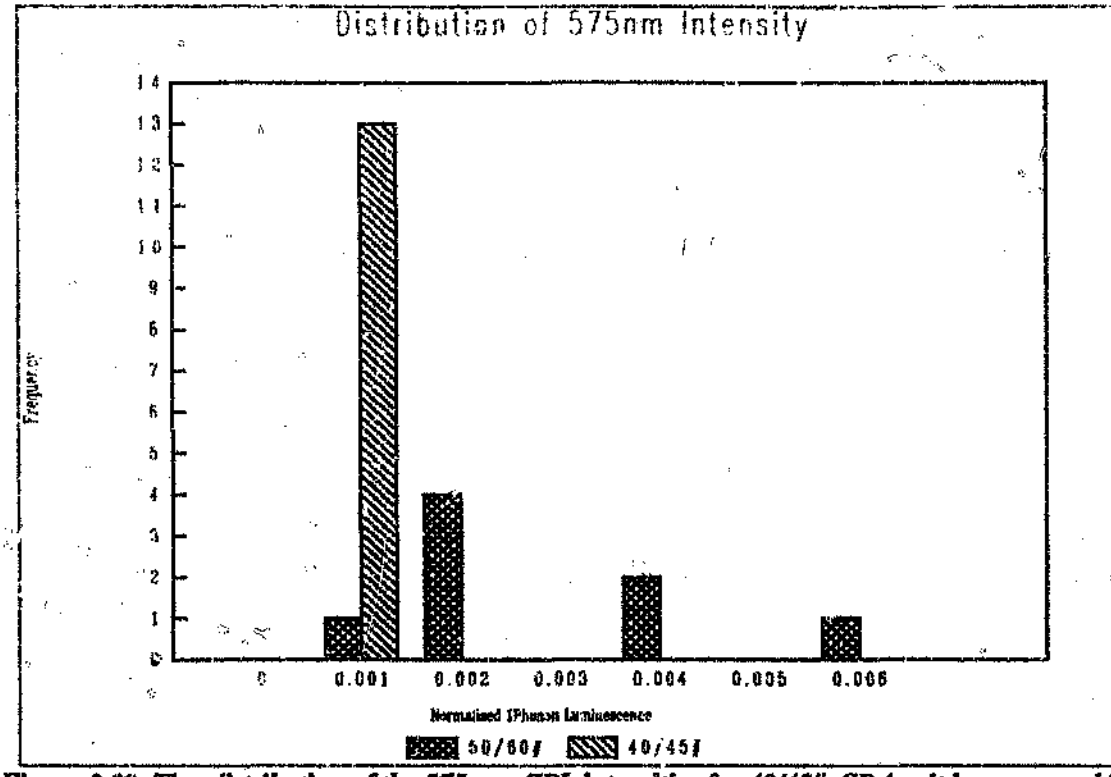

Figure 3.29. The distribution of the 575 nm ZPL intensities for 40/45# SDA grit is narrow, while that of 50/60 # grit is broader and shifted to higher intensities.

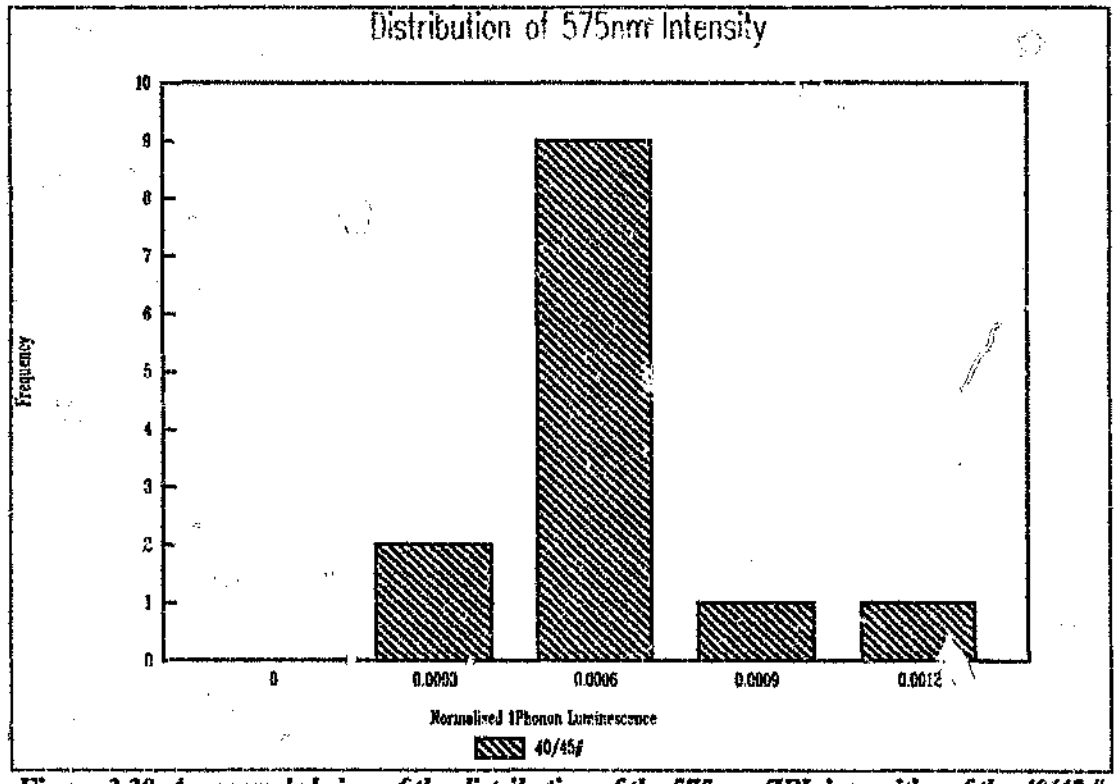

Figure 3.30 An expanded view of the distribution of the 575 nm ZPL intensities of the 40/45 # SDA grit from figure 3.29 above. These all fall into the first interval above by virtue of the choice of interval. Differences in both the variance and mean are significant at 95 %.

3.6 Lineshape Analysis

3.6.1 Analysis of the Shape of the 1.945 eV ZPL

A lineshape resulting from broadening due to independent Gaussian and Lorentzian shapes has an intensity distribution known as a Voigt profile. This can be expressed as :

$$I(\alpha, \nu) = \frac{\alpha}{\pi}\int_{-\infty}^{+\infty} \frac{\exp(-y^2)}{\alpha^2+(\nu-y)^2}dy \qquad ..11$$

Where $\nu = \frac{(\nu-\nu_0)}{\left(\frac{\Gamma'_G}{2}\right)}$, and $\Gamma'_G = (\ln 2)^{-\frac{1}{2}}\Gamma_G$, and Γ_G = Gaussian FWHH

And where $\alpha = \frac{\Gamma_L}{\Gamma'_G}$, (Γ_L = Lorentzian FWHH).
(Posener 1959).

The Voigt profile can be approximated by the bi-quadrated function :

$$I = \frac{I_0}{1+\alpha\left(\frac{(\nu-\nu_0)}{\frac{\Gamma}{2}}\right)^2+(1-\alpha)\left(\frac{(\nu-\nu_0)}{\frac{\Gamma}{2}}\right)^4} \qquad ..12$$

Γ=FWHH, α=0.5 for a Gaussian profile, and α=1 for a Lorentzian profile (Müller 1980).

The ratio of the FWHH of the Lorentzian or Gaussian component occurring in the convolution to the effective FWHH of the final convoluted lineshape, Γ_L/Γ or Γ_G/Γ respectively, are related to the form factor, α in equation 12 above.

The lineshape of the experimentally measured 1.945 eV zero-phonon lines were determined by fitting equation 12 to the suitably scaled spectra. The results are given in table 3.11 below. (Note that the lineshape for O11, the SDA sample S11 sectioned parallel to an {111} face was found to be best

fitted by a superposition of two such Voigt profiles (figure 3.40), possibly as result of the presence of a cracked diamond in the sample (see section 2.2.2). The fitting parameters for the larger of the two components is given in this table, however, this datapoint should be treated circumspectly as regards the FWHH and the lineshape. The measured 1.945 eV ZPLs are illustrated in figures 3.31 to 3.39.

Table 3.11

The curve fitting parameters found for the 1.945 eV ZPL									
Sample	S11	HT11	CDA	O11	C11	COC	COO	Oh	Cv
α	0.970	1	0.821	0.644	0.706	0.869	0.746	0.987	0.611
Γ (cm^{-1})	15.15	25.21	61.94	40.32	35.83	45.10	45.45	14.42	88.10
Γ_L/Γ	0.62	1	0.35	0.20	0.23	0.39	0.26	0.73	0.19
Γ_G/Γ	0.72	0	0.96	1.06	1.04	0.92	1.02	0.59	1.08

Lineshape parameters found by fitting the Voigt profile to the 1.945 eV ZPLs using the approach of Müller (1980).

It should be noted that the monochromator slit widths were at an effective bandpass of 2 cm^{-1}. No effort was made to correct for the effect of instrumental broadening. It has been shown by measurement and calculation (Cary 17 spectrophotometer manual) that an instrument bandpass-to-FWHH ratio of less than 1:10 results in a deviation from the true peak height of less than 0.5%. Hughes (1968), in lineshape analysis work on ZPLs in alkali halides, deemed it unnecessary to correct for instrument broadening for an instrument bandpass-to-FWHH ratio of 1:10. Only two FWHH (that for S11 at 15.15 cm^{-1}, and that for Oh at 14.42 cm^{-1}) had instrument bandpass-to-FWHHs of greater than 1:10). In view of this, the lineshapes for these two ZPLs (Oh and S11) should, perhaps, be treated circumspectly.

In order to graphically display the differences in lineshape, Voigt profiles have been drawn with the formfactors, α, given in the above table but with the FWHH and the maximum intensity, I_0, set constant at arbitrary values. The resultant intensity profiles are given in figures 3.41, 3.42, and 3.43, for the powder samples, the sectioned SDA S11 samples and the single crystal samples respectively. Figure 3.44 gives the profiles for a Gaussian (formfactor $\alpha = 0.5$) and a Lorentzian (formfactor $\alpha = 1$) for reference.The Lorentzian fraction (defined as Γ_L/Γ) and the Gaussian fraction (defined as Γ_G/Γ) are graphically summarised in figures 3.45 and 3.46 respectively.

- For the powder samples it can be seen that the lineshape of the heat treated grit, HT11, is Lorentzian while the SDA powder has a lineshape considerably more Gaussian. That for CDA is almost totally Gaussian.

- For the two sectioned samples of the SDA grit the lineshapes are very similar but considerable more Gaussian than the lineshapes of the powder S11 from which the samples were prepared.

- The single crystals display the whole range of lineshapes, from virtually Lorentzian in the case of Oh to almost Gaussian for Cu. Apart from the cube face of the cubo-octahedral crystal, the lineshapes tend from considerably Lorentzian to Gaussian as the crystal becomes more cubic in morphology.

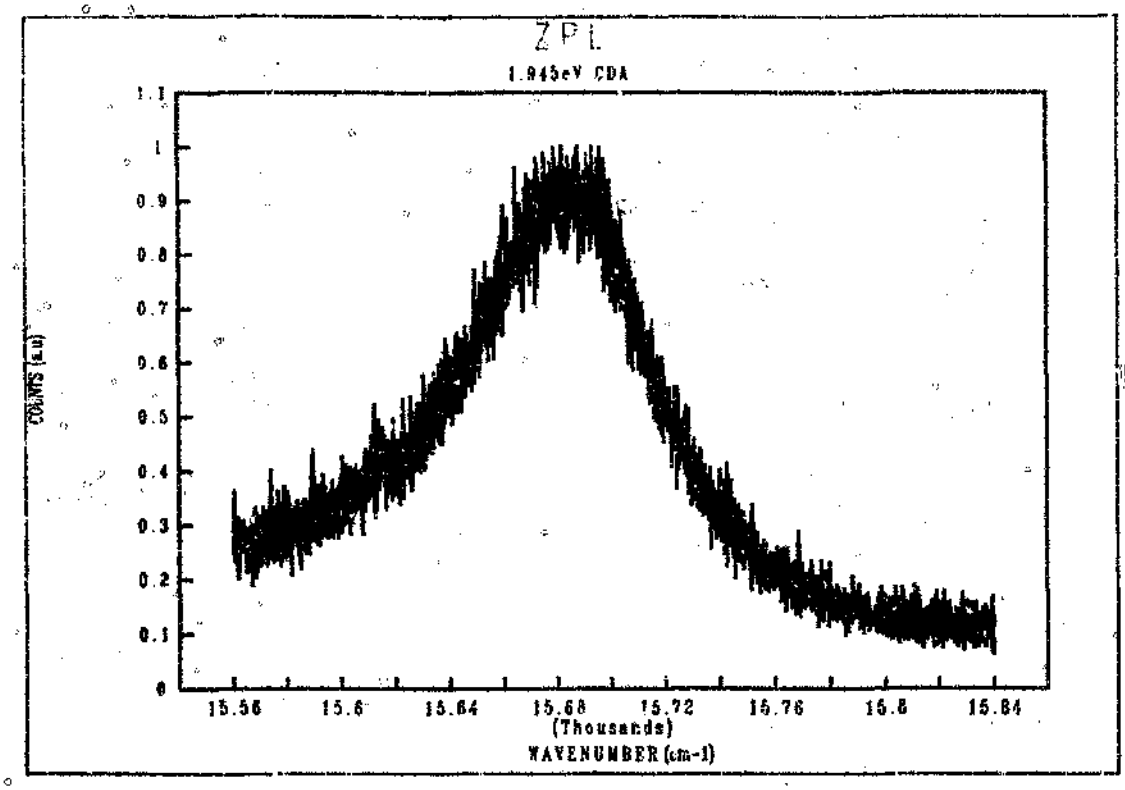

Figure 3.31 Replicate spectra of 1.945 eV ZPL of powder sample of CDA. λ_{exc}=514 nm.

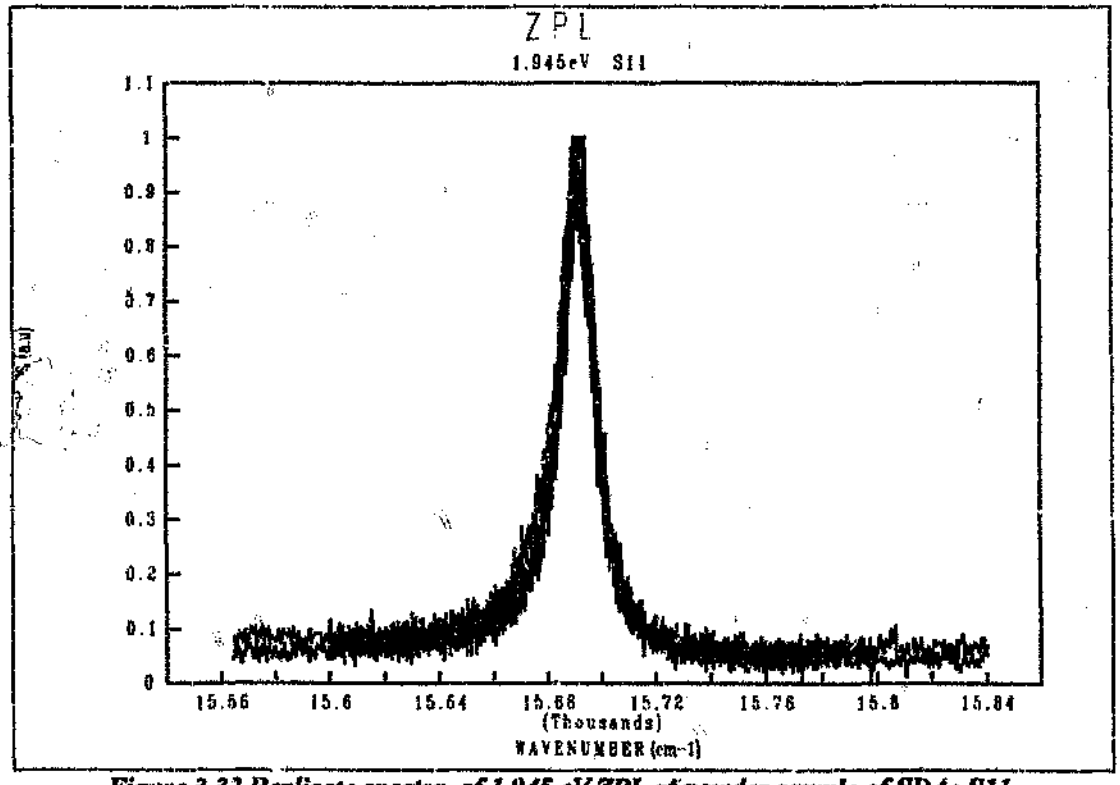

Figure 3.32 Replicate spectra of 1.945 eV ZPL of powder sample of SDA: S11. λ_{exc}=514 nm

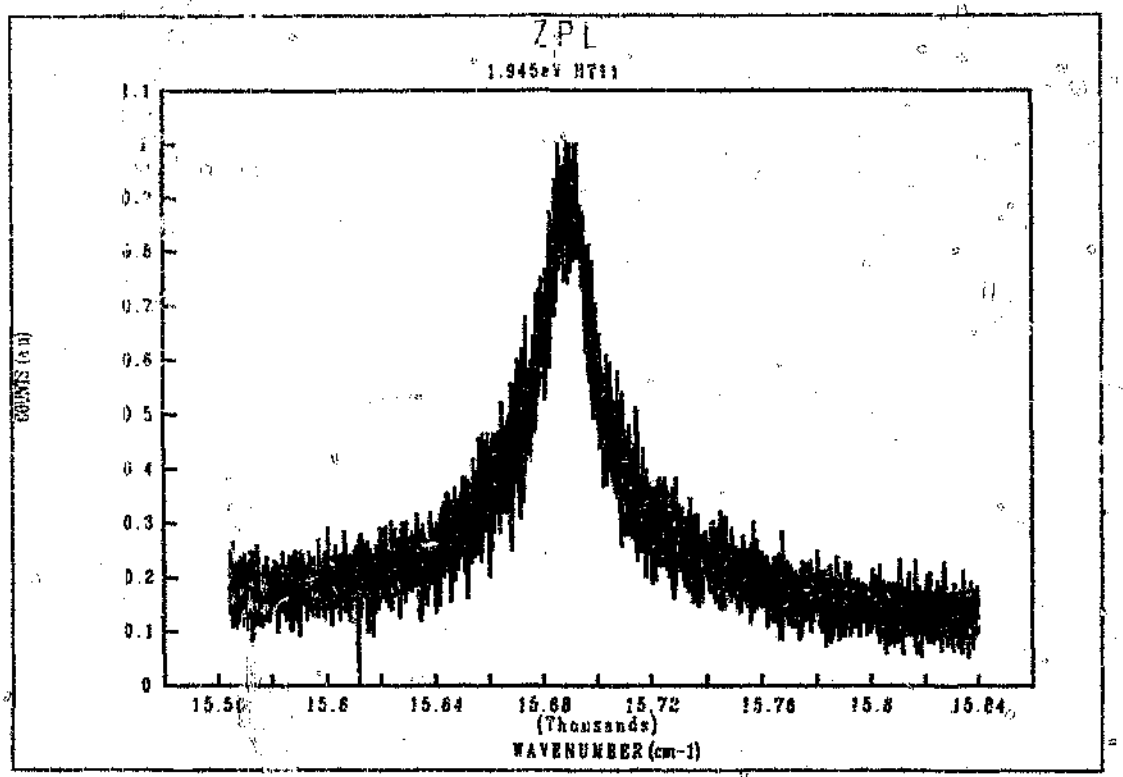

Figure 3.33 Replicate spectra of 1.945 eV ZPL of powder sample of heat treated SDA: HT11. λ_{exc}=514 nm.

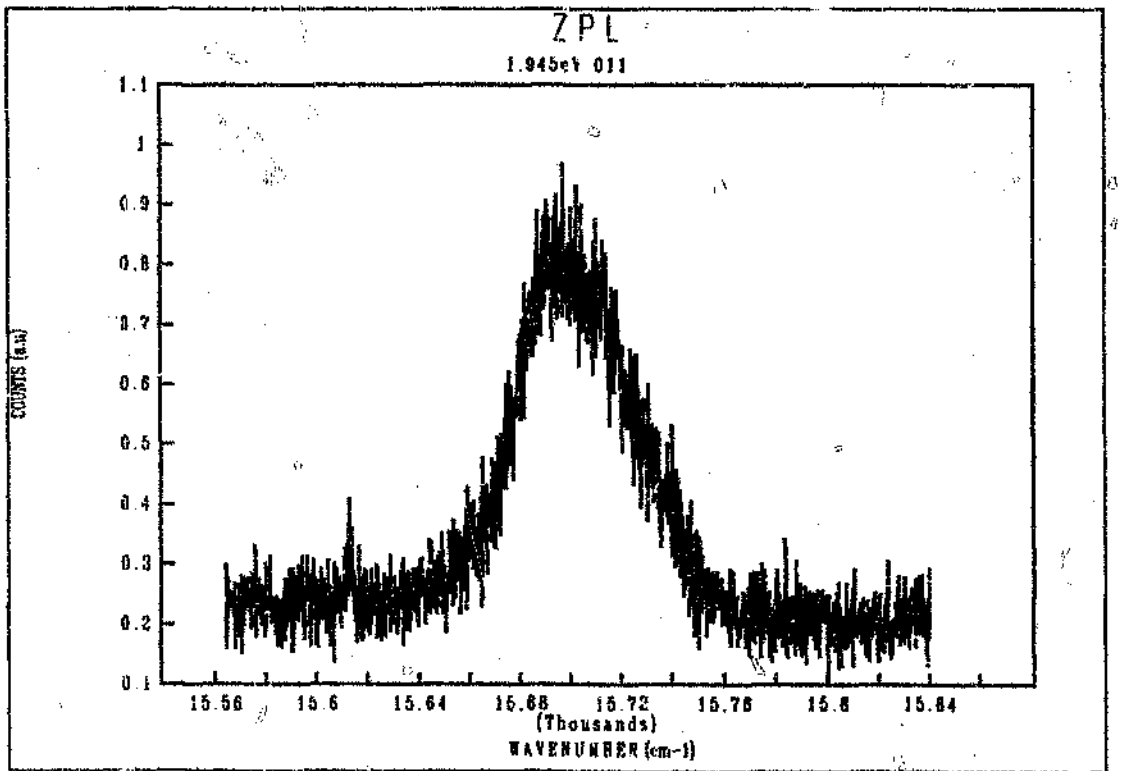

Figure 3.34 Spectrum of 1.945 eV ZPL of {111} sectioned SDA: sample 011. λ_{exc}=514 nm.

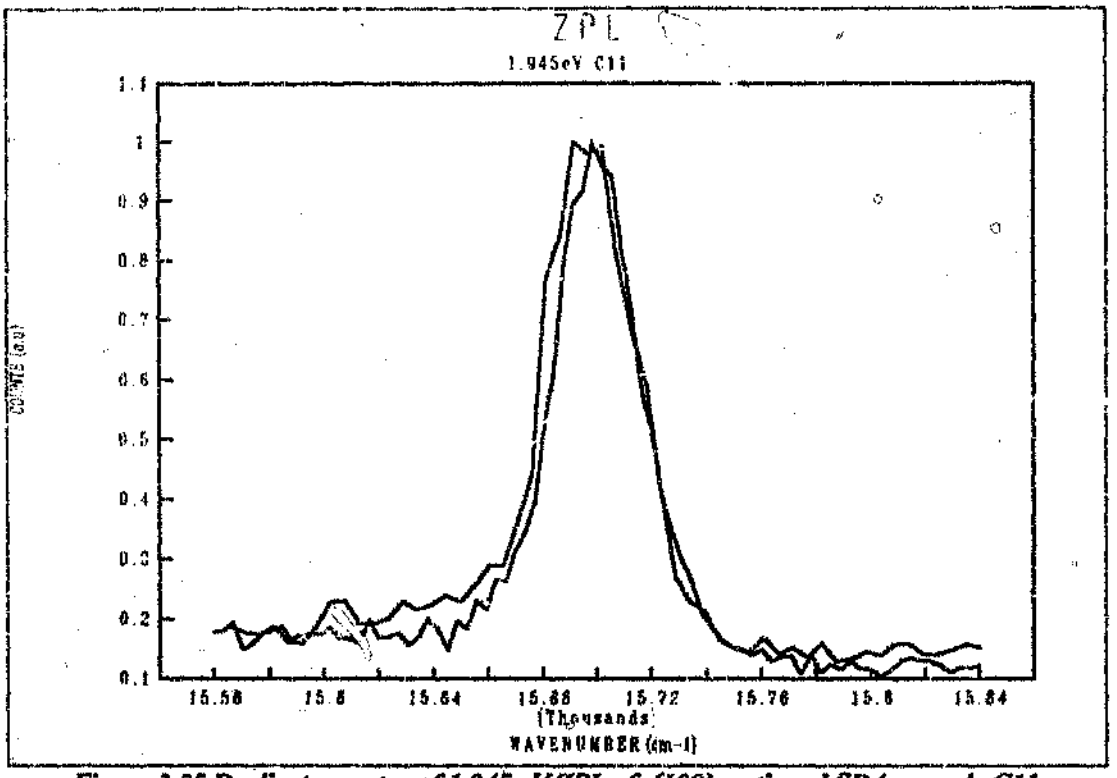

Fipure 3.35 Replicate spectra of 1.945 eV ZPL of {100} sectioned SDA: sample C11.
λ_{exc}=514 nm.

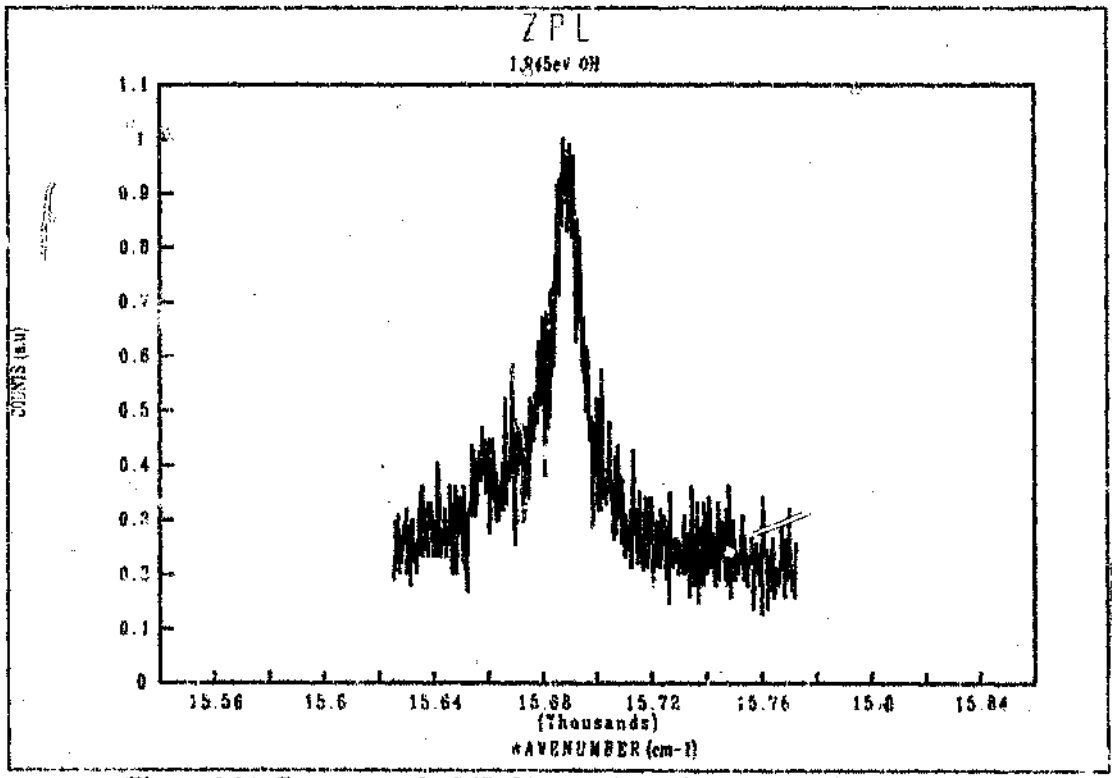

Figure 3.36 Spectrum of 1.945 eV ZPL of octahedral crystal: sample Oh.
λ_{exc}=514 nm.

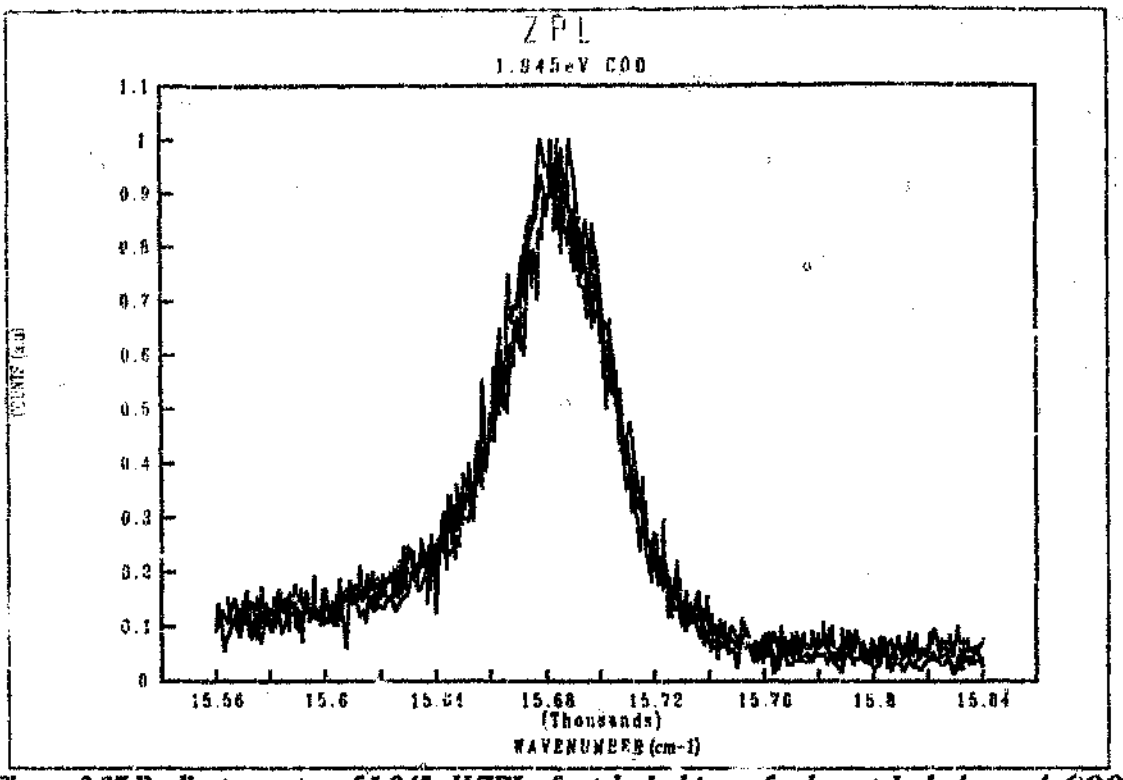

Figure 3.37 Replicate spectra of 1.945 eV ZPL of octahedral face of cubo-octahedral crystal: COO. λ_{exc}=514 nm.

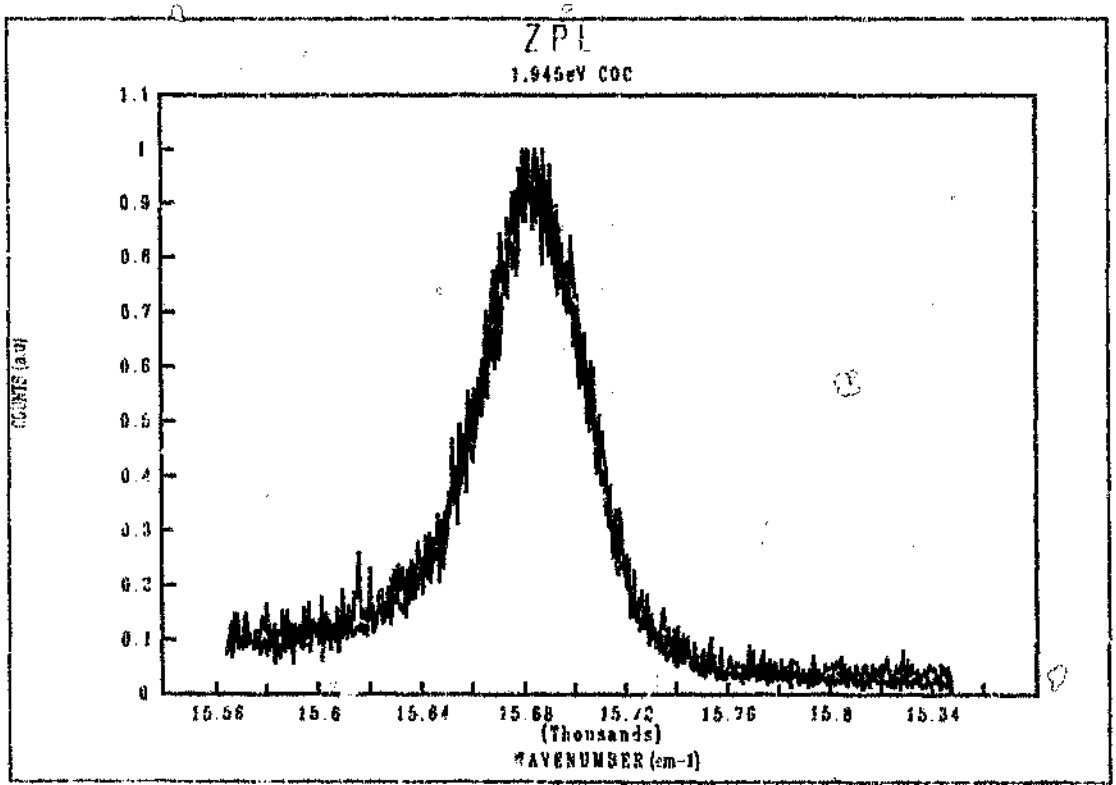

Figure 3.38 Replicate spectra of 1.945 eV ZPL of cubic face of cubo-octahedral crystal: COC. λ_{exc}=514 nm.

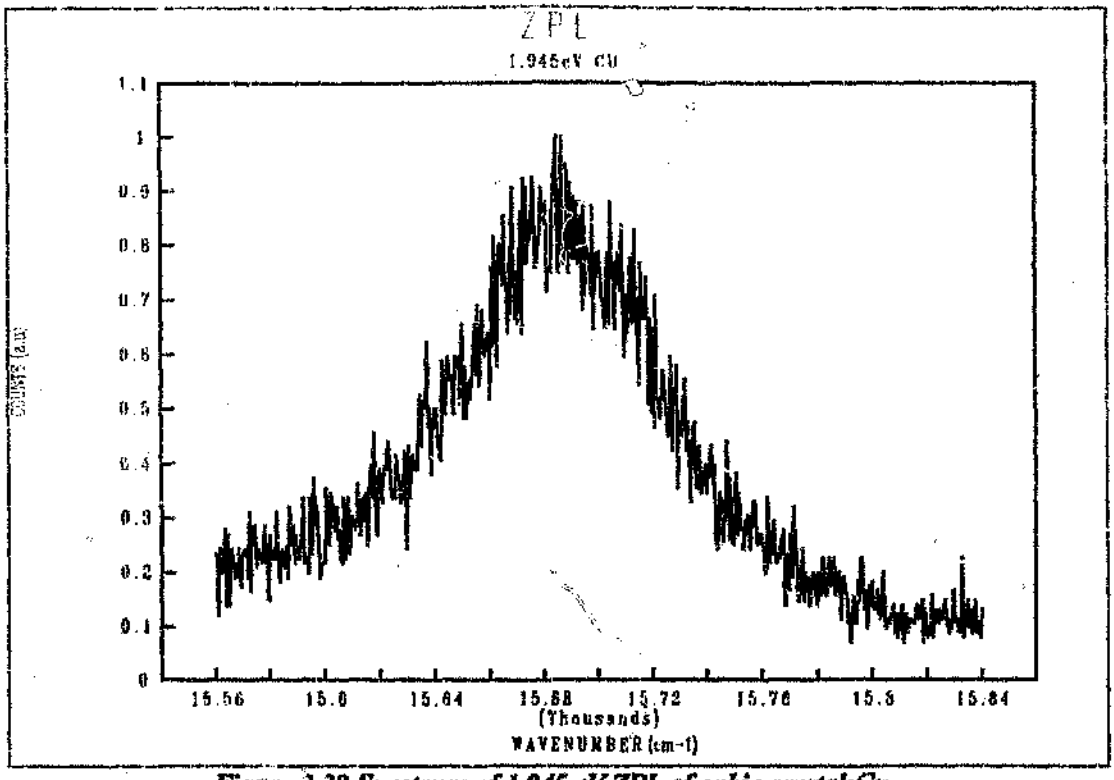

Figure 3.39 Spectrum of 1.945 eV ZPL of cubic crystal:Cu.
λ_{exc}=514 nm.

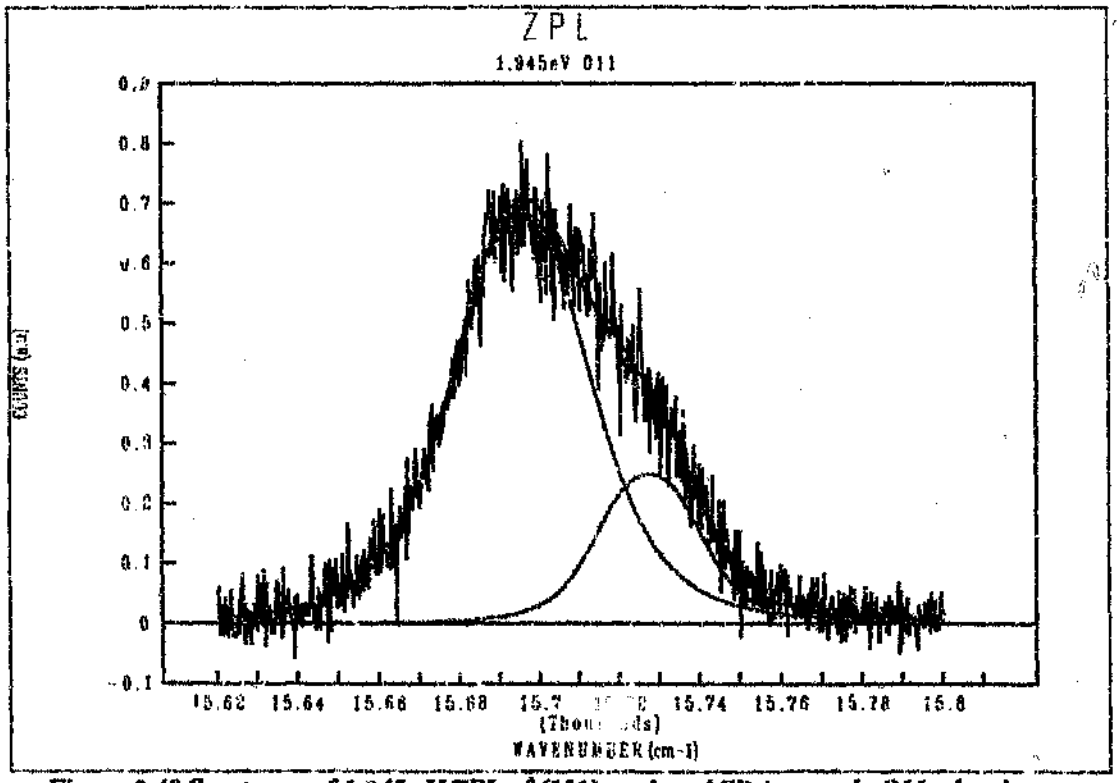

Figure 3.40 Spectrum of 1.945 eV ZPL of {111} sectioned SDA: sample 011, showing deconvolution into two Voigt profile components.
λ_{exc}=514 nm.

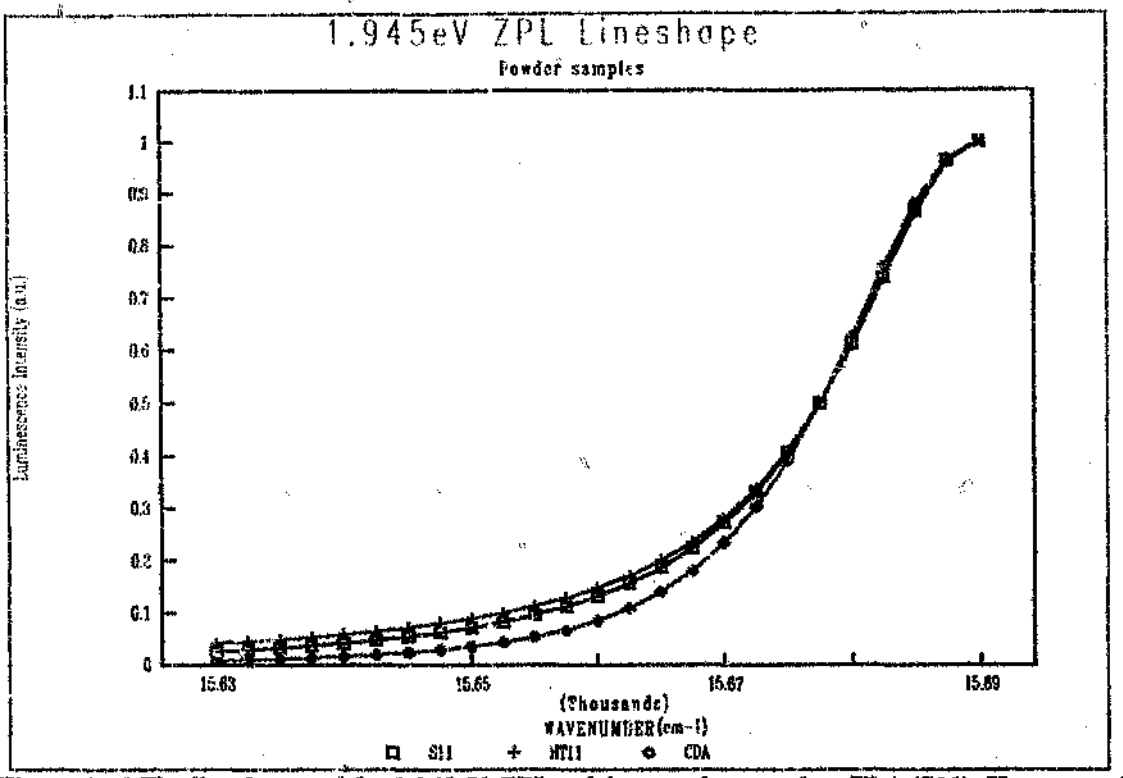

Figure 3.41 The lineshapes of the 1.945eV ZPLs of the powder samples: SDA (S11), Heat treated SDA (HT11), and CDA (CDA).

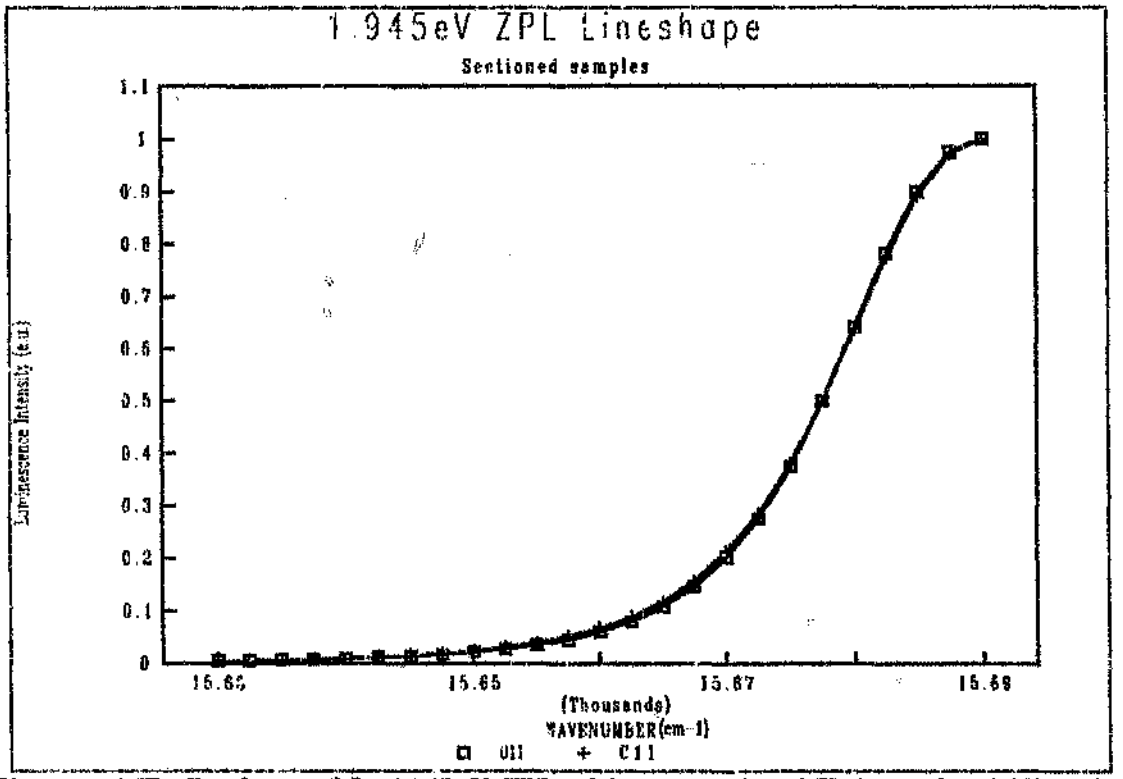

Figure 3.42 The lineshapes of the 1.945 eV ZPLs of the two sectioned SDA samples: {100} section (O11); {111} section (C11). The lineshape given for O11 is the larger Voigt component shown in figure 3.40.

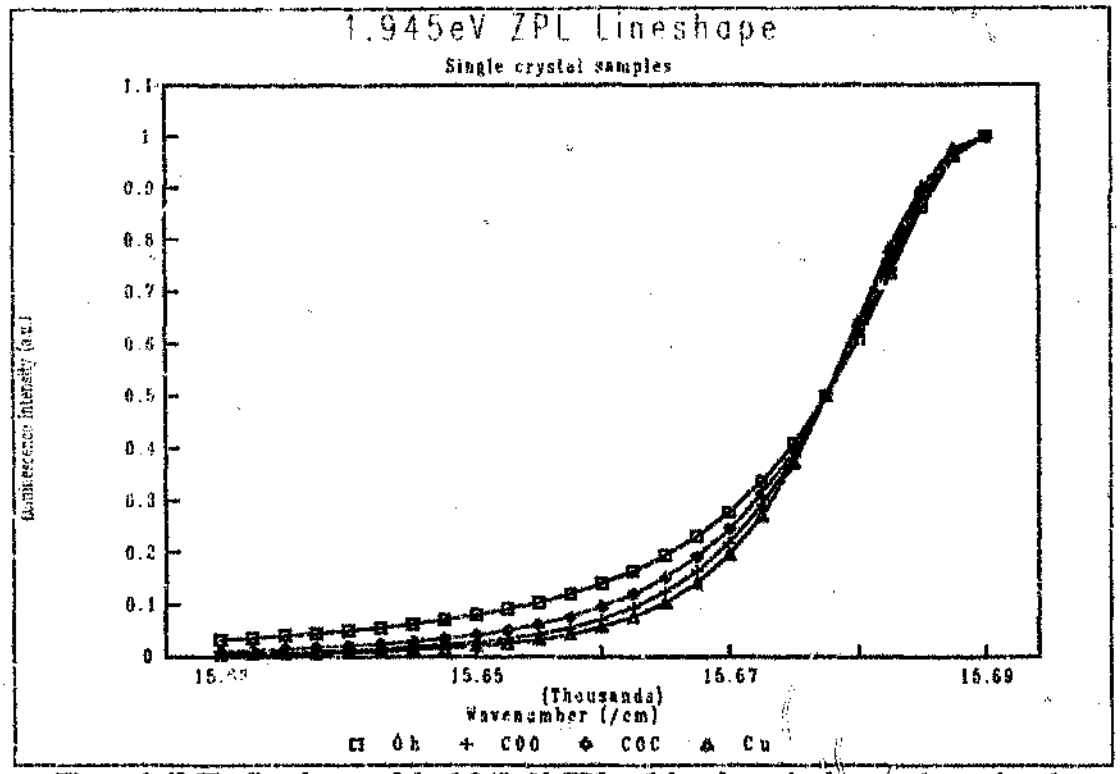

Figure 3.43 The lineshapes of the 1.945 eV ZPLs of the three single crystal samples: the octahedral crystal (Oh), the {111} and {100} faces of the cubo-octahedral crystal (COO and COC), and the cubic crystal (Cu).

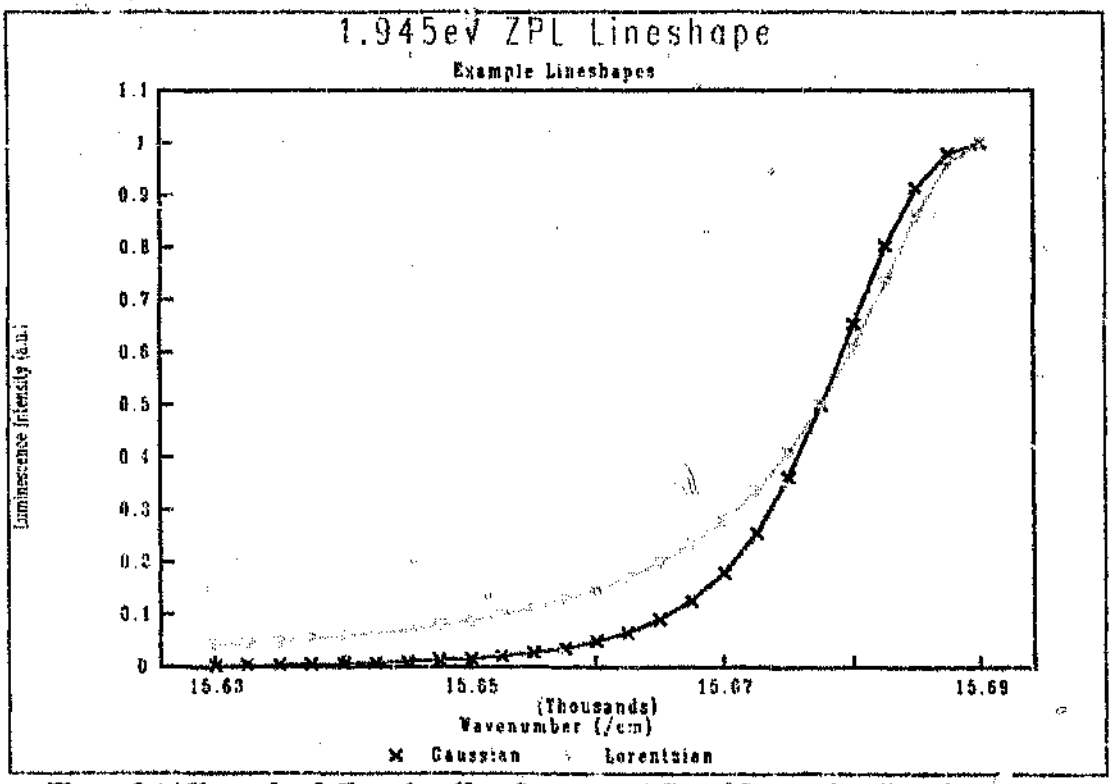

Figure 3.44 Example of Gaussian (formfactor $\alpha = 0.5$) and Lorentzian (formfactor $\alpha = 1$) lineshape.

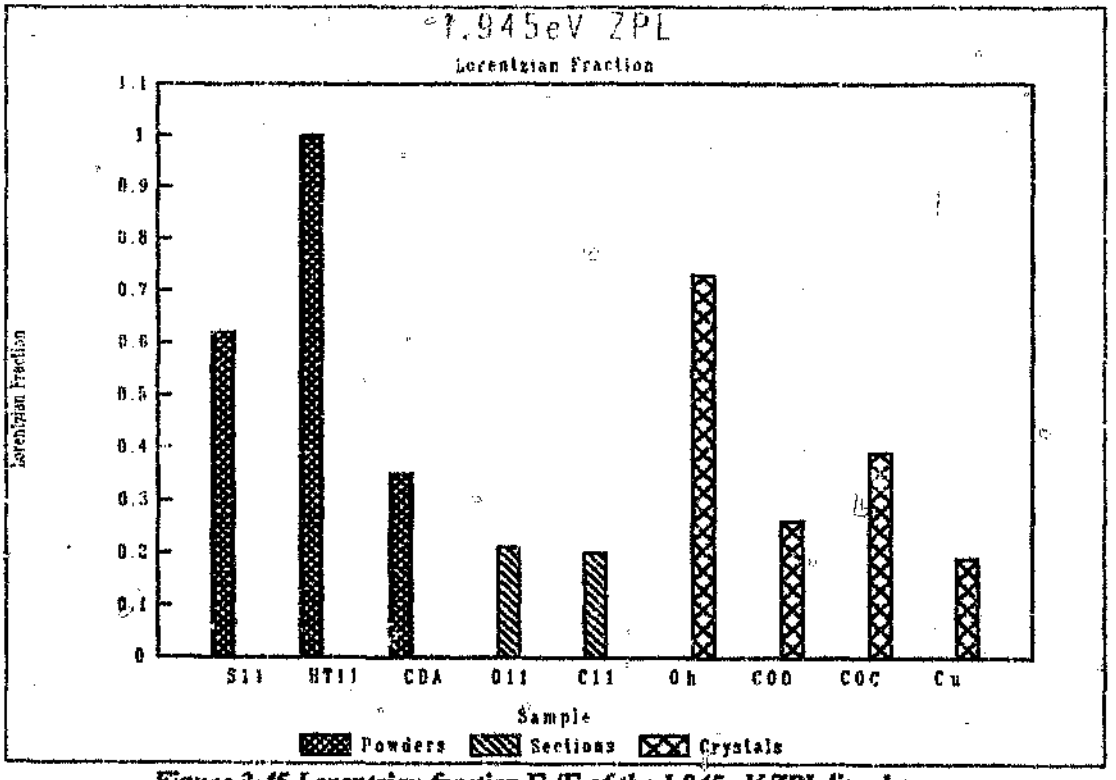

Figure 3.45 Lorentzian fraction Γ_L/Γ of the 1.945 eV ZPL lineshapes.

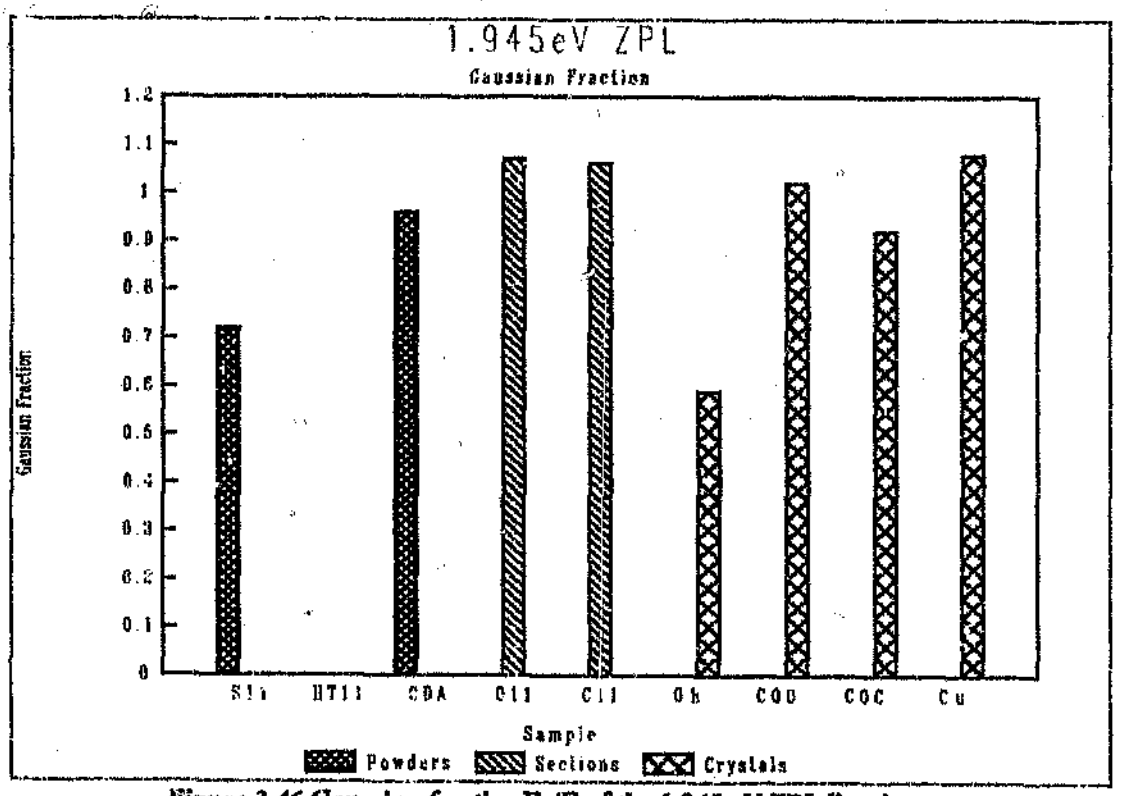

Figure 3.46 Gaussian fraction Γ_G/Γ of the 1.945 eV ZPL lineshapes.

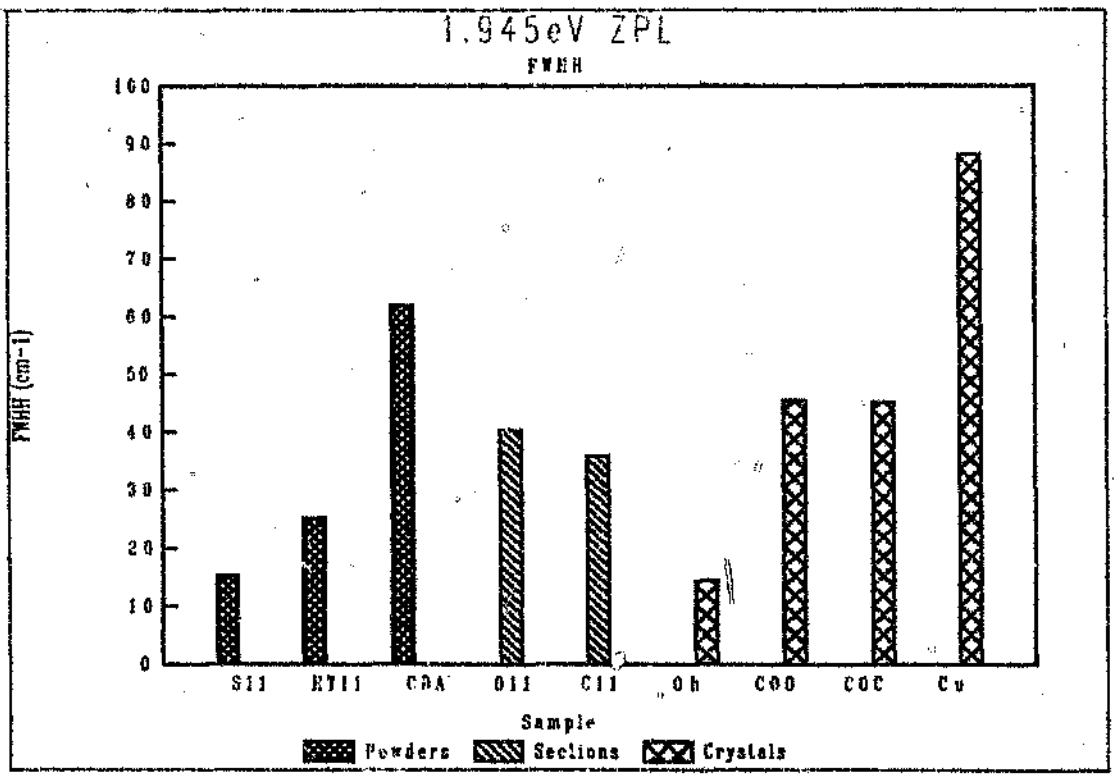

Figure 3.47 Fitted FWHH of the 1.945 eV ZPLs.

3.6.2 Linewidths of the 1.945eV ZPL

The linewidths of the 1.945 eV ZPL are such that Cu> CDA > COO COC O11 C11 > HT11 > S11 > Oh. (Note, that in the case of O11, the FWHH quoted here is that fitted to the major component in the two component fit mentioned in section 3.6.1 above and should be treated with caution.) The FWHH of the fitted 1.945 eV ZPLs are given in table 3.11 above and are shown graphically displayed in figure 3.47.

- For the powder samples, the FWHH of the heat treated SDA powder, HT11, is broader than that of the untreated sample, S11.
- The value for CDA is much broader than that for the two SDA powders.
- The values for the two samples of sectioned SDA crystals embedded in the metal matrix are very similar but are considerably broadened from the values of S11 from which the samples were made.
- The single crystal samples again show a range of line widths from the narrowest value in this work for the truncated octahedral crystal, Oh, through a much higher value for both the cubic and the octahedral face of the cubo-octahedral crystal to the largest value in this work for the cubic crystal, Cu.
- These single crystal samples show a trend of broadened FWHH as the crystal morphology becomes more cubic.

4. DISCUSSION

4.1 Intensities due to Different Defects and Comparison with Previous Work

The three major luminescent systems observed in this work, H3, 1.945 eV and the 575 nm centres have long been noted in natural diamond, generally in association with irradiation and annealing (Walker, 1979). All three are believed to involve vacancies associated with nitrogen: H3 a vacancy with a di-nitrogen (Davies 1977(b)); 1.945 eV - a vacancy with a single substitutional nitrogen (Davies and Hamer 1976); and Zaitsev (1991) has proposed a model for the 575 nm centre involving a vacancy with a single nitrogen in a split interstitial site. As their proposed structures might suggest, the predominant defect formed by irradiation and annealing of natural diamonds is related to the initial diamond type: those types containing predominantly single substitutional nitrogen (Ib) forming the 1.945 eV defect, while those containing di-nitrogen (Type IaA) yielding predominantly H3. The 575 nm centre is formed in all nitrogen containing diamond types after irradiation and annealing.

As discussed in section 1.12, Evans et al (1984) showed that these defects can be formed by means other than irradiation followed by annealing. They showed that the photoluminescence intensity of all three centres is enhanced during high pressure, high temperature sintering of synthetic diamond, the 1.945 eV and the 575 nm luminescence increasing as sintering temperatures increased to about 1500 °C, with both decreasing at higher temperatures while the H3 centre intensity increased. The high pressure, high temperature sintering causes plastic deformation which results in the creation of vacancies. These are mobile at the temperatures involved, and will be trapped at single substitutional nitrogen (the major point defect impurity in synthetic diamond) to form the 1.945 eV centre, and at some more complex defect site involving nitrogen (interstitial nitrogen in the Zaitsev model) to form the 575 nm centre. At temperatures above 1300 °C, the N-V (1.945 eV) defect allows nitrogen to migrate by vacancy enhanced diffusion (Collins 1978) to be trapped by single substitutional nitrogen forming the N-V-N (H3) defect. Ten minutes at 1800 °C at a sintering pressure of 9.5

GPa was sufficient to completely convert all the 1.945 eV and 575 nm defects to H3 (Evans et al 1984).

As discussed in section 1.12 plastic deformation of diamond can be achieved by far less radical means than the above. Brookes et al (1993), using a "soft", conical cubic boron nitride indenter to create plastic deformation of diamond at 1100 °C, observed cathodoluminescence decorating the slip lines created. In the case of synthetic type Ib diamond, the luminescence is due to the 575 nm centre, in the case of type IaA diamond it is due to the H3 centre, and in type IaB it is due to the 491 nm centre (a centre which the authors speculate may be the result of shear on the B centre which consists of four nitrogen atoms). Trapping of vacancies by single substitutional nitrogen to form the 1.945 eV centre is also expected, but while this centre is active in photoluminescence, it is not active in cathodoluminescence. High photoluminescent intensities were, however, measured by the authors for the synthetic diamond after deformation. (The typical mean pressures created by indentation are given by the authors as 8 to 10 GPa.)

Luminescence from H3 is easily seen in both cathodo- and photoluminescence and was noted in **as-grown** synthetics by Collins and Stanley (1985). The presence of the H3, 1.945 eV and the 575 nm defects in as-grown synthetic diamond were also noted in low temperature photoluminescence spectra of synthetic diamond powders by Evans et al (1984). The powders used in the work of Evans et al were MDA, a material similar to the SDA used in this work, but of a much finer particle size. Further studies on similar material were performed by Dodge (1986) and Beard (1987). Examples of synthetic diamond that Dodge studied included MDA, single crystal and crushed SDA. Photoluminescence observed for thirty, relatively large (approximately 1 mm) SDA crystals excited with 488 nm laser irradiation showed H3 luminescence and traces of 1.945 eV luminescence.

As synthetic diamond contains, as its major point defect, single substitutional nitrogen, the production of vacancies during synthesis is highly likely to result in the formation of the 1.945 eV defect. Synthesis temperatures are approximately 1300 °C and

pressures are approximately 5.5 GPa. The pressure, moreover, is not isostatic, but varies throughout the synthesis volume (Fedoseev and Semenova-Tyan-Shanskaya 1986), giving rise to the probability that individual diamond crystals are subjected to shear stresses. These conditions during synthesis make it possible for both the formation of vacancies by the interaction of dislocations, and for their diffusion through the lattice until they are trapped by single substitutional nitrogen to form the 1.945 eV centre, and also for vacancy enhanced migration and aggregation of substitutional nitrogen to form the H3 defect as in the scheme of Evans and co-workers above. Dodge (1986), however, proposed that the bulk of the H3 defect is **grown-in during synthesis**, and suggests a mechanism which successfully explains several features of the H3 luminescence in synthetic diamond which cannot be explained by the vacancy enhanced aggregation scheme: H3 is virtually restricted to the relatively low nitrogen content {100} growth sectors and displays strong linear polarisation with the electric vector parallel to the <100> directions. Dodge also showed that A centres (di-nitrogen) are present in as-grown synthetic diamond by demonstrating an increase in the concentration of H3 after irradiation and annealing at 800 °C for 60 minutes. He suggests that these A centres could only have been formed by the dissociation of grown-in H3.

Beard (1987) examined the possibility of other centres being "grown-in". He concludes that single substitutional nitrogen, or C centres, can be grown in with equal probability on any of the {100}, {111} or {110} faces (which is not in keeping with the observations (e.g., in Burns et al (1990)) that the concentration of C centres depends on the growth zones). Similarly Beard (1987) shows that di-nitrogen, or A centres, can grow-in equally easily on any face, but he shows that the concentration of A centres predicted by a simple statistical argument is too low to be detected by infra red spectroscopy, while that predicted for C centres is easily detectable, in keeping with observations. The 1.945 eV centre is predicted to have a low probability of formation on the {110} and {100} faces, but a slightly larger probability to grow on the {111} face. This argument takes no cognisance of the inhomogeneous concentration of single substitutional nitrogen in the different growth zones of synthetic diamond which results in a markedly higher nitrogen concentration in the {111} growth sectors in most cases

which, alone, should give rise to a higher concentration of 1.945 eV in {111} growth zones. A higher concentration of 1.945 eV centres in {111} growth sectors was experimentally observed in photoluminescence tomography experiments carried out on synthetic diamonds by Van Enckevoort and Lochs (1988) who found that the areas with detectable levels of 1.945 eV luminescence coincide with areas of high single substitutional nitrogen (which also coincided with the {111} growth sector). They suggested a thermal vacancy formation mechanism which would give rise to vacancies uniformly distributed throughout the crystal. Such a situation would indeed produce a distribution of 1.945 eV defects correlated only with the substitutional nitrogen distribution as observed. However, as the thermal production of vacancies invoked by the authors is untenable in view of the high energy of formation of vacancies in diamond viz. 7.2 eV (Bernholc et al 1989), this observation might perhaps be evidence for some grown-in component for either the 1.945 eV defect or of vacancies. (It should be noted that the result from the cubo-octahedral crystal and sectioned SDA in this work do not corroborate the observation of Van Enckevoort and Lochs (1988) as the intensity of the 1.945 eV luminescence from the {100} faces is greater than that from {111} faces in both cases).

In cases of localised production of vacancies such as in regions of plastic deformation, Dodge (1986) noted that the ZPLs of the defects produced were considerably broadened compared to those produced as result of trapping of radiation-induced vacancies. This suggests that the defects produced by plastic deformation were closely spatially correlated with sources of strain associated with the plastic deformation such as dislocations. The observation by Brookes et al (1993) that high levels of 1.945 eV photoluminescence (in addition to the 575 nm cathodoluminescence) were found in the vicinity of high temperature indentation induced plastic deformation is further evidence for the spatial correlation of the distribution of these defects and sources of vacancies such as areas of dislocation interaction.

The creation of 575 nm defects during synthesis is expected to occur in a manner similar to the formation of the 1.945 eV defects, i.e. by vacancy formation, migration and trapping, since it apparently also involves a vacancy trapped at a nitrogen defect.

The distribution of the 575 nm defect would again be determined by the distribution of the both the source of vacancies and the distribution of the nitrogen defect involved. As the nitrogen involved in the 575 nm defect is thought to be in a tetrahedral interstitial site (Zaitsev 1991), the formation of this defect is likely to be correlated with the formation of vacancies, provided there is sufficient substitutional nitrogen present to ensure that some of the interstitials formed are nitrogen interstitials. The interstitial nitrogen is sufficiently stable towards annihilation with vacancies not to recombine to form substitutional nitrogen even after annealing at 1300 °C (Lee et al 1978). Instead, Zaitsev (1991) suggests that it combines with the vacancy to form a stable split interstitial, the 575 nm system.

The above discussion satisfactorily explains the presence of the three major defect types seen in as-grown synthetic diamond in this work :

- **The H3 defect** appears to be grown-in during synthesis, and is largely restricted to the {100} growth sectors. The creation of the H3 defect will depend to some degree on the amount of nitrogen available in the growth medium (as will the uptake of single substitutional nitrogen in the growing diamond). Growth conditions are such that the formation of some H3 and possibly even di-nitrogen A centres by the vacancy enhanced aggregation mechanism is also possible, but at a much lower concentration.

- **The 1.945 eV centre** will be found in the nitrogen rich areas of the diamond, probably near to sites of vacancy formation and will reflect both the degree of vacancy formation and migration during synthesis and the local nitrogen concentration.

- **The 575 nm defect** also requires the formation of vacancies, and the presence of nitrogen in the lattice, but the nitrogen in this case is required in the form of interstitials in tetrahedral sites.

It also predicts that :

- The concentration of H3, since it is grown-in during synthesis, will be related to the available nitrogen in the growth medium, and hence probably to the overall nitrogen content of the diamond, but since it is essentially constrained to the {100} growth sectors, it will also depend on the crystal morphology.

- The concentration of both the 1.945 eV and 575 nm defects will be related to the nitrogen concentration of the diamond (or growth sector in question), **but also to the amount of vacancy formation during synthesis and its distribution.** Either vacancies or the respective nitrogen species involved in these defects may determine the concentration of the 1.945 eV and 575 nm defect centres. An excess of single substitutional nitrogen and a deficiency of vacancies, for example, will result in factors that effect the generation of mobile vacancies becoming critical, while an excess of vacancies and a deficiency of single substitutional nitrogen will cause the single substitutonal nitrogen concentration to become critical.

4.1.1 The Luminescence Intensities from the H3 Defect

In the series of single crystals measured, the intensity of H3 luminescence increases as the crystal morphology progresses from octahedral to cubic (with the exception of the octahedral face of the cubo-octahedral crystal, COO, which has a lower intensity than the octahedral crystal, Oh). This is in keeping with the predicted correlation between the total concentration of H3 and the overall nitrogen uptake of the growing diamond (as the H3 defect involves two nitrogen atoms). As discussed in section 1.5, the concentration of single substitutional nitrogen varies from one growth sector to another in the sequence {111} > {100} >> {113} > {110}, although the {100} growth sector may have the highest nitrogen concentration in "cold shaped", cubic diamond. The **overall** nitrogen concentration of synthetic diamond grown from similar environments (solvent/catalyst, pressure, temperature etc.) is proportional to

the growth rate (Yazu 1985). The growth rate, for situations of similar surrounding metal film thickness (Strong and Haneman 1967), is proportional to the solubility difference between graphite and diamond, which, in turn, is proportional to the overpressure (amount by which the pressure is greater than the equilibrium pressure for the graphite/diamond transition) and inversely proportional to the absolute temperature (Wakatsuki and Takano 1987). Both increasing pressure and decreasing temperature within the diamond stable region will result in a higher growth rate (by moving the growth conditions deeper into the region of diamond thermodynamic stability) as well as a more cubic morphology (Muncke 1979). Thus we might expect, provided that the synthesis environment (solvent/catalyst systems, nitrogen concentration in the growth environment) was constant, that the more cubic crystals grew at a faster rate, and will, by the argument of Yazu (1984) above, contain a higher overall nitrogen concentration. Indeed, Shulshenko et al (1992) have observed the overall nitrogen concentration to increase and the morphology to become more cubic as the growth temperature was decreased for diamond grown from a particular growth environment. Thus, the fact that the overall uptake of nitrogen is more efficient for diamond grown under conditions which result in a more cubic morphology provides a further reason to expect a higher H3 intensity for the more cubic crystals.

In both the case of the sectioned crystals, O11 and C11, and single crystals, COO and COC, where a {100} and a {111} face of the same crystal type was measured, the cubic face displays a higher H3 luminescence as predicted by the model of Dodge (1986) which suggests that H3 is grown-in preferentially on {100} faces during synthesis, and which provides the only satisfactory explanation for the high H3 concentration in the relatively poor nitrogen concentration {100} growth sectors and the observed polarisation of the H3 luminescence.

No change is seen in the H3 luminescence intensity for the SDA powder heat treated at 1120 °C for 40 minutes. While the H3 centre does begin to anneal

out at temperatures above 1000 °C, the data of Collins (1978) shows an imperceptible change in the absorption intensity of H3 in diamond heat treated for 12 hours at 1000 °C.

The exceptionally high H3 concentration of the cubic crystal may arise from the high overall nitrogen concentration found in "cold shaped" diamond (more cubic diamond grown at lower synthesis temperature conditions than usual) (Collins and Lawson 1989, Satoh et al 1990 and Shulshenko et al 1992).

The H3 luminescence intensity measured for the CDA powder is one of the lowest measured. The irregular form of the grains in the CDA powder sample make it difficult to deduce the crystal morphology so the low H3 may arise from either an exceptionally low overall nitrogen concentration, or from a predominantly octahedral morphology (which would imply less cubic growth sectors with their associated grown-in H3 defects).

4.1.2 The Luminescence Intensities from the 1.945 eV Defect

As discussed above, the concentration of 1.945 eV defects is likely to be determined by both the nitrogen concentration and the vacancy concentration, or by one of these should either concentration be far less than the other.

Considering first the concentration of vacancies that are generated under conditions where they are mobile enough to be trapped at the substitutional nitrogen: as mentioned above in section 4.1, thermal formation of vacancies is unlikely in synthetic diamond as the synthesis temperatures are too low for appreciable vacancy formation. The formation of vacancies during growth is unlikely unless stabilised or trapped by another defect (such as the substitutional nitrogens in the case of the grown-in H3 defects). Freshly grown-in vacancies would, by definition, be formed close to the growth surface. Synthesis temperatures are well above the temperature for vacancy diffusion, making the annihilation of such freshly grown vacancies at the

growth surface a likely occurrence, reducing the likelihood of appreciable quantities of grown-in vacancies. It is, however, quite probable that lattice defects such as dislocations are incorporated during crystal growth (as evidenced by the presence of surface growth spirals (Strong and Haneman 1967)). In particular, synthetic diamond almost always contains macroscopic defects in the form of entrapped solvent/catalyst metal inclusions which would be expected to be associated with other lattice defects such as dislocations. Deformation of crystals can result in creation of further dislocations by mechanisms such as multiple cross glide and the operation of Frank-Read sources (Henderson 1972). This dislocation-creation provides the mechanism for slip during plastic deformation. Under certain circumstances, non-conservative dislocation movement occurs which results in the creation of additional vacancies in the wake of the dislocation. The higher the dislocation concentration, the greater the predisposition for the generation of vacancies by non-conservative dislocation movement due to the interaction of dislocations and increased probability of cross slip. The application of shear stress can thus act both as the source of dislocations and vacancy creation.

The sources of stress required for plastic deformation of the sort discussed above to occur may be the result of factors external to or internal to the diamond. External factors will include shear stresses occurring in the synthesis cell as the result of the interaction of adjacent crystals (in the case of high nucleation densities) or by shear stresses generated during and after solidification and depressurisation of the solvent/catalyst. Both of these would occur at temperatures far in excess of the 500 °C required for vacancies to be mobile. They may also be the result of internal effects in the diamond crystals such as the effect of heat treatment on solvent/catalyst inclusions. During heat treatment of synthetic diamond crystals, the entrapped solvent/catalyst metal inclusions catalyse the conversion of diamond to graphite, allowing the reaction to assume significant levels at relatively low temperatures (800 °C for nickel inclusions, and 750 °C for nickel and cobalt films on diamond surfaces in UHV (Evans 1992)). This reaction can be simply viewed as reverse diamond

synthesis, the diamond synthesis solvent/catalysts reducing the activation energy barrier for the conversion of metastable diamond to its thermodynamically stable form - graphite. In the case of catalysis by internal inclusions, the very large volume increase on converting diamond to graphite will result in the build up of large internal strains around the inclusion. These strained regions centred around the inclusions can be seen in birefringence microscopy of heat treated diamond and, in severe cases, the internal stress can be sufficient to result in cleavage of the diamond (Dickerson and Fish 1992). Further work by Dickerson (1993) has shown that 575 nm cathodoluminescence is observed around these internal inclusions after heat treatment at 1100 °C. The above suggests that internal graphitisation catalysed by solvent/catalyst inclusions in heat treated synthetic diamond can result in plastic deformation and the associated creation of vacancies which can migrate to be trapped at other point defects such as substitutional nitrogen in a manner similar to that observed by Brookes et al (1993) for indentation of diamond at elevated temperatures.

We now consider the arguments for the effect of the overall nitrogen concentration on the 1.945 eV defect concentration: for diamonds which are subjected to the same shear pressures during synthesis and otherwise end up with similar vacancy concentrations, one might expect the 1.945 eV concentration to increase with the nitrogen concentration, hence, from the argument given above (section 4.1.1), to increase as the morphology becomes more cubic. This is indeed observed for the suite of single crystals measured in this work. In the case where cubic and octahedral faces **of the same crystal** were compared, one would expect, on the basis of the observation that the relative nitrogen concentration in the various growth sectors varies in the sequence {111} >> {100} > {113} > {110} (Woods and Lang 1975 and Burns et al 1990) , that the 1.945 eV concentration should be greater in the octahedral growth sectors. This is **not** observed in this case. The 1.945 eV intensity was found to be higher in the cubic growth sectors of the pairs of samples where measurements were taken on both cubic and octahedral faces of

the same crystal (COC > COO, C11 > O11). This might suggest that a higher vacancy concentration existed in the cubic growth sectors compared to the octahedral growth sectors of the same crystal.

The observation of increased intensity of the 1.945 eV luminescence in the heat treated SDA powder (HT11 > S11) can be explained in terms of increased vacancy formation by the effect of temperature and the presence of internal inclusions as described above. An enhanced concentration of 575 nm defects might also be anticipated in terms of this mechanism. The failure to detect 575 nm luminescence in this case might be related to the rather high detection limit for this centre in photoluminescence compared to the ease with which it can be detected by cathodoluminescence.

The high intensity of 1.945 eV luminescence in the CDA powders may also be explained in terms of enhanced vacancy creation and trapping, induced in this case by the robust growth conditions (high growth and nucleation rates) used in order to attain the irregular and friable crystal characteristics of this material (Wedlake 1979). The high nucleation densities would increase the probability of interparticle interactions and shear stresses as a consequence of volume collapse as graphite converts to diamond, while the high growth rates may be expected to increase the dislocation density, further increasing the likelihood of generating vacancies by non-conservative dislocation movement under the effect of shear stresses.

4.1.3 The Luminescence Intensities from the 575 nm Defect

As the 575 nm defect also comprises a vacancy and lattice damage involving nitrogen, conditions favouring the 1.945 eV centre will also favour the 575 nm centre. While it is not detected in all cases, the intensity of the 575 nm luminescence correlates reasonably well with that of the 1.945 eV centre as predicted in cases where both centres are observed.

4.2 Statistical Analysis

This discussion relates to measurements of the luminescence of powder samples excited by a focused laser beam of spot size smaller than or equal to the individual grain size in a powder sample ("small area luminescence", section 2.2.3.2). The spectra measured in this fashion yield results which vary considerably for repeat measurements on the same powder sample as discussed in section 2.2.3.2. The data can, however, be treated as representing sub-samples of each sample type.

4.2.1 Correlations between Different Defects within Samples

Here analysis (section 3.5.1.2) of the correlations between photoluminescent features WITHIN individual sub-samples is discussed.

Since all the defects under discussion, H3, 1.945 eV and 575 nm , involve the same components, namely vacancies and nitrogen, a situation favouring the formation of one of these defects in such a sub-sample is thus highly likely to also favour the formation of the other, hence correlations between all of these within the same sub-sample might have been expected. However, as discussed above, the concentration of H3 is determined by the overall nitrogen uptake by the {100} growth sectors during growth while the 1.945 eV defect concentration is likely to be determined by the concentration of mobile vacancies generated, since the vacancy concentration is likely to be the limiting factor in the formation of the 1.945 eV defect

It is quite probable, on the other hand, that the concentration of the nitrogen species required for the formation of 575 nm defects would be related to that of the single substitutional nitrogen required for the formation of the 1.945 eV defect, and, since both defects contain a vacancy, one would expect to find a correlation between these two defect types. This is indeed observed for all sub-samples measured (see table 3.8 and figure 3.24).

It is possible, given that only a small fraction of the available nitrogen might be expected to be found as interstitials, that an excess of mobile vacancies occurs. The nitrogen concentration in such a situation will determine the final concentration of the 575 nm defect centres as it does for the H3 defect concentration. In such a case, one would expect to find a correlation between the concentrations of these defect types. This is observed in the case of the fine 50/60 # grit sub-samples, but not in the case of the coarser (>50 #) sub-samples (see table 3.9 and figure 3.23). This suggests that an excess of mobile vacancies were present in the case of the finer grit, but not for the coarser grit, possibly because these finer crystals were somehow subjected to higher levels of shear stresses during the synthesis cycle or were perhaps exposed to them for longer.

The above argument regarding the vacancy concentration in the coarser and the finer grits also suggests that the concentration of 1.945 eV and 575 nm defect centres should be lower in the case of the coarser (>50 #) grit. This is observed to be so (clearly shown in figure 3.24).

Because the H3 defect is essentially restricted to the {100} growth sectors, while the 1.945 eV and 575 nm defects may occur in any growth sectors, the predicted correlation between concentrations of the 1.945 eV or the 575 nm defect and the H3 defect may be affected by the relative fractions of {100} and {111} growth sectors probed by the luminescence technique (or by the morphology if one or more entire crystals are probed). This argument further supports the suggestion that the CDA powder sample crystals contain little {100} growth sectors (the CDA sample displayed one of the highest 1.945 eV, intensities (suggesting a history of abundant mobile vacancies) but one of the lowest H3 intensities).

4.2.2 Frequency Distributions

This discussion covers the analysis (section 3.5.2) of the distribution of the luminescent intensities measured on many different sub-samples (as opposed to analysing the trends of relative luminescent intensities within individual sub-samples as discussed in the previous section).

The frequency distributions for the three types of defect concentrations for the three defect types in SDA grit samples basically reiterate the trends indicated by the correlation analysis. The H3 intensity varies over a larger range and to higher levels for the coarser grits than for the finer grits; both the 1.945 eV and the 575 nm intensity varies far more and to far higher levels for the finer grits. These observations may be satisfactorily explained by the arguments presented in the preceding discussion: coarser particle size indicates faster growth rate and hence a higher proportion of cubic growth sector and higher overall nitrogen uptake, both conducive to higher H3 concentrations; the higher intensities from the 575 nm and 1.945 eV luminescence in the finer particles must, from the arguments presented in the preceding section, arise from a greater availability of vacancies to be trapped at the two types of nitrogen-containing sites to produce the 575 nm and 1.945 eV defects respectively. The higher vacancy availability probably arose because the finer grits were subjected to greater shear stresses or were subjected to these stresses for greater periods.

The narrower H3 intensity distributions for the finer grit suggest that this grit is of a more uniform morphology, or grew in more uniform nitrogen concentration environments. The narrower distributions observed for the vacancy related defect intensities for the coarser grits suggests that the coarser grits were exposed to a more uniformly stressed environment than the finer grits.

4.3 Lineshape Analysis

4.3.1 Linewidths

In the simplest analysis, the inhomogeneous strain broadening of the ZPL can be ascribed to an average strain, lumping all the sources of the strain together. In this scenario, a larger FWHH indicates a greater average strain in the sample. The larger FWHH observed for HT11 compared to S11 suggests that heat treatment of SDA powder increases the strain in the crystals in agreement with the increased birefringence and other signs of heat treatment induced strain and plastic deformation observed by Dickerson and Fish (1992). The sectioned crystals of the SDA powder sample S11 show increased linewidth compared to the powders. The fact that a crystal cracked during cooling (as a result of the greater thermal expansivity of the metal compared to that of the diamond) is testimony to the stressed state of the sectioned crystals during measurement which is again in keeping with the general hypothesis that the observed line broadening can be attributed to strain in the crystal. The two broadest ZPLs observed were for CDA powder and the cubic crystal, Cu. An increased level of lattice imperfection and/or increased substitutional nitrogen concentration resulting from a faster growth rate was invoked above to explain a higher 1.945 eV luminescence in these two samples. The former suffices to explain the observed broad ZPLs in this instance. (It also explains the general trend of increasing linewidth for increasing cubic growth sector fraction in the series Oh, COO, COC, Cu, with the exception of COO which does not display a narrower linewidth for this octahedral face compared to the cubic face of this cubo-octahedral crystal.). Shulshenko (1992) noted a correlation between metal inclusion concentration and the cubic morphology of the crystals resulting from growth at lower temperatures (and hence higher overpressures). Any such increased metal inclusion concentration in the more cubic crystals would result in increased lattice imperfection such as dislocations. This, in turn, would give rise to higher vacancy concentrations and hence higher 1.945

eV concentration, all of which would contribute towards increased ZPL broadening.

This general approach to linewidths can be taken a little further by using the following relationship between the observed linewidth of the 1.945 eV ZPL and the average internal stress present in the sample noted by Evans et al (1984), namely S=W/10 where S is the stress in GPa and W is the linewidth in meV. Results of the application of this relationship are illustrated in figure 4.1.

These results can be compared with a calculated value of 0.25 for the Ib diamond used for the work of Davies and Hamer (1976), 0.7 to 1.8 GPa inferred from the 575 nm ZPL width for combustion flame grown single crystal diamond film by Graham and Ravi (1992), 2 to 6.5 GPa for commercial SYNDITE (sintered polycrystalline) compacts (Evans et al 1984), and 0.42 to 0.73 GPa calculated from the linewidths measured for carbonado (naturally sintered diamond) by Dodge (1986). The average stresses are seen to compare favourably with those of the non-sintered diamond types measured by the above authors.

4.3.2 Lineshapes

In the section 1.12 above, Stoneham's (1969) statistical approach to line broadening was discussed. It predicts that the lineshape of inhomogeneously broadened ZPLs range from Gaussian to Lorentzian as the predominant source of strain ranges from line defects to point defects. As the theory is strictly only applicable to single crystals, only spectra of single crystals Oh, COC, COO, Cu can be considered. These crystals display a wide range of lineshapes but, in general, a trend of increasing Gaussian fraction is seen for the more cubic crystals. Again the cubic face of the cubo-octahedral crystal (COC) proves an exception, displaying a lower Gaussian fraction than the octahedral face.

The argument of increasing lattice disorder with the faster growth rates observed for the more cubic morphologies again appears to apply, the Gaussian lineshape specifically suggesting increasing dislocation concentration. This is consistent with the increased vacancy concentration suggested above to explain the increased 1.945 eV formation; the efficiency of vacancy creation via shear stress-induced dislocation interaction would be increased by a higher dislocation concentration.

Of course, the possible role of the "near neighbour effect" (Davies 1970(b)) discussed in section 1.12 may be a contributing factor to the Gaussian component, especially in crystals such as Cu which are expected to have a higher concentration of single substitutional nitrogen. (The "near neighbour effect" is the consequence of the existence of a minimum distance from a luminescing centre, within which no defect centre may occur without combining to form a different, aggregated centre. Davies (1970(b)), using a continuum approach, showed that this effect gives rise to a Gaussian contribution to the lineshape, and is more marked for higher nitrogen concentrations). These lineshape predictions were recently confirmed by Orth et al (1993) using an approach which assumed a discrete lattice.

When both line defects and point defects are present, the longer range stress fields of the line defects are expected to dominate any line broadening, so the "near neighbour effect" is likely to be less important for samples such as these synthetic diamonds which would probably contain substantial dislocation concentrations, especially crystals such as Cu with its obvious metal inclusions. The fact that longer range stress fields are associated with dislocations might also explain why such effects of the proposed higher point defect concentration in more cubic crystals are swamped by the proposed increasing dislocation concentration.

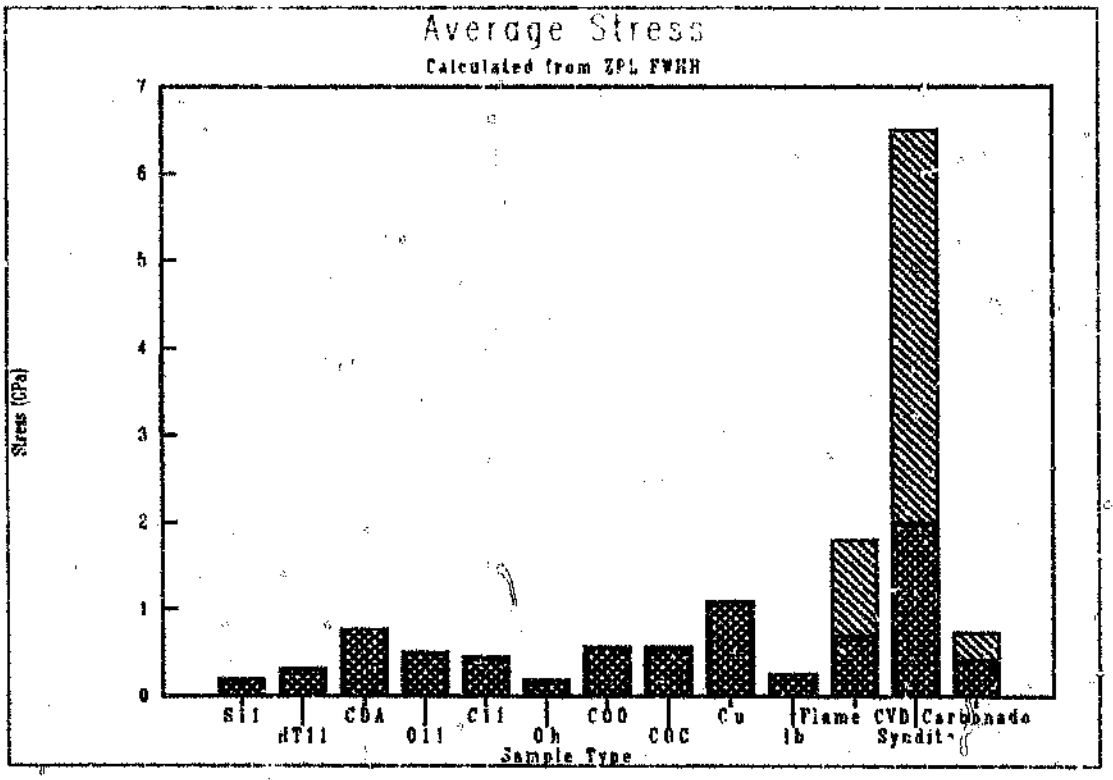

Figure 4.1 Estimation of stress in diamond from the FWHH by the method of Evans et al (1984). The less densely shaded portions of the bars indicate the range of stress reported for the respective diamond types.

4.4 Summary

The luminescence observed in the suite of diamond types used in this work is in keeping with that observed by several other authors for synthetic diamond; the defects indicated are to be expected from the known high substitutional nitrogen concentration in synthetic diamond, together with the factors which would give rise to vacancies.

A more cubic morphology is indicative of a faster growth rate, which, in turn has been correlated with a higher overall uptake of nitrogen from the growth environment. As all three defects considered here involve nitrogen, the intensity of luminescence observed for these defects is expected to correlate with the proportion of cubic growth sector. This is generally observed for all three defect types: H3, 1.945 eV and 575 nm.

Correlations are observed in some cases between the luminescence intensity of different defects measured on the same samples. In particular, the 1.945 eV and 575 nm defect intensities are correlated and the 575 nm and the H3 defect intensities are correlated in the case of the finer 50/60 # grit, but not in the case of the coarser >50 # grit. It is possible to argue that this latter case arises from a greater availability of mobile vacancies in the finer 50/60 # grit during the synthesis process, possibly as a consequence of exposure to greater or more prolonged shear stresses.

The substitutional nitrogen concentration is expected to be higher in the octahedral growth sectors than in the cubic growth sectors. The 1.945 eV intensity is expected to follow suite. The contrary is observed, suggesting that a larger vacancy concentration is initially generated in the cubic growth sectors compared to that in the octahedral growth sectors and the trapping of these vacancies at substitutional nitrogen results in the higher 1.945 eV concentration.

The CDA powder sample showed both extremely low H3 intensity and extremely high 1.945 eV intensity. This suggests a far higher concentration of vacancy generation in these crystals, commensurate with the robust growth conditions used to create this

type of diamond. It also suggests a relatively low fraction of {100} growth sectors which would be expected to contain H3 centres.

SDA diamond powder heat treated for 40 minutes at 1120 °C differs little from a similar, untreated powder in the intensity of the H3 luminescence, but the heat treated sample displays a significantly higher 1.945 eV intensity. This is in keeping with the large strains and plastic deformation expected as result of internal graphitisation catalysed by solvent/catalyst inclusions under these conditions.

The arguments concerning vacancy concentration used to explain the 1.945 eV intensity generally explain the FWHH observed in this work: In general, the linewidth increases as the crystal morphology becomes more cubic, suggesting a faster and hence less perfect crystal growth. The heat treated sample of SDA diamond powder has an increased linewidth compared to the untreated sample. The CDA sample displays an exceptionally broadened 1.945 eV ZPL, in keeping with the high degree of crystal imperfection predicted from its high vacancy concentration inferred from its high 1.945 eV intensity. The sectioned crystals were stressed by thermal contraction of the metal matrix in which they were encased to such an extent that some crystals fractured. The linewidths of these crystals were broadened as expected.

Analysis of lineshape for the single crystal samples generally confirm the suggestions that the imperfection of the lattice (manifested as the line defect concentration) increases for more cubic crystals, possibly as result of a more rapid growth rate.

4.5 Conclusions and Suggestions for Further Work

4.5.1 Conclusions

The aim of this study was to evaluate the usefulness of photoluminescence as a means of generating information on the growth history of various types of synthetic diamond. The following conclusions may be drawn in this regard :

The correlation of the luminescent intensity of the H3 defect with the fraction of cubic growth sector present in the diamond predicted from the observed restriction of H3 to these growth sectors is confirmed in this work. A general trend of increasing H3 intensity with cubic morphology and an increased intensity for luminescence measured on cubic faces compared to that measured on octahedral faces for the same diamond is observed. As more cubic morphology is associated with a higher excess pressure, and hence growth rate, this correlation means that the H3 intensity is indeed an indicator for growth conditions.

The luminescence intensity from the two vacancy related defects, 575 nm and 1.945 eV, correlates with the expected degree of crystal imperfection (as evidenced in the increase in the intensities for increasing cubic nature of the single crystals) or expected plastic deformation (as in the case of the heat treated SDA). A relative enhancement of the luminescence due to these two defects for finer grit samples from the same synthesis run suggests that the finer grit experienced a greater exposure to mobile vacancy generation than the coarser grit from the same synthesis run.

The FWHH is broadened by inhomogeneous strain as anticipated from similar factors to those predicated for the vacancy related defects.

The ZPL lineshape generally displays an increasing Gaussian fraction for the more cubic crystals, suggesting an increasing concentration of line defects for the more cubic crystals.

4.5.2 Suggestions for Future Work

The three defect types discussed in this work all involve nitrogen in the diamond lattice. The measurement of nitrogen concentrations in the powders

and crystals used for photoluminescence measurements would enable a more conclusive study to be done.

The observation of ZPL broadening, changes in lineshape, and changes in the 1.954 eV (and possibly 575 nm) intensities for the heat treated SDA powder sample compared to the untreated sample suggest that photoluminescence measurements of single crystals or powders is a potentially useful means of monitoring, indirectly, the stresses built up in the crystal by internal graphitisation and thermal expansion of the inclusion.

The several observations concerning photoluminescence intensity of the different defects and crystal size for powders grown in the same synthesis runs should be confirmed on a wider range of particle sizes (mostly on finer samples as the changes appear to flatten off for the coarser sizes). In particular, the suggestion that the finer grit samples have been subjected to greater shear stresses or subjected for longer, if confirmed, means that photoluminescence could provide a means of monitoring the shear stresses in synthesis capsules.

The fact that both the intensity of the 575 nm and 1.945 eV defects and the ZPL width are increased by the presence of dislocations or the vacancies associated with them suggest that the defect intensities should correlate with the linewidth (in similar crystals). This suggested correlation should be investigated.

REFERENCES

Anthony T R, Banholzer W F, Fleischer J F, Wei L, Kuo P K, Thomas R L and Pryor R W 1990 *Phys. Rev.* **B42**, 1104

Beard D R 1987 *PhD Thesis*, University of Reading, UK

Berman R 1979 *The properties of diamond* ed J E Field (London: Academic Press)

Bernholc J, Antonelli A, Wang C, Davis R F 1989 *Materials Science Forum* **38**, 713

Bernholc J, Kajihara S A, Wang C, Antonelli A and Davis R F 1992 *Materials Science and Engineering*, **B11**, 265

Bezrukov G N, Butuzov V P and Laptev V A 1972 *Soviet Phys. Dokl.* **16**, 800

Brookes C A 1992 *The properties of natural and synthetic diamond* ed J E Field (London: Academic Press)

Brookes C A, Brookes E J, Howes V R, Roberts S G and Waddington C P 1990 *J. Hard Mater.* **1**, 3

Brookes E J, Collins A T and Woods G S 1993 *J. Hard Mater.* **4**, 97

Burns R C, Cvetkovic V, Dodge C N, Evans D J F, Rooney M T, Spear P M and Welbourn C M 1990 *J. Cryst. Growth* **104**, 257

Burns R C and Davies G J 1992 *The properties of natural and synthetic diamond* ed J E Field (London: Academic Press)

Busch D M 1979 *The properties of diamond* ed J E Field (London: Academic Press)

Busch J V, Dismukes J P, Nallicheri N V and Walton K R 1991 *Applications of diamond films and related materials* ed Y Tzeng, M Yoshikawa, M Murakawa and A Feldman (Elsevier Science Publishers) 623

Cannon P and Conlin E T 1964 *International Congress on the Reactivity of Solids*, 5th, Munich, 362

Chrenko R M, Strong H M and Tuft R E 1971 *Phil. Mag.* **23**, 313

Chrenko R M, Tuft R E and Strong H M 1977 *Nature* **270**, 141

Collins A T 1978 *International Conference on Defects and Radiation Effects in Semiconductors* Nice, 327

Collins A T 1980 *J. Phys. C: Solid State Physics* **13**, 2641

Collins A T 1991 *New Diamond Science and Technology MRS Int. Conf. Proc.* 659

Collins A T 1992 *Diamond and Related Materials* **1**, 457

Collins A T 1993 *Physica* **B185**, 284

Collins A T, Kanda H and Burns R C 1990 *Phil. Mag.* **B61**, 797

Collins A T and Lawson S C 1989 *Phil. Mag. Lett.* **60**, 117

Collins A T, Stanley M 1985 *J. Phys. D: Appl. Phys.* **18**, 2537

Davey S T, Evans T and Robertson S H 1984 *J. Mater. Sci. Lett.* **3**, 1090

Davies G 1970(a) *J. Phys. C: Solid St. Phys.* **3**, 2474

Davies G 1970(b) *International Conference on the Physics of Semiconductors*, 10th, Cambridge Mass., 277

Davies G 1971 *J. Phys. D: Appl. Phys.* **4**, 1340

Davies G 1972 *J. Phys. C: Solid State Phys.* **5**, 2534

Davies G, 1974 *J. Phys. C: Solid State Phys.* **7**, 3798

Davies G 1977(a) *The Chemistry and Physics of Carbon* ed. P L Walker and P A Thrower **13** (New York : Marcel Dekker Inc.)

Davies G 1977(b) *Diamond Research* (London: Industrial Diamond Information Bureau) 15

Davies G 1977(c) *J. Phys. C.*: Solid State Phys. **12**, 2551

Davies G 1981 *Rep. Prog. Phys.* **44**, 787

Davies G and Collins A T 1993 *Diamond and Related Materials* **2**, 80

Davies G and Hamer M F 1976 *Proc. R. Soc. Lond.* **A348**, 285

Davies G, Lawson S C, Collins A T , Mainwood A and Sharp S J 1992 *Phys. Rev.* **B46**, 13157

DeVries R C 1991 *J. Mater. Educ.* **13**, 387

Dickerson C B 1993 *Private Communication*

Dickerson C B and Fish M L 1992 *Unpublished abstracts: Diamond Conference,* Cambridge 25

Dodge C N 1986 *PhD Thesis*, University of Reading, UK

Dyer H B, Raal F A, Du Preez L and Loubser J H N 1956 *Phil. Mag.* **11**, 763

Evans S 1992 *The properties of natural and synthetic diamond* ed. J E Field (London: Academic Press Limited)

Evans T, Davey S T and Robertson S H 1984 *J. Mater. Sci.* **19**, 2405

Fedoseev D V and Semenova-Tyan-Shanskaya A S 1986 *Sverkhtverdye Materialy* **8**, 3

Fedoseev D V and Semenova-Tyan-Shanskaya A S 1987 *Sov. Phys. Dokl.* **32**, 515

Field J E 1979 *The properties of diamond* ed J E Field (London: Academic Press)

Field J E 1991 *Surface and Coatings Technology* **47**, 631

Field J E 1992 *The properties of natural and synthetic diamond* ed J E Field (London: Academic Press)

Giardini A A and Tydings J E 1962 *American Mineralogist* **47**, 1393

Giling L J and Van Enckevoort W J P 1985 *Surface Science* **161**, 567

Graham R J and Ravi K V 1992 *Appl. Phys. Lett.* **60**, 1310

Hanley P L, Kiflawi I and Lang A R 1977 *Phil. Trans. R. Soc.* **A284**, 329

Harris J W 1992 *The properties of natural and synthetic diamond* ed. J E Field (London: Academic Press)

Henderson B 1972 *The structures and properties of solids* 1 ed B R Coles (London: Edward Arnold)

Hughes A E 1968 *J.Phys. Chem. Solids* **29**,1461

Kaiser W and Bond W L 1959 *Phys. Rev.* **115**, 857

Kamiya Y and Lang A R 1965 *J. Appl. Phys.* **36**, 579

Kanda H, Setaka N, Ohsawa T and Fukunaga O 1981 *J. Cryst. Growth* **51**, 6229

Kawarada H, Yokota Y, Mori Y, Nishimura K, Ito T, Suzuki J, Mar K-S, Wei J and Hiraki A 1989 *SPIE 1055 Raman Scattering, Luminescence, and Spectroscopic Instrumentation in Technology* 162

Klyuev A Yu, Naletov A M and Nepsha V I 1982 *(Zh. Fiz. Khim)* **56**, 528

Koivula 1993 *Gems and Gemology* (Summer) **26**, 300

Kurdadze Sh A, Loladze N T and Martovitskii V P 1992 *Neorganicheskie Materialy* **28**, 969

Lang A R, Moore M and Walmsley J C 1992 *The properties of natural and synthetic diamonds* ed J E Field (London: Academic Press)

Lee Y H, Brosious P R, Corbett J W 1978 *Phys. Stat. Solidi.* **A50** 237

Loubser J H N and van Wyk J A 1977 *Diamond Research* (London: Industrial Diamond Information Bureau) 16

Malogolovets V G, Vishnevskii A S and Povarennykh A S 1978 *Dokl. Akad. Nauk. SSSR* **243**, 111

Malogolovets V G, Ivakhnenko S A and Chipenko G V 1993 *Sverkhtverdye Materialy* **15**, 7

Miyamoto M, Akaishi M, Yamaoka S and Fukanaga O 1991 *Kobelco Technology Review No 12*, 28

Müller E W, Mosfun - *A new and versatile Mössbauer fitting program* (Mössbauer Effect Data Centre NC USA, 1980)

Muncke G 1979 *The properties of diamond* ed J E Field (London: Academic Press)

Nevstruev G F, Katsay M Ya and Ilnitskaya G D 1992 *High Pressure Research* **9**, 296

Novikov N V and Boriimsky A I 1992 *High Pressure Research* **9**, 128

Orth D L, Mashl R J and Skinner J L 1993 *J. Phys.: Condens. Matter* **5** 2533

Perevertailo V M 1992 *High Pressure Research* **9**, 284

Ponahlo J 1992 *J. Gemm.* **23**, 3

Posener D G 1959 *Aust. J. Phys.* **12**, 184

Robertson S H 1984 *PhD Thesis*, University of Reading, UK

Satoh S, Nakashima T, Tsuzuji K and Yazu S 1990 *High Pressure Research* **5**, 926

Seal M 1992 *The properties of natural and synthetic diamond* ed J E Field (London: Academic Press)

Sellschop J P F 1992 *The properties of natural and synthetic diamond* ed J E Field (London: Academic Press)

Shulshenko A A, Varga L and Hidasi B 1992 *Refractory Metals and Hard Materials* **11**, 285

Spiegel M R 1988 *Schaum's outline of theory and problems of statistics* 2nd ed. (New York: McGraw-Hill Publishing Company)

Stoneham A M 1969 *Reviews of Modern Physics* **41**, 82

Strong H M 1989 *Am. J. Phys.* **57**, 794

Strong H M and Chrenko R M 1971 *J. Phys. Chem.* **75**, 1838

Strong H M and Hanneman R E 1967 *J. Chem. Phys.* **46**, 3668

Sunagawa I 1984 *Materials science of the earth's interior* ed I Sunagawa (Tokyo: Terra Scientific Publishing Company)

Sunagawa I 1990 *J. Cryst. Growth* **99**, 1156

Sussman R S 1993 *Industrial Diamond Review* **53**, 63

Tomlinson P N 1992 *The properties of natural and synthetic diamond* ed J E Field (London: Academic Press)

Underhill L G, 1985 *"Introstat"*, 4th Ed., (Cape Town: Juta and Co. Ltd.)

Vagarali S, Lee M and DeVries R C 1990 *J. Hard Mater.* **1**, 233

Van Enckevoort W J P and Lochs H G M 1988 *J. Appl. Phys.* **64**, 434

Vins V G, Feigelson B N, Eliseev A P, Patrin N S, Patrenin Yu V and Nekhaev P Yu 1991 *Sverkhtverdye Materialy* **13**, 21

Wakatsuki M 1984 *Materials science of the earth's interior* ed I Sunagawa (Tokyo: Terra Scientific Publishing Company)

Wakatsuki M 1991 *XIII AIRAPT - Int. Conf. on High Pressure Science and Technology*, Bangalore 671

Wakatsuki M and Takano K J 1987 *High-Pressure Research in Mineral Physics* 203

Walker J 1979 *Rep. Prog. Phys.* **42**, 1605

Wedlake R J 1979 *The properties of diamond* ed J E Field (London: Academic Press)

Wentorf R H 1965 *Advances in Chemical Physics* **9** ed I Prigogine (New York: Interscience Publishers)

Wierzchowski W, Moore M, Makepeace A P W and Yacoot A 1991 *Journal of Crystal Growth* **114**, 209

Wilks E M and Wilks J 1965 *Physical properties of diamond* ed R Berman (Oxford: Clarendon Press) 371

Woods G S 1970 *Phil. Mag.* **22**, 1081

Woods G S 1971 *PhD Thesis.* University of the Witwatersrand

Woods G S 1973 *Diamond Research* (London: Industrial Diamond Information Bureau) 25

Woods G S 1986 *Proc. R. Soc. Lond.* **A407**, 219

Woods G S and Lang A R 1975 *J. Cryst. Growth* **28**, 215

Yazu S 1985 *European Patent* **0 136 408 A1**

Zaitsev A M, Ulyashin A G and Husein Ali Nur 1991 *Sverkhtverdye Materialy* **13**, 18

Author: Fish Michael Lester.
Name of thesis: Optical properties of synthetic diamond of different synthesis origin.

PUBLISHER:
University of the Witwatersrand, Johannesburg
©2015

LEGALNOTICES:

Copyright Notice: All materials on the University of the Witwatersrand, Johannesburg Library website are protected by South African copyright law and may not be distributed, transmitted, displayed or otherwise published in any format, without the prior written permission of the copyright owner.

Disclaimer and Terms of Use: Provided that you maintain all copyright and other notices contained therein, you may download material (one machine readable copy and one print copy per page)for your personal and/or educational non-commercial use only.

The University of the Witwatersrand, Johannesburg, is not responsible for any errors or omissions and excludes any and all liability for any errors in or omissions from the information on the Library website.